NATIONAL ADVISORY COMMITTEE FOR AERONAUTICS

TECHNICAL NOTE 2476

AN EMPIRICAL METHOD PERMITTING RAPID DETERMINATION

OF THE AREA, RATE, AND DISTRIBUTION OF WATER-DROP

IMPINGEMENT ON AN AIRFOIL OF ARBITRARY SECTION

AT SUBSONIC SPEEDS

By Norman R. Bergrun

Ames Aeronautical Laboratory
Moffett Field, Calif.

NACA

Washington

September 1951

TECHNICAL NOTE 2476

AN EMPIRICAL METHOD PERMITTING RAPID DETERMINATION
OF THE AREA, RATE, AND DISTRIBUTION OF WATER-DROP
IMPINGEMENT ON AN AIRFOIL OF ARBITRARY SECTION
AT SUBSONIC SPEEDS

By Norman R. Bergrun

SUMMARY

An empirical method for the determination of the area, rate, and
distribution of water-drop impingement on airfoils of arbitrary section
is presented. The procedure represents an initial step toward the
development of a method which is generally applicable in the design
of thermal ice-prevention equipment for airplane wing and tail sur-
faces. Results given by the proposed empirical method are expected
to be sufficiently accurate for the purpose of heated-wing design,
and can be obtained from a few numerical computations once the velocity
distribution over the airfoil has been determined.

The empirical method presented for incompressible flow is based
on results of extensive water-drop trajectory computations for five
airfoil cases which consisted of 15-percent-thick airfoils encompassing
a moderate lift-coefficient range.   The differential equations per-
taining to the paths of the drops were solved by a differential
analyzer.

The method developed for incompressible flow is extended to the
calculation of area and rate of impingement on straight wings in sub-
sonic compressible flow to indicate the probable effects of compressi-
bility for airfoils at low subsonic Mach numbers.

INTRODUCTION

The design of thermal ice-prevention equipment for airplane wing
and tail surfaces has progressed to the point where the amount and
distribution of heat flow can be calculated for specified flight and
icing conditions (reference 1). This design procedure requires infor-
mation as to the area, rate, and distribution of water-drop impinge-
ment on the leading edge of the airfoil section being analyzed. At the
present time, an approximation of area and rate of water-drop impinge-
ment is achieved by using a method involving the substitution of a
circular cylinder for the airfoil leading edge, as suggested in

references 1 and 2. This substitution method is adequate for design purposes for some combinations of cylinder diameter and drop size, but it can produce sizable errors for other combinations (references 1, 3, and 4).

A second means of estimating the area and rate of water–drop impingement on airfoils is provided by reference 3. This method is more accurate than the cylinder substitution method, but the calculation procedure is somewhat laborious and, as a result, its use is not too practicable in a complete design study where a large number of trajectories are usually required.

To establish a procedure which would eliminate the laborious computations of water–drop trajectories in the design of wing thermal ice–prevention equipment, it became apparent that a large number of water–drop trajectories would be required for study. Experience with calculating trajectories by the method of reference 3 had shown that the pattern of water–drop impingement for drop sizes usually encountered in flight can be related most directly to velocity distribution over the surface of the airfoil. Airfoil shape itself appeared to have an effect on the pattern of impingement, but to a lesser degree than velocity distribution. Five airfoil cases were chosen as being the minimum which could be expected to provide sufficient data to include the effects of these two factors. Water–drop trajectories were computed for these five cases.

This report presents the results of the water–drop–trajectory computations. From a generalization of these data, a method is derived that permits a relatively rapid determination of the area, rate, and distribution of water–drop impingement for a fairly large number of airfoil surfaces of arbitrary profile. The derivation and limitations of this method and the procedure for its use are presented herein. The water–drop trajectories for the five airfoil cases were computed on the differential analyzer at the University of California, Los Angeles, under contract with the NACA; and appreciation is extended to the staff of the University for its aid and cooperation during the conduct of the program.

SYMBOLS

The following nomenclature is used throughout this report:

a   airfoil mean–line designation, fraction of chord from leading edge over which design load is uniform

a_d instantaneous drop–acceleration ratio, dimensionless

A_O area normal to flow direction outlined by several trajectories at free—stream conditions, square feet

A_s area of impingement outlined on an airfoil surface by trajectories starting at free—stream conditions from an initial area of A_O, square feet

c chord length of airfoil, feet

C concentration factor $\left(\dfrac{dA_O}{dA_s}\right)$, dimensionless

C_d drag coefficient of drop, dimensionless

c_l section lift coefficient, dimensionless

C_p pressure coefficient $\left[1-\left(\dfrac{U_a}{V}\right)^2 \right]$, dimensionless

C_{p_M} pressure coefficient at Mach number M, dimensionless

E collection efficiency of airfoil, percent

G rate of change of velocity along the stagnation stream-line at the stagnation point $\left[\dfrac{d(U_a/V)}{dS}\bigg|_{\Psi=0} \right]$, dimensionless

h frontal height of airfoil, fraction of chord

k slope of airfoil contour at a particular chordwise position, dimensionless

L length of span, feet

m liquid—water content of icing cloud, pounds of water per cubic foot of air

M Mach number, dimensionless

M_a weight rate of water—drop impingement per unit of surface area, pounds per hour, square foot

M_s weight rate of impingement of water drops on a body, per unit span, pound per hour, foot

P ratio of the vector difference between the local air and drop velocities to free—stream velocity $\left(\dfrac{\overline{U}_a-\overline{U}_d}{V}\right)$, dimensionless

r   radius of drop, feet

R   Reynolds number for drop at relative velocity PV $\left(\dfrac{2PVr}{\nu}\right)$

R_V Reynolds number for drop at free-stream velocity V $\left(\dfrac{2Vr}{\nu}\right)$

s   distance along airfoil surface from leading edge, positive on upper surface and negative on lower surface, feet

S   distance along water-drop trajectory, fraction of chord

t   time, seconds

t_e equivalent ellipse thickness ratio for a low-drag airfoil $\left(\dfrac{2\rho}{t_{max}}\right)$, fraction of chord

t_{max} maximum thickness of airfoil, fraction of chord

u   component of local velocity parallel to chord line, feet per second

U   local velocity of air or drop, feet per second

v   component of local velocity perpendicular to chord line, feet per second

V   free-stream air velocity, feet per second

x,y   rectangular coordinates for a system of axes having the origin at the airfoil leading edge and the x axis, positive toward the trailing edge, lying along the airfoil chord, fraction or percent of chord

x',y' rectangular coordinates for a system of axes having the origin at the airfoil leading edge and the x' axis, positive in the free-stream direction, lying parallel to free-stream direction, fraction or percent of chord

Δy total airfoil-ordinate intercept established by two impinging trajectories starting from infinity at a distance Δy_0 apart, fraction of chord

Δy_0 distance between two trajectories at infinity, fraction of chord

Δy_{o_t} distance between two trajectories which start at infinity and impinge tangentially on the airfoil, fraction of chord

α angle of attack, degrees

β Prandtl-Glauert factor, equal to $(1-M^2)^{1/2}$, dimensionless

γ specific weight, pounds per cubic foot

θ angular displacement between local velocity and x axis, degrees

ν kinematic viscosity of air, square feet per second

ρ airfoil leading-edge radius, fraction of airfoil chord

τ time scale $\left(\dfrac{tV}{c}\right)$, dimensionless

ψ scale modulus $\left(9\,\dfrac{\gamma_a}{\gamma_d}\times\dfrac{c}{r}\right)$, dimensionless

Ψ stream function, dimensionless

Subscripts

a   air

av   average

cr   critical

d   drop

e   effective

l lower surface

M   conditions at a particular Mach number

max   maximum

o   initial condition

s   condition at airfoil surface

t   tangential

u   upper surface

DERIVATION OF THE METHOD

The method, derived herein, for calculating area, rate, and distribution of drop impingement assumes that airfoil velocity distribution can be considered as the primary factor influencing the paths of water drops which approach an airfoil. Hence, it was desired to find a relatively simple relation between the airfoil velocity distribution (which in itself is a function of airfoil contour) and the area, rate, and distribution of impingement. Accordingly, trajectories around airfoils of known surface velocity distribution were obtained for analysis, and, from this information, generalizations were made as to the behavior of drops in the presence of the different airfoil velocity fields.

Description of Procedure Used to
Obtain Water–Drop Trajectories

The five airfoil cases selected for the water–drop–trajectory investigation are listed in the following table:

Case	Airfoil	Angle of attack (deg)	c_l	Leading–edge radius (percent chord)
1	15–percent–thick symmetrical Joukowski	0	0	2.67
2	Do	2	.22	2.67
3	Do	4	.44	2.67
4	15–percent–thick cambered Joukowski	0	.44	2.67
5	NACA 65_2–015 (symmetrical)	4	.44	1.505

This table shows the systematic changes in the variables which affect velocity distribution. Cases 1, 2, and 3 were intended to reveal the effects of systemmatically altering airfoil velocity distribution by changing angle of attack; case 4, compared to cases 1

and 3, the effects of altering velocity distribution by the addition
of a basic load distribution obtained by cambering the mean line;
and cases 3 and 5, the effects of changing general airfoil shape for
a given angle of attack and lift coefficient. The upper- and lower-
surface velocity distributions over the forward region of each of the
five airfoils are shown in figure 1. Velocity distributions for
Joukowski airfoils are used where possible because the required veloc-
ity components in the field of flow are more readily obtained than for
most other airfoils. It is noted in figure 1 that the variables
selected did not result in a wide variety of velocity distributions,
but it is believed that these distributions are of sufficient scope to
allow a generalization of the trajectory data, at least for cases in
which there are no marked nose-pressure peaks.

The water-drop-trajectory computations were made to encompass
a speed range of 100 to 350 miles per hour (assuming incompressible
flow), a drop-diameter range of 20 to 100 microns, and a variation
in altitude from sea level to 20,000 feet. Airfoil chord length was
varied from 3 inches to 30 feet. These variables were combined into
the dimensionless parameters, ψ and R_V, which then were used as
the independent variables throughout the trajectory computations.
The range in values of ψ and R_V resulting from a combination of
each minimum value and a combination of each maximum value of the three
constituent variables is about 150 to 20,000 for ψ and about 35 to
1000 for R_V. These ranges in ψ and R_V encompass most other pos-
sible combinations of the selected values of speed, drop size, altitude,
and chord length, but the data calculated for these ranges in ψ and
R_V are not necessarily limited to the particular values of the con-
stituent variables used to establish the ranges in ψ and R_V.

The problem of obtaining area, rate, and distribution of water-
drop impingement on an airfoil is one of determining the solution to
a set of simultaneous differential equations yielding the trajectory
or path which a water drop will follow. These equations, a derivation
of which may be found in reference 5, are essentially those which result
from imposing conditions of dynamic equilibrium on a drop moving in an
air stream. In dimensionless form, the equations are

$$\frac{d(u_d/V)}{d\tau} = \frac{\psi}{R_V} \left(\frac{C_d R}{24}\right) \left(\frac{u_a}{V} - \frac{u_d}{V}\right) \tag{1}$$

$$\frac{d(v_d/V)}{d\tau} = \frac{\psi}{R_V} \left(\frac{C_d R}{24}\right) \left(\frac{v_a}{V} - \frac{v_d}{V}\right) \tag{2}$$

$$\left(\frac{R}{R_V}\right)^2 = \left(\frac{u_a}{V} - \frac{u_d}{V}\right)^2 + \left(\frac{v_a}{V} - \frac{v_d}{V}\right)^2 \tag{3}$$

Basically, equations (1) and (2) define the acceleration of a drop at any instant in orthogonal (x and y) directions. Consequently, a double integration of these equations, starting from a selected initial point (x_0, y_0), yields x and y values necessary to plot a drop trajectory. Equation (3) is required to proceed with the solutions of equations (1) and (2). In performing the integrations, knowledge of the quantity $C_d R/24$ (the ratio of the actual drag coefficient given by Stokes law of resistance) is required; also required are magnitudes of the air—velocity components u_a/V and v_a/V as a function of drop location relative to the body. (See reference 5.) Variation of the term $C_d R/24$ with local Reynolds number R was taken from reference 6, while the variation of the air—velocity components u_a/V and v_a/V throughout the flow field was obtained analytically for the Joukowski airfoils. In the case of the NACA 65_2–015 airfoil, however, the velocity distribution throughout the flow field was obtained by an electrolytic analogy method.[1]

In carrying out the differential analyzer computations for the five airfoil cases, the general procedure was to assign values to the terms ψ and R_V in equations (1), (2), and (3), to establish initial conditions, and then to obtain the water—drop—trajectory traces from the analyzer. For each combination of ψ and R_V selected, several trajectories were traced until the two trajectories were found, one for the upper surface and one for the lower surface, which were tangent to the airfoil surface at the point of drop impact. The importance of these two tangential trajectories lies in the fact that all drops between the tangential trajectories hit the airfoil and all drops outside will miss. In some cases, after the tangential trajectories were

---

[1]The electrolytic analogy method was based on the fact that the streamlines in an inviscid incompressible fluid and the equipotential lines in an electrical field are governed by the same equations. By means of this analogy and suitably constructed apparatus, velocities at any point in the flow field around a body could be measured directly. Accuracy of the electrolytic analogy method of obtaining velocities was assessed by comparing measured velocities with theoretically calculated values for two bodies. Comparisons were made for a small cylinder, with and without circulation, and for a 15—percent—thick Joukowski airfoil (of various chord lengths) with and without circulation. For optimum test conditions, the accuracy in velocities was about ±5 percent out to approximately one—half chord forward of the airfoil. Between one—half and one chord length forward of the airfoil, velocities could be obtained with an estimated accuracy of ±10 percent.

established, the distance between them was divided into six approximately equal spaces, and trajectories started at the boundary of each space were traced. These intermediate trajectories were used to obtain an indication of the distribution of water-drop impingement over the airfoil surface.

Water-Drop-Trajectory Data

All the tangential trajectories, and the trajectories traced for distribution of impingement, are presented for the five airfoil cases in figures 2 through 6. The drop trajectories, which were calculated for assigned values of the independent variables ψ and R_V directly yield values of trajectory starting ordinates and surface positions of drop impingement. These variables, which, by the method of analysis shown in reference 1, can be used to determine the values of the dependent variables, area, rate, and distribution of impingement, are tabulated in tables I through V for each of the airfoil cases. Also included in the tables are the velocity components of the drops at the point of impingement.

Manner in Which Water-Drop-Trajectory Data
Were Generalized

The objective in generalizing the water-drop-trajectory data obtained from the differential analyzer is to establish a relatively simple method for determining the impingement pattern of water drops on an arbitrarily selected airfoil at a given attitude for specified values of ψ and R_V. It is desirable that application of such a method should require only information which is usually available for the airfoil profile, or which is easily procured, such as the pressure distribution. Therefore, the first part of this section will present the reasoning associated with deriving such a method for incompressible flow from the results of the trajectory data; the latter part is devoted to an extension of the basic method to subsonic compressible flow.

Generalization in regard to area of water-drop impingement.— In order to determine the area of water-drop impingement on the leading edge of an airfoil for specified meteorological and flight conditions, the values of s/c for the trajectories which impinge tangentially on the upper and lower surfaces must be obtained. In computational methods like those of references 3, 5, and 6, the procedure essentially has been to select values of ψ and R_V and then to determine the trajectory. Various trajectories are computed until the tangential trajectory for the upper and lower surfaces is found. The two

tangential trajectories located determine the farthest positions of
drop impingement on the airfoil surface for the selected values of ψ
and R_V and permit calculating area of impingement from the equation

$$A_s = \left[\left(\frac{s}{c} \right)_{u_t} - \left(\frac{s}{c} \right)_{l_t} \right] L_c$$

In the derivation of the empirical method, herein presented, the
reverse procedure was employed; that is, a point on the airfoil was
selected (s/c) and the corresponding ψ and R_V values which are
associated with the tangential trajectories at that point were deter-
mined. The nature of the relationship between s/c and the parame-
ters ψ and R_V is shown in figure 7. Data for the figure are those
of table IV for the cambered airfoil at zero angle of attack and a
lift coefficient of 0.44. From figure 7, it can be seen that any
specified value of s/c in the figure can correspond to an infinite
number of combinations of R_V and ψ. Consequently it becomes
necessary to select values of one variable and to solve for the other.
In the derivation of the method of this report, values of R_V are
assumed and corresponding values of ψ are computed.

If the data of figure 7 could be made available for all airfoils
of interest, the problem of determining s/c for various values of
ψ and R_V would, of course, be simple. Because obtaining such data
for all airfoils is impractical, the problem in the general case
arises in determining the relation between R_V, ψ, and s/c. To
determine this relationship, equations (1), (2), and (3) are utilized
to derive an expression for the scale modulus ψ, which is

$$\psi = \frac{a_d \, R_V}{\left(\dfrac{C_d R}{24} \right)\left(\dfrac{R}{R_V} \right)} \tag{4}$$

where

$$a_d = \sqrt{ \left[\frac{d(u_d/V)}{d\tau} \right]^2 + \left[\frac{d(v_d/V)}{d\tau} \right]^2 }$$

Equation (4) expresses generally the relation between ψ and R_V
at all points in a trajectory, and, therefore, it is applicable at the
airfoil surface for an arbitrarily selected value of s/c which corre-
sponds to some particular tangential trajectory. It remains to

establish the values of $C_dR/24$, R/R_V, and a_d for the selected value
of s/c. Actually, since $C_dR/24$ is a known function of R, the
problem reduces to approximating R/R_V and a_d at the airfoil sur-
face.

Evaluation of R/R_V at airfoil surface: To determine R/R_V
the method of this report is based on a graphical solution utilizing
the hodograph plane. It is in this connection that the trajectory
data from the differential analyzer are plotted in the hodograph
plane in figure 8 for each of the five airfoil cases. To show the
general relation of drop velocities to air velocities, the hodograph
of air at the airfoil surface is also shown for each case. It is
interesting to note in figure 8 that the velocity components for all
drops, regardless of the combination of ψ and R_V, can be repre-
sented by one faired curve.[2] Of particular interest, however, is the
fact that the hodograph for the drops, for both upper and lower air-
foil surfaces, always passes through the point $u_d/V = \cos\alpha$,
$v_d/V = \sin\alpha$. Thus, in the simplest case of an airfoil at zero
angle of attack, the hodograph of the drops always passes through
an abscissa value of unity because this point corresponds physically
to the point of maximum airfoil thickness where straight-line tan-
gential trajectories always impinge upon the airfoil with free-stream
air velocity. The coordinates at the origin of the air and drop
hodographs correspond physically, of course, to the airfoil stag-
nation point.

To show the connection between the results of the trajectory
data for the five airfoil cases and the case of an arbitrary airfoil,
figure 9 is presented. Figure 9(a) depicts several water-drop
trajectories in the physical plane impinging tangentially at the
same point s/c on an airfoil which is at an angle of attack α.
These trajectories, for purposes of explanation, may be assumed to
correspond to various points on a line of constant s/c in figure 7.
Accordingly, there is an infinite number of particular combinations

---

[2]An inspection of figure 8(e) will show that, for the upper surface
of the NACA 65_2-015 airfoil, the curve was not faired through all
the data points. The reason is that the velocity components for
some of the data points were in error. This can be shown by noting
that every data point will not fall on a line connecting the origin
and a point on the air hodograph having the same s/c value as the
data point. Each data point must lie on such a line because the
slope of a trajectory tangential to the airfoil at some s/c posi-
tion and the slope of the airfoil at the same s/c position are
equal. The data points in figure 8(e) considered to be inconsistent
with this criterion are designated with tag marks and are not
heavily relied upon for establishing the drop hodograph.

of ψ and R_V which are affine to any particular position of tangential drop impingement $(s/c)_t$. In figure 9(a), a single vector representing the drop velocity for all the trajectories is drawn tangentially to the airfoil at the point of drop impingement. Only one vector is shown because the tangential trajectory hodographs presented in figure 8 indicate that all drops impinging tangentially at a common point may be considered to have the same velocity. Also shown in figure 9(a) is a vector representing the air velocity at the point of impingement for the trajectories. The angle between the drop- and air-velocity vectors and the x axis is designated by the angle θ. In figure 9(b), a typical air and drop hodograph is shown and the same vectors as shown in the physical plane are indicated. It should be noted that the difference in length of air and drop vectors at a particular s/c position is numerically equal to the value of R/R_V given by equation (3).

As can be seen from figure 8, all five airfoils exhibit the same characteristic in regard to the single-valued nature of the term R/R_V with chordwise position, and it will be assumed that all other airfoils will display the same characteristic. However, in order to calculate values of R/R_V for an arbitrary airfoil, both hodographs of the air and of the tangential trajectories are required. The hodograph of the air velocity at the airfoil surface is easily obtained from the velocity distribution over the airfoil, but the shape of the hodograph for the tangential trajectories is more difficult to obtain. This is because the data of figure 8 yield only the information that the tangential-trajectory hodograph always will pass through the point $u_d/V = 0$, $v_d/V = 0$ and the point $u_d/V = \cos \alpha$, $v_d/V = \sin \alpha$.

With two points on the trajectory hodograph always known, it was concluded that, if one more point could be established, preferably where the vertical-velocity component reaches the maximum value, the general shape of the trajectory hodograph would be reasonably ascertainable. It was noted from the hodographs in figure 8 that peak values of v_a/V and v_d/V were at nearly the same location on the airfoil surface. That is, values of $v_{a_{max}}/V$ and $v_{d_{max}}/V$ nearly always fall on a straight line through the origin, and it remains to determine just where on the line the value of $v_{d_{max}}/V$ will fall. In this connection, it was decided to compare, for the five airfoil cases, values of the vertical component of relative velocity between drop and air attained at the position of maximum vertical air velocity. Accordingly, values of $(v_{a_{max}}/V) - (v_{d_{max}}/V)$ and $v_{a_{max}}/V$ were obtained from figure 8 and these are plotted in figure 10. An inspection of the data in figure 10 shows that the four Joukowski airfoil cases provide data sufficient to establish a relation between $(v_{a_{max}}/V) - (v_{d_{max}}/V)$ and $v_{a_{max}}/V$; but too little

information is available for the NACA 65-series sections to firmly
establish a relation between $(v_{a_{max}}/V) - (v_{d_{max}}/V)$ and $v_{a_{max}}/V$.
The point plotted in figure 10 for the NACA 65_2-015 airfoil upper
surface does not lie on the curve established by the Joukowski air-
foil data, and a question arises as to whether this difference is
real or due to a possible improper fairing in figure 8(e) of the
upper-surface drop hodograph. While this question cannot be resolved
until further data are available, qualitatively it would seem that
the drop velocities should tend to approach more nearly the air
velocities in the case of low-drag airfoils because these shapes
are not so conducive to abruptly altering the paths of water drops.

To show how figure 10 can be used as an aid in the construction
of the drop hodograph for an airfoil of arbitrary profile and
attitude, figure 11 is presented. The procedure is first to draw
the air hodograph and establish $v_{a_{max}}/V$. Then, the maximum vertical
velocity of the tangential-trajectory hodograph is determined as
being less than $v_{a_{max}}/V$ by the amount $(v_{a_{max}}/V) - (v_{d_{max}}/V)$ in
accordance with the curve in figure 10. The value of $v_{d_{max}}/V$ so
determined is assumed to lie on a straight line connecting the
origin and $v_{a_{max}}/V$. The position of $v_{d_{max}}/V$ along the radial line
determines the value of $(R/R_V)_{v_{a_{max}}}$ at that particular position.
Values of R/R_V for other s/c positions are taken, as a first
approximation, as being in the same ratio to the air velocity at the
particular s/c position as the value of R/R_V at $v_{a_{max}}/V$ is to
U_a/V at $v_{a_{max}}/V$ (curve A in figure 11). Values of R/R_V calcu-
lated in this manner usually are too large near the point
$u_d/V = \cos\alpha$, $v_d/V = \sin\alpha$ (point X, figure 11), so that a drop
hodograph so constructed would probably not pass through this point
as it should. To overcome this discrepancy in the drop hodograph
as computed by a proportion based on the peak point of the air
hodograph, a curve without reflex is faired tangentially into the
proportional drop hodograph from the point $u_d/V = \cos\alpha$,
$v_d/V = \sin\alpha$. The combination of the proportional curve and the
faired curve comprises the drop hodograph, which is labeled curve B
in figure 11. For the five airfoil cases, maximum deviations of
the drop hodographs obtained by the foregoing method from the drop
hodographs in figure 8 were of the order of 15 percent.

Two other methods were considered for establishing drop hodo-
graphs. One method assumed R/R_V to maintain a constant value equal
to the value prevailing at the point $u_d/V = \cos\alpha$, $v_d/V = \sin\alpha$.

The other method assumed the ratio $\dfrac{R/R_V}{U_a/V}$ to maintain a constant
value determined by the value of R/R_V and U_a/V at the point
$u_d/V = \cos \alpha$, $v_d/V = \sin \alpha$. The drop hodographs given by each of
these two methods also are shown for the example in figure 11. The
curves are labeled C and D, respectively. These two methods have
the advantage of not requiring the use of the hodograph and fig-
ure 10; however, they are considerably more inaccurate (maximum
deviations from the drop hodographs for the five airfoil cases being
in the order of 30 percent) due to the neglect of factors of apparent
influence on the drop trajectories. Use of either one of these
latter two methods is suggested for particular airfoil cases which
might happen to fall beyond the scope of the data presented in fig-
ure 10.

After the tangential-trajectory hodograph has been established
in relation to the hodograph for air, values of R/R_V are available
for various chordwise positions on the airfoil. These values are used
in equation (4) for arbitrarily selected values of R_V and s/c.
Since values of R_V are arbitrarily selected, values of R are
ascertainable. Furthermore, values of the term $C_d R/24$ can be calcu-
lated because $C_d R/24$ is a function of R in accordance with
table VI. Thus, to solve equation (4), the only other term to be
evaluated is a_d.

Evaluation of the drop-acceleration term a_d: The remaining
term to be evaluated in equation (4) is the acceleration of the drop
at the airfoil surface a_d. To determine the variation of this term
with chordwise position, values of a_d were calculated from the
trajectory data by equation (4) for each of the airfoil cases presented
in tables I through V. The procedure used in making the calculations
was to compute the value of R/R_V by utilizing values of the
orthogonal drop-velocity components from tables I through V for
corresponding values of ψ and R_V. The term was calculable through
knowledge of R/R_V and R_V. The terms R/R_V, $C_d R/24$, R_V, and ψ were
then substituted into equation (4) and solved for a_d. The results
of this procedure are presented in figure 12 for each of the five
airfoil cases.

An inspection of figure 12 shows that drop acceleration at the
surface of the airfoil, like the hodograph of drop velocities for
tangentially impinging trajectories, can be considered a single rela-
tion regardless of the combinations of ψ and R_V. How the singular
nature of the acceleration values arises can be shown by rewriting
equation (4) as follows:

$$a_d = \psi \left(\frac{C_d}{24}\right)\left(\frac{R}{R_V}\right)^2_t \qquad (5)$$

However, since the term $(R/R_V)_t$ is taken to be constant for a given position on the surface, equation (5) may be written

$$a_d = (const) \; \psi C_d \qquad (6)$$

where the constant depends on the chordwise position and the value of $(R/R_V)_t$ at that position. Thus, according to equation (6), it is apparent that, if the product of ψ and C_d remains constant for various values of R_V at a given chordwise position, then the value of a_d also will remain constant. Hence, to show the constancy of a_d at various chordwise positions for various R_V values, products of ψ and C_d were calculated for every combination of ψ and R_V presented in tables I through V for the five airfoils. The procedure used was to select a value of R_V and to derive C_d by using the value of $(R/R_V)_t$ noted on the hodograph for the s/c position corresponding to the particular R_V value chosen. The products of ψC_d were compared with other ψC_d products corresponding to the same physical point on the airfoil; but these latter products were calculated by using values of ψ obtained from a plot of the tabulated values of ψ and s/c for various values of R_V. This procedure was adopted in order to obtain products corresponding to farthest positions of impingement not given directly in tables I through V. Comparisons of the products are made in tables VII through XI. These comparisons show that, for a given s/c position, the product of ψ and C_d generally is of the same order of magnitude for a wide range of ψ and R_V values, particularly at the lower values of s/c. Therefore, the assumption that a_d is constant for a particular chordwise position seems fairly well justified.

The problem of evaluating drop acceleration now has been reduced to finding, for a number of s/c positions on the airfoil, a value of a_d which corresponds to each s/c value chosen.

In approximating the drop acceleration at a point where the drop trajectory is tangent to the airfoil surface, several procedures are possible, as was the case with the term R/R_V. Of the various procedures investigated, the one which will be presented herein is considered most acceptable because the resultant accuracy is commensurate with that produced by the most accurate procedure presented for obtaining R/R_V. In addition, the procedure is simple in application. For this procedure, the approximation is made that the tangential acceleration of a drop at a given point on the surface

is the same as the acceleration of the air along the airfoil surface
at the same point.[3] The equation used to express the drop acceler-
ation in terms of air velocity at the airfoil surface is:

$$a_d = \frac{U_a}{V} \times \frac{d(U_a/V)}{d(s/c)} \tag{7}$$

The velocity gradient term in equation (7) can be evaluated simply
by plotting U_a/V against s/c, and obtaining the slope of the
resulting curve at the desired s/c positions.

Results obtained by using equation (7) to approximate values
of a_d for the five airfoil cases are shown in figure 12 where
the calculated point values are denoted by square symbols. It will
be noted that equation (7) appears to provide good results for the
symmetrical Joukowski airfoil case (fig. 12(a)), and over most of
the lower surface of each of the other four airfoil cases (figs. 12(b),
12(c), 12(d), and 12(e)). For these latter four airfoil cases,
equation (7) provides upper-surface drop-acceleration values toward
the leading edge of the airfoil which appear in good agreement with
the trajectory data; but farther aft, the ability of equation (7)
to predict appropriate values diminishes appreciably, particularly
for the Joukowski and NACA 65_2-015 airfoils at 4° angle of attack
(figs. 12(c) and 12(e)). In these instances, the inability of
equation (7) to yield drop acceleration values fairly far aft on
the airfoil surface apparently is because the drops impinging in
this region have sufficiently large inertia so as not to respond to
the very rapid changes in surface-air velocities prevailing near
the position of maximum air velocity. Except quite near the leading
edge, the trajectories are fairly straight, indicating that the
impinging drops do not respond appreciably to the vertical components
of air velocity. Thus, it seemed that a suitable representation of
drop acceleration for the case of an airfoil with a velocity peak
located near the leading edge might be obtained by assuming that the

---

[3] Only the tangential component of drop acceleration needs to be
approximated since the normal component of drop acceleration can
be shown to be equal to zero at the point of drop impingement
for tangential trajectories. That the normal acceleration of the
drop is zero at the point of impingement can be shown by writing
the equations expressing dynamic equilibrium of a drop. The terms
involving the drop and air velocities are resolved normally and
tangentially. A substitution of the boundary conditions at the
point of impingement shows that the normal acceleration must equal
zero at this point.

drop acceleration was influenced mostly by the x components of air velocity. In equation (7), then U_a/V would be replaced by u_a/V so that

$$a_d = \frac{u_a}{V} \times \frac{d(u_a/V)}{d(s/c)} \tag{8}$$

Equation (8) was used to calculate additional drop-acceleration values for the upper surfaces of the airfoils presented in figure 12 and the results obtained are compared in these figures with drop acceleration values given by the trajectory data. The points calculated by equation (8) are shown as triangles in figure 12, and represent a good approximation of the upper surface a_d values fairly far aft on these surfaces.

The question arises as to whether it would be possible in the general case, when the differential analyzer data points shown in figure 12 were not present, to detect the inadequacy of equation (7) to represent the correct values of a_d. In this connection it should be noted that the point on the curve for $a_d = 0$ can always be selected because this point corresponds to the chordwise position of the tangentially impinging straight-line trajectory having the maximum s/c intercept. This particular trajectory can always be established by constructing a line tangent to the upper surface of the airfoil and parallel to the free-stream velocity. With this point located it would be quite evident that the square data points (equation (7)) in figure 12(e), for instance, could not represent the correct curve, and that equation (8) should be used to obtain additional points to provide a reasonable guide. The technique of fairing a curve, through calculated drop-acceleration values, to a value of zero acceleration at the extreme position of drop impingement can be used also for the lower surface of airfoils; but the technique can be applied only in those instances where the airfoil angle of attack is sufficiently low to permit a straight-line trajectory to impinge tangentially at some point on the airfoil surface.

Summary of calculation of scale modulus ψ : The two preceding subsections have shown how the terms in equation (4) can be evaluated to obtain values of ψ for selected R_V values at chosen positions on the airfoil surface. However, a special procedure for evaluating ψ at the stagnation point is necessary, since equation (4) cannot be used to evaluate the scale modulus at or very near the stagnation point. This procedure is more suitably discussed in connection with the section on rate of impingement which follows.

For a further verification of the calculation of scale modulus, appendix A includes a comparison of results of empirical calculations of farthest position of impingement with results obtained from formal solutions of the trajectory equations for five airfoils.

Generalization in regard to rate of impingement.- Another quantity of interest to the designer of an aircraft thermal-ice-prevention system is rate of drop impingement on an airfoil. An expression for weight rate of drop impingement per unit length of span, according to reference 7, is given by

$$M_S = 3600 V m \Delta y_{o_t}' \tag{9}$$

In order to evaluate the rate of impingement M_S, the term $\Delta y_{o_t}'$ must be known. When methods like those of references 3, 5, and 6 are employed, $\Delta y_{o_t}'$ can be determined directly from the calculated trajectories which impinge tangentially upon the airfoil. For an empirical procedure where no trajectories are available, however, determination of $\Delta y_{o_t}'$ must be based upon quantities which are known. Preceding sections have shown that $(s/c)_{u_t}$ and $(s/c)_{l_t}$ can be established as a function of ψ for various values of R_V; hence, the airfoil ordinates corresponding to the farthest position of drop impingement on the upper and lower surfaces y_{u_t} and y_{l_t} also can be ascertained as a function of ψ for various values of R_V. Because values of y_{u_t} and y_{l_t} can be obtained readily for a wide range of ψ and R_V values, the data were examined for a relationship involving Δy_{o_t} (for small angles of attack, Δy_{o_t} is approximately equal to $\Delta y_{o_t}'$) and the quantity $y_{u_t} - y_{l_t}$ which will be called Δy_t. In this regard, Δy_{o_t} was compared to Δy_t over the range of ψ and R_V values presented in tables I through V for the five airfoil cases. The results are shown in figure 13.

An inspection of figure 13 shows that, for each airfoil, the ratio of Δy_{o_t} to Δy_t can be considered linear with respect to the log of the scale modulus ψ for various R_V values. The linearity exists for values of $(\Delta y_o/\Delta y)_t \leq 0.8$ for the Joukowski airfoils, and a value of $(\Delta y_o/\Delta y)_t \leq 0.9$ for the NACA 65_2-015 airfoil; but this linearity appears to be characteristic only of airfoils as cylinder data from reference 6, when plotted in the same manner, do not show this property. In figures 13(c) and (e), the ratio noticeably exceeds unity, the reason being that the projected frontal height h (equal to $\Delta y_{o_t}'$ for the limiting case of straight-line trajectories) exceeds the airfoil maximum thickness when the airfoil

angle of attack is other than zero. Of special interest in figure 13, however, is the fact that the ratio $(\Delta y_0 / \Delta y)_t$ must become zero at some particular value of ψ for a given value of R_V. This "critical" value of ψ can be calculated from an aerodynamic property of the airfoil. According to reference 6, for symmetrical bodies at zero angle of attack, the critical value of ψ (i.e., values greater than that for which no drops impinge on the body) is given by

$$\psi_{cr} = 4R_V \left. \frac{\partial(u_a/V)}{\partial x} \right|_{\psi=0} \qquad (10)$$

For symmetrical bodies at an attitude other than $0°$, or for unsymmetrical bodies at an arbitrary attitude, the same form of equation (10) applies, but with the notation slightly altered, thus

$$\psi_{cr} = 4R_V \left. \frac{\partial(U_a/V)}{\partial S} \right|_{\psi=0} \qquad (11)$$

This change is made because the small drop which just impinges at the stagnation point of the airfoil closely follows the stagnation streamline which, in the general case, is not a straight line. For simplicity, though, equation (11) shall be written

$$\psi_{cr} = 4R_V G \qquad (12)$$

In order to use equation (12), the problem presents itself of assigning a value of G for the case of an aribtrary airfoil. Fortunately, the problem is relieved by the fact that the answers sought, s/c and E, are effected only in a minor way by variations in G.[4] Thus, it was believed that for determining G the airfoil could be replaced by a shape more amenable to calculation. It was assumed that a symmetrical Joukowski airfoil would be representative of that type section having maximum thickness fairly well forward, and an ellipse representative of that type section having maximum thickness well aft (low-drag airfoils). Since the major factors influencing the value of G are thickness and angle of attack,

---

[4]Calculations have shown that negligible changes in s/c and E are incurred for a change in G as large as 10 percent.

calculations of G were made for a symmetrical Joukowski airfoil and an ellipse of different thickness and lift coefficients.[5] The results of these calculations are presented in figure 14. The data in 14(a) are intended for use with airfoils resembling Joukowski airfoils, and may be used directly. The data in figure 14(b) are intended for use with low-drag profiles; however, it is first necessary to establish an "equivalent ellipse" thickness ratio for the low-drag section being used. An equivalent ellipse is defined for the purposes of figure 14(b) as an ellipse having its leading-edge radius equal to the leading-edge radius of the airfoil, and a thickness equal to the airfoil maximum thickness. The major axis of the ellipse is thus established, and the ellipse thickness ratio can be computed. An equation expressing the thickness ratio of the equivalent ellipse in terms of the airfoil leading-edge radius and thickness ratio is:

$$t_e = \frac{2\rho}{t_{max}} \tag{13}$$

With the aid of figure 14, the value of ψ_{cr} for a large number of airfoils can be estimated for any R_V value in accordance with equation (12). Not only does this value correspond to the condition of zero rate of impingement, but it corresponds to the condition of zero area of impingement. Hence, the critical value of ψ can be used for obtaining an additional point for area of impingement computations, and this value will correspond to the s/c value at the stagnation point.

While the condition of no drops impinging on the airfoil surface yields one point on the curves, $(\Delta y_o/\Delta y)_t$ versus log ψ, at least one more point is required for each value of R_V in order to establish the linear relationships observed in figure 13. To locate a second point on an isopleth of R_V, it is desirable to determine a value of ψ corresponding to a chosen value of $(\Delta y_o/\Delta y)_t$ somewhat less than unity. The reason for this specification is to procure a spread in the values of $(\Delta y_o/\Delta y)_t$ used to establish the linear relationships between $(\Delta y_o/\Delta y)_t$ and log ψ, for isopleths of R_V which were noted in figure 13.

---

[5]No account is taken of the effect of a cambered profile on the velocity gradient G. The reason for this is that tests with an electrolytic tank have shown that the effects of camber are very small in comparison with the effects of thickness, and calculations have shown that only large variations in G are important in affecting the values of s/c and E.

In developing a procedure for determining what value of ψ is associated with a specified value of $(\Delta y_o/\Delta y)_t$ on an isopleth of R_V, the data from the five airfoil cases were examined for values of some parameter, related to $(s/c)_{u_t}$ and $(s/c)_{l_t}$, which could be used to fix the value of ψ. The parameter used to supply the necessary values was the efficiency of drop impingement E. The relationship between E and $(\Delta y_o/\Delta y)_t$ is given by

$$E = \left(\frac{\Delta y_o}{\Delta y}\right)_t \left(\frac{\Delta y_t}{t_{max}}\right) \tag{14}$$

Equation (14) can be derived by starting from the definition of E in terms of the initial drop trajectory ordinates

$$E = \frac{\left(y_{o_u}{}' - y_{o_l}{}'\right)_t}{h} \times \frac{\Delta y_{o_t}{}'}{h} \tag{15}$$

At the small angles of attack associated with most flight conditions, h in equation (15) can be replaced by t_{max} and $\Delta y_{o_t}{}'$ by Δy_{o_t} so that

$$\Delta y_{o_t} = E t_{max} \tag{16}$$

Then, if both sides of equation (16) are divided by Δy_t and the terms rearranged, equation (14) is obtained.

The trajectory data for the five airfoil cases provided, for different values of R_V, relatively constant values of E corresponding to a value of[6] $(\Delta y_o/\Delta y)_t = 0.8$. These efficiency values were

---

[6]The procedure utilized was to determine from curves of $(\Delta y_o/\Delta y)_t$, as a function of ψ (fig. 13), the value of ψ at which $(\Delta y_o/\Delta y)_t = 0.8$ for different values of R_V. Then, data from tables I through V were used to establish curves of E as a function of ψ for the same values of R_V. On the efficiency curves, the value of E corresponding to $(\Delta y_o/\Delta y)_t = 0.8$ for a particular value of R_V could be determined by locating, for the same R_V value, the value of ψ which was established from curves of figure 13 to correspond to $(\Delta y_o/\Delta y)_t = 0.8$.

used to obtain an average efficiency value for each airfoil case.
Then, by using equation (14), an average value of $\Delta y_t/t_{max}$ could
be computed for each airfoil case by using the average efficiency
values and a value of $(\Delta y_o/\Delta y)_t = 0.8$. The results are presented
in the following table:

Case number	Efficiency of impingement, E (percent)								Average value for each case	$\dfrac{\Delta y_t}{t_{max}}$
	R_V									
	16	32	64	128	256	512	1024	2048		
I	– –	77.5	– –	77.0	– –	75.5	– –	78.0	77.0	0.963
II	76.0	– –	74.5	– –	75.5	– –	77.5	– –	75.8	.948
III	72.0	– –	73.0	– –	72.0	– –	70.5	– –	71.8	.898
IV	77.0	– –	82.0	– –	86.0	– –	82.0	– –	81.7	1.022
V	55.0	– –	59.0	– –	56.5	– –	55.0	– –	56.4	.705

The values of $\Delta y_t/t_{max}$ tabulated in the preceding table exhibit
some variation between airfoil cases, and figure 15 is presented to
show this variation when $\Delta y_t/t_{max}$ is assumed to be a function only of
angle of attack. In figure 15, a curve is presented for the Joukowski
airfoils, but not for the NACA 65_2-015 airfoil because the trajectory
data provides only one point. Until additional information is avail-
able on the variation of $\Delta y_t/t_{max}$ with angle of attack, it is recom-
mended that the variation shown in figure 15 be used. It is possible,
then, to determine, for a given value of R_V, an approximate value of
ψ at which $(\Delta y_o/\Delta y)_t = 0.8$. The procedure which may be used for
determining this value of ψ is shown graphically in figure 16. From
curves of $(s/c)_{u_t}$ and $(s/c)_{l_t}$ as a function of log ψ for a
specified value of R_V (fig. 16(a)), curves of y_{u_t} and y_{l_t} as a
function of log ψ are established for the same value of R_V
(fig. 16(b)). For the relation shown by figure 16(b), there is a
value of $\Delta y_t/t_{max}$ which is the same as the one chosen from the rela-
tion in figure 15 corresponding to the airfoil angle of attack. This
particular value of $\Delta y_t/t_{max}$ corresponds to the ψ value at which
$(\Delta y_o/\Delta y)_t = 0.8$ for the particular R_V value chosen (fig. 16(c)),
and the second point on an isopleth of R_V for $(\Delta y_o/\Delta y)_t$ as a
function of log ψ is thereby determined.

The previous discussion has shown how values of Δy_{o_t} may be obtained for various ψ and R_V values. However, in the design of a thermal ice-protection system, by the method discussed in reference 1, it is sometimes more convenient to determine the rate of water-drop impingement by using the airfoil collection efficiency E rather than by using the term $\Delta y_{o_t}'$. In such circumstances, equation (9) becomes

$$M_s = 3600 \, V_m \, E \, t_{max}$$

wherein E is given by equation (14). When equation (14) is used and the angle of attack is other than zero, the limit efficiency value corresponding to straight-line trajectories will be greater than unity because h usually is somewhat greater than t_{max}.

Appendix A includes a comparison of results of calculations of efficiency of impingement by the empirical method of this report with results obtained from formal solutions of the trajectory equations for the five airfoil cases.

Generalization in regard to distribution of impingement.— Of secondary importance in the design of heated wings is the distribution of water-drop impingement over the length of interception along the airfoil surface. However, knowledge of distribution of water drops over an airfoil is sometimes quite useful and, therefore, a discussion of the subject is believed worthwhile.

An examination of the trajectory data did not reveal any direct way to obtain an empirical functional relation between impingement distribution, scale modulus, and free-stream-drop Reynolds number. Therefore, a graphical construction was resorted to in order to approximate the distribution of drop impingement over an airfoil surface. That a graphical procedure could be used in this manner was found by examining plots of the concentration factor[7] C as a function of s/c for various combinations of ψ and R_V. Typical variations of these factors are presented in figure 17 calculated from data for the five airfoil cases. For each of the airfoil cases presented in figure 17, two curves represented by solid lines are shown. One curve is typical for combinations of ψ and R_V corresponding to curved trajectories, and the other curve is typical for the combination of ψ and R_V corresponding to straight-line trajectories ($\psi=0$, value of R_V arbitrary). The curve for $\psi=0$ is obtained by drawing a number of straight-line trajectories to the airfoil to obtain values of the concentration factor, $C = dA_o/dA_s$, and represents the locus of maximum possible values of C. This curve, which will be referred to as a limit curve, can always be obtained for a given airfoil because

---

[7]The use of the concentration factor C in the computation of heat requirement due to drop impingement is discussed in reference 1.

straight-line trajectories can always be reproduced, but the curves for
values of C less than maximum cannot be obtained because the shapes
of the curved trajectories corresponding to these values cannot be
determined. Because of the shape of the C distribution curves noted
for the five airfoil cases in figure 17, a triangular distribution
has been found useful to represent approximately the distribution
curves for curved trajectories. If a triangular distribution is
assumed, as shown by a dashed line for each of the airfoil cases, in
figure 17, the following equation may be written for the maximum value
of C on the triangular distribution:

$$\int_{s_{l_t}}^{s_{u_t}} C\,ds = \frac{1}{2}\,C_{max}\,(s_{u_t} + s_{l_t})$$

from which

$$C_{max} = \frac{\displaystyle\int_{s_{l_t}}^{s_{u_t}} C\,ds}{(s_{av})_t} \qquad (17)$$

The denominator of equation (17) can be evaluated from the curves of
farthest positions of tangential drop impingement. The numerator may
be evaluated from the equation

$$\int_{s_{l_t}}^{s_{u_t}} C\,ds = Eh \qquad (18)$$

so that

$$C_{max} = \frac{Eh}{(s_{av})_t} \qquad (19)$$

That the relation expressed in equation (18) exists can be shown
by recalling from equations (9) and (15) that the total weight rate of
drop impingement on an airfoil may be written as

$$M_s = 3600\,Vm\,Eh \qquad (20)$$

Equation (20) may also be written as the summation, between the farthest
positions of impingement, of the local weight rates of impingement per
unit surface area, thus

$$M_s = \int_{s_{l_t}}^{s_{u_t}} M_a \, ds \qquad (21)$$

According to reference 1, M_a in equation (21) can be expressed by

$$M_a = 3600 \, V_m C \qquad (22)$$

where

$$C = dA_o/dA_s \qquad (23)$$

By substitution of the value of M_a from equation (22) into equation (21), the result is obtained that

$$M_s = 3600 \, V_m \int_{s_{l_t}}^{s_{u_t}} C \, ds \qquad (24)$$

Then, by comparing equations (20) and (24), equation (18) can be obtained.

Use of equation (19) permits the calculation of C_{max} for a triangular distribution because all the terms of the right-hand member are known. The value of C_{max} is taken to be on a line connecting the points $C=1.0$, $s/c=0$, and $C=0$, and s/c for the stagnation point. The reason for this assumption is that the very large drops are very little deviated from their paths, and the very small drops tend to follow the stagnation streamline.

The value of C_{max} obtained from equation (19) always will be low. However, if the triangular approximation is altered to correspond more nearly to the shape of the limit curve for the C values, while retaining the enclosed area the same as the triangular area, more accurate concentration-factor values can be obtained. The altering of the curve is an attempt to establish the locus of concentration-factor values as it would be given by data obtained for calculated trajectories.

Generalization in regard to calculating area and efficiency of impingement at high subsonic speeds.— With the advent of airplanes in the 500 to 600 miles per hour speed range, considerable interest has been shown in the effects which compressibility may have on area and rate of drop impingement.

The differential analyzer computations for the five airfoil cases of this study were made to encompass airspeeds up to about 350 miles per hour on the basis that any effects of compressibility could be neglected. Consequently, no corrections to the velocity field were introduced for any of the airfoils to account for compressibility. However, for higher speeds, the effects of compressibility would be expected to become more pronounced and some method of taking compressibility into account should be considered.

The effects of compressibility: In compressible flow below the critical Mach number, streamlines at a large distance forward of the airfoil have nearly the same shape as for incompressible flow. Nearer the airfoil, deviations of the compressible flow streamlines from the incompressible flow streamlines are greater (reference 8). Thus, in compressible flow, drops may be considered to start at infinity at the same initial conditions as they would for incompressible flow, but terminate on the airfoil surface at velocities governed by the local compressible-flow surface-air velocities. These velocities are, in general, higher than corresponding incompressible-flow velocities; therefore, compressibility may have some effect on farthest position and efficiency of drop impingement.

If it is presumed that drops in compressible flow react to a change in surface-air velocities (due to changes in flow field arising from compressibility) in much the same manner as drops react to changes in flow field caused by a change in airfoil basic thickness, load distribution, or angle of attack, the same general procedure used to calculate farthest position and rate of impingement for incompressible flow can be applied to the calculations for compressible flow.

To obtain the air hodograph for compressible flow when experimental data are not available, the equation

$$\left(\frac{U_a}{V}\right)_M = \left[1 + \frac{1-(1 + 0.7025M^2 C_{P_M})^{0.2883}}{0.2025M^2}\right]^{1/2} \tag{25}$$

(taken from reference 9) may be used to evaluate the magnitude of the velocity vectors. The pressure coefficient, C_{P_M}, in equation (25) can be calculated using the Prandtl-Glauert equation

$$C_{P_M} = \frac{1}{\beta} \times C_p$$

where

$$\beta = \sqrt{1-M^2}$$

and C_p is the pressure coefficient at a point on the airfoil surface when the flow is incompressible. The pressure coefficient C_p is related to the surface-air velocity at the same point on the surface by the equation

$$C_p = 1 - \left(\frac{U_a}{V}\right)^2 \qquad (26)$$

Values of U_a/V used in equation (26) to calculate various values of C_p are the same as those used to establish the air hodograph for incompressible flow.

Effect of compressibility on the farthest position and efficiency of drop impingement: Because of incompressible-flow hodograph is altered to another shape for compressible flow, the drop hodograph also will be modified, utilizing the procedure developed for the incompressible case. The changes in the drop and air hodographs in turn alter the values of a_d and $(R/R_V)_t$ at points along the airfoil surface. According to equation (4), if changes in a_d and the product $(R/R_V)_t \, (C_d R/24)$ are not proportionate, the scale modulus will be altered for given $(s/c)_t$ and R_V values. To show the effect of compressibility on the scale modulus, some calculations of farthest position and efficiency of drop impingement were made for the 15-percent-thick Joukowski airfoil at zero lift and M=0.6 (which is near the critical value). A value of $R_V=225$ was chosen for the calculations (430 mph, 15,000 ft, 0° F, and drop diameter of 25 microns). The results of these computations are compared in figure 18 with empirical results for incompressible flow. Figure 18(a), which presents the farthest position of drop impingement as a function of scale modulus, shows that the scale modulus has been increased slightly over most of the range in $(s/c)_t$ for the isopleth of R_V chosen. This result is equivalent to the farthest position of impingement being increased from the value of $(s/c)_t$ corresponding to the same ψ and R_V value in incompressible flow. For the conditions chosen, the increase in farthest position of impingement is small and, for most practical purposes, may be neglected. Figure 18(b) shows that compressibility also slightly increases impingement efficiency. This result can be explained by equation (14) which indicates that increases in E are effected by increases in either the value of $(\Delta y_o/\Delta y)_t$ or Δy_t, or both. Increases in the values of both of these terms, for given ψ and R_V values, occur

for increased values of farthest position of impingement, and hence impingement efficiency is increased. The increase in efficiency due to compressibility for the same airfoil also is small and, like the increases in farthest position of drop impingement, may be neglected for most practical purposes. It should be noted, though, that the computations for farthest position and efficiency of impingement were made for a relatively low Mach number (0.6), and that somewhat larger changes in both parameters for given ψ and R_γ values may be possible for airfoils having appreciably higher critical Mach numbers. However, it is suggested that the empirical method as applied to compressible flow not be used for airfoil sections having high critical Mach numbers (0.9) in view of the fact that no data exist for giving validity to the extrapolation of the method of this report to compressible flow.

PROCEDURE FOR USING THE METHOD TO CALCULATE AREA,
RATE, AND DISTRIBUTION OF WATER-DROP
IMPINGEMENT ON AN ARBITRARY AIRFOIL

Previous sections have shown how the empirical method of this report may be applied to determine area, rate, and distribution of impingement for an arbitrary airfoil in either incompressible or compressible flow. The procedure to be followed in using the method will now be explained by means of an example of the computations in the case of an NACA 23015 airfoil, in incompressible flow, at $c_l = 0.5$. The detailed computation procedure in this example is arranged in a form believed to be most readily usable; and the various phases of the computations are presented in a step-wise manner, each phase consisting of several operations for ease in following the procedure. The procedure for compressible flow is nearly the same as for incompressible flow, hence, only the procedure for incompressible flow is illustrated. However, where differences in procedure would occur for the case of compressible flow, these are noted.

Area of Impingement

The procedure for calculating area of impingement consists primarily in determining values of $(s/c)_{u_t}$ and $(s/c)_{l_t}$. The following steps explain how the empirical relations derived from the trajectory data are used to determine these values, and figure 19 incorporates necessary accompanying graphical relationships.

Step 1: The following curves are needed for use during the computation procedure:

(a) A large-scale plot of the airfoil (fig. 19(a))

(b) A plot of s/c versus x for both upper and lower surfaces (fig. 19(b))

(c) A plot of k for various x positions (fig. 19(c))

(d) Chordwise distribution of incompressible-flow air velocities over the airfoil surface (fig. 19(d))

Step 2: Construction of the air hodograph:

(a) On a coordinate system using vertical air-velocity components as ordinates and horizontal velocity components as abscissas, measure values of air velocity as vectors emanating from the origin. (These values are obtained from the velocity distribution (fig. 19(d)) established in step 1(d)). The slope of the velocity vectors with respect to the horizontal axis is determined by the shape-factor curve established in step 1(c). Figure 19(e) illustrates this step for the NACA 23015 airfoil.

(b) Connect the end points of all vectors noting that the envelope curve (the hodograph) passes through the origin for the physical coordinates corresponding to the stagnation point. Refer to figure 19(e) for illustration.

(c) For compressible flow over a straight wing below the critical Mach number, compute the velocities for the air hodograph from

$$\left(\frac{U}{V} \right)_M = \left[1 + \frac{1-(1+0.7025M^2 c_{p_M})^{0.2883}}{0.2025M^2} \right]^{1/2}$$

Step 3: Construction of drop hodograph:

(a) From the hodograph established in step 2(b) (incompressible flow) or step 2(c) (compressible flow), note the maximum value of vertical air-velocity component $v_{a_{max}}/V$ for both upper and lower surfaces. For the NACA 23015 airfoil, the air hodograph shows that $v_{a_{max}}/V$ for

the upper surface is 0.915 and for the lower surface, 0.39.

(b) Using figure 10, determine the value of $(v_{a_{max}}/V) - (v_{d_{max}}/V)$
for both surfaces. A subtraction of $(v_{a_{max}}/V) - (v_{d_{max}}/V)$ from
$v_{a_{max}}/V$ will yield the vertical location of $v_{d_{max}}/V$. Project
$v_{d_{max}}/V$ horizontally for each surface until it intersects the ray
connecting the origin and $v_{a_{max}}/V$. In this manner, the value
of $(R/R_V)_t$ corresponding to $v_{a_{max}}/V$ is determined graphically.
In the case of the NACA 23015 airfoil, $(v_{a_{max}}/V) - (v_{d_{max}}/V)$ for
the upper surface is 0.245 and for the lower surface, 0.068.
These values are measured from the air hodograph (fig. 19(f))
to provide values of $(R/R_V)_t$ corresponding to upper and lower
surface values of $v_{a_{max}}/V$.

(c) Establish the vector passing through the origin and inclined
with the horizontal axis at an angle equal to the airfoil angle
of attack. The length of this vector is made equal to unity
(fig. 19(f)).

(d) For both airfoil surfaces, establish an approximate
tangential-trajectory hodograph which follows the equation

$$\frac{u_d}{V} = \left(\frac{u_d}{V}\right)_{v_{a_{max}}} \times \frac{u_a/V}{(u_a/V)_{v_{a_{max}}}} \qquad (27)$$

The hodograph determined by equation (27) for the upper
surface of the NACA 23015 airfoil is designated as curve A
in figure 19(g) and as curve B for the lower surface. When
equation (27) provides, for either the upper or lower surface,
a drop hodograph which fails to pass through the point
$u_d/V = \cos \alpha$, $v_d/V = \sin \alpha$ (point X in fig. 19(g)), a curve
should be faired from point X to connect tangentially with the
approximate drop hodograph as determined by equation (27).
In the example case, neither the upper nor lower surface
drop hodographs passes through point X, and therefore curves
are faired from this point to the approximate drop hodographs.
The faired curves are labeled C and D in figure 19(g) for the
upper and lower surfaces, respectively. For the upper surface,
the approximate drop hodograph almost passes through point X,
so little difficulty is experienced in fairing a connecting
curve. However, for the lower surface, the approximate drop
hodograph deviates considerably from point X leaving a larger
latitude for fairing a curve from this point than was the

case for the upper surface. In this instance, the contour
of the air hodograph was followed as a guide in fairing a
curve from point X to the approximate drop hodograph. The
combination of curves A and C for the upper surface, and
curves B and D for the lower surface, comprise the resultant
tangential-trajectory hodograph for each surface.

(e) Convert the x values used in the air hodograph of
figure 19(e) to s/c values by utilizing the relationship
in figure 19(b) between x and s/c. This step is shown
also in figure 19(g).

(f) Measure the values of $(R/R_V)_t$ as determined by the
drop and air hodographs in figure 19(g) and plot these
values against their corresponding s/c positions. This
step is performed in figure 19(h) for the upper and lower
surfaces of the NACA 23015 airfoil.

Step 4: Calculation of drop-acceleration values at the air-
foil surface.

(a) Use the air-velocity distribution over the airfoil
surface (fig. 19(d)) and the relation between x and s/c
(fig. 19(b)) to establish the relation required between
U_a/V and s/c for both upper and lower surfaces.
Equation (7) then can be used to calculate values for a_d.
Values obtained for a_d by equation (7) are plotted
against their respective surface positions s/c, and this
is done in figure 19(i) for the upper and lower surfaces
of the NACA 23015 airfoil.

(b) Include in the plot of a_d versus s/c (fig. 19(i))
the value of s/c at which a_d is zero on each surface.
The value of s/c at which a_d is zero corresponds to
the extreme position of tangential drop impingement on
the airfoil surface. For each surface, the extreme
position of drop impingement can be obtained by drawing
two straight-line trajectories in the free-stream direction,
one tangent to the airfoil upper surface and the other
tangent to the lower surface. The point of tangency for
each straight-line trajectory defines the s/c value
corresponding to an a_d value of zero. For the NACA 23015
airfoil at a lift coefficient of 0.5, the extreme position
of impingement on the upper surface is at s/c=23.0 and
on the lower surface, at s/c=53.0.

(c) For each surface, fair a curve through the calculated values of a_d to the value of s/c found in step 4(b) corresponding to a_d of zero. This step is also performed in figure 19(i). On the upper surface, values of a_d given by equation (7) were considered in error over a small range of s/c near the peak in the velocity distribution curve (fig. 19(d)), and consequently little weight was given the points in this region when extending the faired curve to $a_d=0$ at the extreme position of drop impingement. A few additional points can be calculated by equation (8) to aid in the fairing of the drop-acceleration curve, but since in this example the extreme position of impingement is fairly far forward ($s/c = 23.0$) and equation (7) will yield positive a_d values for s/c values as far aft as 11 percent, use of equation (8) was deemed unnecessary.

Step 5: Computation of scale moduli corresponding to arbitrarily selected values of farthest position of impingement.

(a) Using drop-acceleration values obtained from figure 19(i) of step 4 and $(R/R_V)_t$ values from figure 19(h) of step 3, calculate values of scale modulus ψ from equation (4). The computations are made for arbitrarily selected values of R_V and s/c. Values of $C_d R/24$ required for solving equation (4) can be obtained from interpolation of the data presented in table VI, or preferably from a semi-logarithmic plot of the data. A small range of tabulated $C_d R/24$ values, including the values involved in the computation of ψ for the NACA 23015 airfoil is shown graphically in figure 19(j). The computations of ψ for the NACA 23015 airfoil are shown in the following table:

				CALCULATION OF SCALE MODULI FOR CHOSEN AREAS OF IMPINGEMENT AND DIFFERENT R_V VALUES			
				$R_V=10$			
s/c	a_d	$a_d R_V$	$(R/R_V)_t$	R	$\dfrac{C_d R}{24}$	$\left(\dfrac{R}{R_V}\right)_t \times \dfrac{C_d R}{24}$	ψ
				UPPER SURFACE			
5	8.6	86	0.365	3.65	1.42	.518	166
10	2.8	28	.405	4.05	1.45	.586	48
15	1.0	10	.412	4.12	1.46	.600	17
20	.2	2	.405	4.05	1.45	.586	4
				LOWER SURFACE			
5	2.7	27	0.10	1.0	1.17	0.117	231
10	1.0	10	.12	1.2	1.20	.144	70
20	.6	6	.10	1.0	1.17	.117	51
30	.35	3.5	.085	.85	1.14	.097	36
40	.17	1.7	.072	.72	1.13	.081	21
45	.10	1.0	.070	.70	1.12	.078	13
				$R_V=100$			
				UPPER SURFACE			
5	8.6	860	0.365	36.5	2.88	1.05	819
10	2.8	280	.405	40.5	3.00	1.21	230
15	1.0	100	.412	41.2	3.02	1.24	80
20	.2	20	.405	40.5	3.00	1.21	16
				LOWER SURFACE			
5	2.7	270	0.10	10	1.80	0.180	1500
10	1.0	100	.12	12	1.90	.228	439
20	.6	60	.10	10	1.80	.180	333
30	.35	35	.085	8.5	1.72	.146	240
40	.17	17	.072	7.2	1.64	.118	144
45	.10	10	.070	7.0	1.63	.114	88

Step 6: Establishing the curves of farthest position of impingement.

(a) Plot the values of ψ calculated in step 5 against the corresponding values of s/c as ordinates for isopleths

of R_V. Use a semilogarithmic scale, plotting the ordinates arithmetically. This is done for the NACA 23015 airfoil in figure 19(k).

(b) On the plots of s/c begun in step 6(a), denote by lines drawn at constant s/c values the value of extreme position of drop impingement on each upper and lower surface. For the NACA 23015 airfoil, at a lift coefficient of 0.5, the extreme positions of impingement have been found in step 4(b) as being at $s/c=23.0$ on the upper surface, at $s/c=53.0$ on the lower surface.

(c) Calculate from equation (12) the critical-scale modulus value for each isopleth of R_V. The value of G required to evaluate equation (12) for either incompressible or compressible flow can be obtained from figure 14. The value of Ψ_{cr} calculated for a given value of R_V corresponds to s/c at the stagnation point. Values of Ψ_{cr} calculated from equation (12) for different values of R_V also should be plotted on the graph of farthest position of impingement (fig. 19(k)) begun in step 6(a). Since the NACA 23015 airfoil can be considered to have the same type of profile as Joukowski airfoils, figure 14(a) is used to obtain a value of G for evaluating equation (12). For a value of $c_l=0.5$ and a thickness ratio of 0.15, figure 14(a) shows the value of G to be 37.5. When this value of G is used in equation (12), Ψ_{cr} has the following values:

R_V	Ψ_{cr}
10	1500
100	15000

(d) For each isopleth of R, fair a curve through the values of s/c plotted in steps 6(a) and 6(c) (fig.19(k)). These curves should approach asymptotically, as a limiting value, the farthest position of drop impingement for the upper and lower airfoil surfaces. Figure 19(k) then may be used for design purposes by determining the values of $(s/c)_u$ and $(s/c)_l$ for particular values of Ψ and R_V.

Rate of Impingement

The procedure for the determination of the total rate of impinge-ment, as has been explained in reference 1, consists of summing the rate of water-drop impingement for each of the drop sizes in an assumed

drop-size distribution. This is possible for each size of drop by use of the equation:

$$M_s = 3600 \ EV \ my_{max}$$

The values of V, m, and y_{max} are directly obtainable from a knowledge of the nature of the icing conditions and the airfoil shape. The procedure for calculating efficiency of impingement consists essentially of evaluating equation (14). The following steps explain how the empirical relationships derived from the trajectory data are used to solve equation (14), and figure 20 is presented to show the necessary accompanying graphical relationships.

Step 1.— The following relationship should be established for use during the computational procedure: s/c as a function of y/c for both upper and lower surfaces. This relationship is shown for the NACA 23015 airfoil in figure 20(a).

Step 2.—Establishing $(\Delta y_o/\Delta y)_t$ as a function of ψ for isopleths of R_V.

(a) Using the farthest position of impingement curves (fig. 19(k)), establish the airfoil ordinates at points of tangential drop impingement as a function of $\log \psi$ for isopleths of R_V. This is done in figure 20(b) for the NACA 23015 airfoil for R_V values of 10 and 100.

(b) On the curves established in figure 20(b), establish the values of ψ at which $(\Delta y_o/\Delta y)_t = 0.8$. This can be done by using figure 15 which provides, for different angles of attack, values of $\Delta y_t/t_{max}$ corresponding to the value of $(\Delta y_o/\Delta y)_t = 0.8$. For the NACA 23015 airfoil (assuming the NACA 23015 airfoil to be similar in profile to the Joukowski airfoils), figure 15 gives $\Delta y_t/t_{max} = 0.9$ at $\alpha = 3.6^\circ$. This value can be used in figure 20(b) to determine the values of ψ corresponding to $(\Delta y_o/\Delta y)_t = 0.8$, by locating the ψ values at which $\Delta y_t = 0.9 t_{max}$. For the NACA 23015 airfoil, these ψ values in figure 20(b) are taken to be:

R_V	ψ
10	28
100	130

(c) Construct a semilogarithmic plot, assigning values of scale moduli as abscissas (logarithmic scale) and values of $(\Delta y_0 / \Delta y)_t$ as ordinates (arithmetic scale). Then, for each particular chosen value of R_V, plot the values of ψ_{cr} corresponding to a value of $(\Delta y_0 / \Delta y)_t = 0$ and also the values of ψ corresponding to a value of $(\Delta y_0 / \Delta y)_t = 0.8$. This is done in figure 20(c) for the NACA 23015 airfoil. In figure 20(c), the values of ψ_{cr} are denoted by circles and the values of ψ at $(\Delta y_0 / \Delta y)_t = 0.8$ are denoted by squares.

(d) Using the points plotted in step 2(c), connect with a straight line each pair of points having the same R_V value. This procedure establishes $(\Delta y_0 / \Delta y)_t$ as a function of ψ for isopleths of R_V and is illustrated in figure 20(c) for the NACA 23015 airfoil. The curves in figure 20(c) have been extrapolated to approach a limit value of $(\Delta y_0 / \Delta y)_t = 1.13$ which corresponds to $h/t_{max} = 1.09$ for straight-line tangential trajectories.

Step 3.—Calculation of impingement efficiency:
(a) Equation (14) now is used to calculate impingement efficiency for various ψ and R_V values. To evaluate equation (14) for a selected value of R_V, record values of $(\Delta y_0 / \Delta y)_t$ for arbitrary values of ψ from the relationship (fig. 20(c)) established in step 2(c). For the same ψ values, obtain corresponding Δy_t values directly from the curves established (fig. 20(b)) in step 2(c).

(b) Plot the values of E obtained in (a) above against the corresponding values of scale modulus in isopleths of R_V. A semilogarithmic scale is recommended, with values of E being plotted as ordinates on the arithmetic scale (fig. 20(d)). Figure 20(d) then may be used for design purposes by determining values of E for particular values of ψ and R_V.

Distribution of Impingement

Distribution of impingement is considered defined, as explained in reference 1, when values of the concentration factor C are determined over the region of drop impingement. The empirical procedure consists first of evaluating distribution of impingement for straight-line trajectories. By establishing the distribution of impingement for straight-line trajectories, a limit curve (the locus of maximum values of C) is obtained which can be used as a guide modifying an approximate distribution for the particular trajectories of interest. Figure 21 is presented to illustrate the steps involved for the NACA 23015 airfoil. These steps are subsequently described.

Step 1.—Impingement distribution on an airfoil caused by straight—line trajectories (the limit curve).

(a) To determine the impingement distribution on an airfoil for straight—line trajectories, the procedure is to plot the airfoil contour and draw several straight—line trajectories, in a streamwise direction, so that they impinge upon the airfoil. The two tangential trajectories should be included. This procedure is illustrated in figure 21(a) for the NACA 23015 airfoil.

(b) For each trajectory appearing in the plot made in (a), note the trajectory starting ordinates and the corresponding positions of impingement, s/c. Plot these values, using position of impingement s/c as abscissas, and fair a curve through the points (fig. 21(b)).

(c) Establish concentration factor values for arbitrarily selected values of position of impingement by obtaining the slope, at various points, of the curve plotted in (b). A plot of these concentration factor values against position of impingement values yields the limit curve corresponding to straight—line trajectories. Note that the maximum value is always unity at the airfoil leading edge, and the minimum values are zero at the extreme position of tangential drop impingement.

Step 2.—Determining impingement distribution for an arbitrary value of scale modulus and free—stream Reynolds number.

(a) Calculate a maximum value of concentration factor from equation (19). Values of s/c and E needed to evaluate this equation for a selected value of R_V and various values of ψ may be obtained from efficiency and farthest position of impingement curves already established. For the NACA 23015 airfoil, the value of C_{max} becomes

$$C_{max} = \frac{Eh}{(s_{av})_t} = \frac{(0.75)(0.164)}{1/2(0.135+0.45)} = 0.42$$

for a value of $\psi = 100$ and a value of $R_V = 100$.

(b) Plot the value of C_{max} obtained in (a) against position of impingement, s/c. Assume that C_{max} lies on a straight line connecting the points $C=1.0$, $s/c=0$, and $C=0$ for s/c at the stagnation point. See figure 21(c).

(c) Using the value of C_{max} obtained in step (b), form a triangular distribution of drop impingement by drawing straight lines from the point C_{max} to the points $(s/c)_{u_t}$, C=0 and $(s/c)_{l_t}$, C=0. This step is also illustrated in figure 21(c).

(d) Modify the triangular distribution established in (c) to conform to the general shape of the distribution curve established in step 1(c) for straight-line trajectories. In performing this modification, the value of C_{max} is usually increased such that the new curve contains the same area as did the triangular distribution. The modified curve is shown in figure 21(c) for a particular combination of ψ and R_V. For other combinations of ψ and R_V that may be needed for design purposes, other figures similar to figure 21(c) would have to be constructed.

EVALUATION OF THE EMPIRICAL METHOD
DEVELOPED IN THIS REPORT

The degree to which the final values of farthest position and efficiency of drop impingement as calculated herein depend upon the accuracy of determination of the intermediate quantities $(R/R_V)_t$, a_d, and G was investigated by determining the effect of arbitrarily altering these three quantities a given percentage. With this procedure, the effect on farthest position and efficiency of impingement can be appraised for the selected changes in the three variables; also, some concept can be gained of the approximate error in the empirical method itself. When computations were made for the 15-percent-thick symmetrical Joukowski airfoil at $\alpha = 4^0$, and the values of $(R/R_V)_t$, a_d, and G were altered by ±10 percent in all possible combinations, it was found for farthest position of impingement that in no case was changing G significant. The combination of positive and negative changes providing the largest change in ψ resulted in a change in s/c of about 2-percent chord over most of the range in values of ψ. The empirical method contributed an additional change of only about 1/2-percent chord. For efficiency of impingement, the effect of a change in the term G alone was to make a change in efficiency of about 0.5 percent; the combination of positive and negative changes in $(R/R_V)_t$ and a_d providing maximum change in ψ made a change in efficiency of about 3 percent over most of the range in ψ values. As compared with these changes, the approximations of the empirical method led to efficiency of impingement values which differed from the differential analyzer values by about -15 percent.

While the foregoing values will not be necessarily representative for all other airfoils, they nevertheless seem to indicate the order of magnitude of error in area and efficiency of impingement to be expected when the error in the terms $(R/R_V)_t$, a_d, and G can be kept within ±10 percent. Whether this sort of accuracy always can be realized by using the procedures suggested in this report can be ascertained only as more water-drop trajectory data become available.

CONCLUDING REMARKS

Results of water-drop trajectory data obtained from a differential analyzer have provided a basis for the initial development of a general method for empirically determining area, rate, and distribution of water-drop impingement on airfoil sections of arbitrary profile. The method, as applied to the incompressible-flow regime, is more firmly established for airfoils resembling the Joukowski airfoils investigated than for low-drag airfoils, since the basic data were obtained for four Joukowski airfoil cases and only one low-drag section. Because the differential analyzer data were obtained only for cases involving incompressible flow, the method as applied to compressible flow will not provide area and rate-of-impingement data having as much validity as the data for incompressible flow. There is no doubt that further water-drop trajectory data are needed, particularly for thin airfoils (order of 5-percent thick) at high speeds, and airfoils at high angle of attack (in the neighborhood of 12°). Whether these new data would revise the procedure presented herein, replace it, or substantiate it remains to be seen. Until such data are available, however, the method of this report should provide more complete and accurate information on the rate, area, and distribution of water-drop impingement on an arbitrary airfoil than any other known empirical means.

Ames Aeronautical Laboratory,
     National Advisory Committee for Aeronautics,
          Moffett Field, Calif., May 8, 1951.

APPENDIX A

COMPARISON OF RESULTS OF EMPIRICAL CALCULATIONS OF
FARTHEST POSITION AND EFFICIENCY OF IMPINGEMENT
WITH RESULTS OBTAINED FROM FORMAL SOLUTIONS OF
TRAJECTORY EQUATIONS FOR SIX AIRFOILS

After a new design method has been developed based on a limited
amount of data, it is desirable, but not always possible, to evaluate
the accuracy of the method by applying it to cases where checks on the
method exist. Unfortunately, in this investigation no experimental data
exist and very little calculated data are available on water-drop trajec-
tories beyond that reported herein. However, there is some justification
for checking the results of this method against the more accurate calcu-
lations for the five airfoil cases since these data (except for distri-
bution of impingement) were used only to establish a procedure which,
when applied, would not necessarily yield the same values for area and
percent impingement as the data. Consequently, the empirical relation-
ships just established were applied to the five airfoil cases, and
values of farthest position and efficiency of impingement were then
obtained and compared with the results of the differential analyzer
study. These comparisons for farthest position and efficiency of im-
pingement are shown in figures 22 and 23, respectively. In addition, a
comparison is made in figures 24 and 25 for a 12-percent-thick Joukowski
airfoil computed by the method of reference 3, and also by the method of
this report.

In examining figures 22 and 24, which compare farthest position of
impingement values, it can be seen that the calculated points compare
fairly well with curves obtained as a result of formal solutions of the
trajectory equations. A favorable comparison also appears to exist in
the case of efficiency of impingement, as is shown by the curves in fig-
ures 23 and 25. Discrepancies exist, but these may be expected in view
of the empirical relations used as a basis for the computations. It
will be noticed that values of farthest position of impingement were not
obtained for values approaching the limit position of drop impingement
on upper and lower surfaces. This omission is due to the fact that the
values of drop acceleration approach zero as the farthest position of
impingement approaches the limit values on both upper and lower surfaces.
As a result, scale moduli corresponding to these positions of impinge-
ment are difficult to obtain accurately because a small error in drop
acceleration makes a large error in scale modulus. For all practical
purposes, though, inability to calculate points near the limit values
makes little difference because the conditions in this range are seldom
realized in flight.

Since the empirically calculated values for both farthest position and efficiency of impingement are in reasonable agreement with the theoretical values, it appears to be justifiable to presume that calculations can be made with reasonable accuracy for other airfoils, at least in the same angle-of-attack range. Extension to other airfoils of the method using the hodograph technique tacitly includes the assumption that the vertical components of the tangential drop velocities bear the same relation to the maximum vertical velocities of the air as established in figure 10 for the five airfoils of this study.

REFERENCES

1. Neel, Carr B., Bergrun, Norman R., Jukoff, David, and Schlaff, Bernard A.: The Calculation of the Heat Required for Wing Thermal Ice Prevention in Specified Icing Conditions. NACA TN 1472, 1947.

2. Patterson, D. M.: A Simplified Procedure for the Determination of Heat Requirements for Ice Protection of Fixed Areas of Aircraft. Central Air Documents Office, Technical Data Digest, vol. 14, no. 4, 15 February 1949, pp. 15-23.

3. Bergrun, Norman R.: A Method for Numerically Calculating the Area and Distribution of Water Impingement on the Leading Edge of an Airfoil in a Cloud. NACA TN 1397, 1947.

4. Neel, Carr B., Jr.: Calculation of Heat Required for Wing Thermal Ice Prevention in Specified Icing Conditions. S.A.E. Quarterly Transactions, vol. 2, no. 3, July 1948, pp. 369-378.

5. Guibert, A. G., Janssen, E., and Robbins, W. M.: Determination of Rate, Area, and Distribution of Impingement of Waterdrops on Various Airfoils from Trajectories Obtained on the Differential Analyzer. NACA RM 9A05, 1949.

6. Langmuir, Irving, and Blodgett, Katherine B.: A Mathematical Investigation of Water Droplet Trajectories. General Electric Co. Rep., 1945. (Also available as Army Air Forces Tech. Rep. No. 5418, Feb. 1946, and as Dept. of Commerce Pub. P. B. No. 27565.)

7. Glauert, Muriel: A Method of Constructing the Paths of Raindrops of Different Diameters Moving in the Neighborhood of (1) a Circular Cylinder, (2) an Aerofoil, Placed in a Uniform Stream of Air; and a Determination of the Rate of Deposit of the Drops on the Surface and the Percentage of Drops Caught. R.&M. No. 2025, British A.R.C., 1940.

8. Stack, John: Compressible Flows in Aeronautics. Jour. Aero. Sci., vol. 12, no. 2, April 1945, pp. 127-148.

9. Allen, H. Julian, and Nitzberg, Gerald E.: The Effect of Compressibility on the Growth of the Laminar Boundary Layer on Low-Drag Wings and Bodies. NACA TN 1255, 1947.

TABLE I.— RESULTS FROM DIFFERENTIAL ANALYZER STUDIES OF WATER–DROP
IMPINGEMENT ON A 15–PERCENT–THICK SYMMETRICAL JOUKOWSKI AIRFOIL

$$[c_l=0; \ \alpha=0^\circ]$$

Figure number	ψ	R_V	y_0	Surface	s/c	u_d/V	v_d/V
1(a)	2	128	0.074	Upper[1]	0.265	1.0	0
1(a)	2	128	−.074	Lower[1]	−.265	1.0	0
1(b)	8	512	.074	Upper[1]	.273	.997	.004
1(b)	8	512	−.074	Lower[1]	−.273	.997	−.004
1(c)	32	2048	.072	Upper[1]	.262	.997	.013
1(c)	32	2048	−.072	Lower[1]	−.262	.997	−.013
1(d)	4	32	.073	Upper[1]	.273	1.0	.012
1(d)	4	32	−.073	Lower[1]	−.273	1.0	−.012
1(e)	16	128	.070	Upper[1]	.244	1.005	.023
1(e)	16	128	.045	Upper	.068	.99	.013
1(e)	16	128	.020	Upper	.021	.982	.009
1(e)	16	128	−.020	Lower	−.021	.982	−.009
1(e)	16	128	−.045	Lower	−.068	.99	−.013
1(e)	16	128	−.070	Lower[1]	−.244	1.005	−.023
1(f)	64	512	.0655	Upper[1]	.225	1.004	.043
1(f)	64	512	−.0655	Lower[1]	−.225	1.004	−.043
1(g)	256	2048	.058	Upper[1]	.188	1.007	.092
1(g)	256	2048	.040	Upper	.058	.949	.069
1(g)	256	2048	.020	Upper	.023	.931	.029
1(g)	256	2048	−.020	Lower	−.023	.931	−.029
1(g)	256	2048	−.040	Lower	−.058	.949	−.069
1(g)	256	2048	−.058	Lower[1]	−.188	1.007	−.092
1(h)	8	8	.059	Upper[1]	.197	.994	.078
1(h)	8	8	−.059	Lower[1]	−.197	.994	−.078
1(i)	32	32	.056	Upper[1]	.185	.992	.089
1(i)	32	32	−.056	Lower[1]	−.185	.992	−.089
1(j)	128	128	.0485	Upper[1]	.150	.989	.149
1(j)	128	128	−.0485	Lower[1]	−.150	.989	−.149
1(k)	512	512	.038	Upper[1]	.108	.941	.225
1(k)	512	512	−.038	Lower[1]	−.108	.941	−.225
1(l)	2048	2048	.025	Upper[1]	.072	.856	.349
1(l)	2048	2048	−.025	Lower[1]	−.072	.856	−.349
1(m)	64	8	.0255	Upper[1]	.078	.870	.321
1(m)	64	8	.018	Upper	.031	.693	.192
1(m)	64	8	.008	Upper	.010	.698	.061
1(m)	64	8	−.008	Lower	−.010	.698	−.061
1(m)	64	8	−.018	Lower	−.031	.693	−.192

[1]Denotes tangential trajectories.

TABLE I.— CONCLUDED

Figure number	ψ	R_V	y_o	Surface	s/c	u_d/V	v_d/V
1(m)	64	8	−0.0255	Lower[1]	−0.078	0.870	−0.321
1(n)	256	32	.021	Upper[1]	.073	.828	.359
1(n)	256	32	−.021	Lower[1]	−.073	.828	−.359
1(o)	1024	128	.015	Upper[1]	.052	.741	.451
1(o)	1024	128	.010	Upper	.020	.572	.198
1(o)	1024	128	.005	Upper	.009	.563	.109
1(o)	1024	128	−.005	Lower	−.009	.563	−.109
1(o)	1024	128	−.010	Lower	−.020	.572	−.198
1(o)	1024	128	−.015	Lower[1]	−.052	.741	−.451
1(p)	4096	512	.0110	Upper[1]	.038	.584	.452
1(p)	4096	512	−.0110	Lower[1]	−.038	.584	−.452
1(q)	16384	2048	.004	Upper[1]	.022	.329	.469
1(q)	16384	2048	−.004	Lower[1]	−.022	.329	−.469
1(r)	512	8	.0035	Upper[1]	.023	.355	.514
1(r)	512	8	−.0035	Lower[1]	−.023	.355	−.514
1(s)	8192	128	.0020	Upper[1]	.015	.251	.401
1(s)	8192	128	−.0020	Lower[1]	−.015	.251	−.401
1(t)	32768	512	.0005	Upper[1]	.016	.187	.459
1(t)	32768	512	−.0005	Lower[1]	−.016	.187	−.459

[1]Denotes tangential trajectories.

TABLE II.— RESULTS FROM DIFFERENTIAL ANALYZER STUDIES OF WATER–DROP
IMPINGEMENT ON A 15–PERCENT–THICK SYMMETRICAL JOUKOWSKI AIRFOIL

$$[c_l = 0.22, \quad \alpha = 2°]$$

Figure number	ψ	R_V	y_o	Surface	s/c	u_d/V	v_d/V
2(a)	4	256	—0.0046	Upper[1]	0.236	1.001	0.041
2(a)	4	256	—.1548	Lower[1]	—.316	.998	.035
2(b)	16	1024	—.0055	Upper[1]	.223	1.003	.044
2(b)	16	1024	—.1539	Lower[1]	—.310	.998	.030
2(c)	2	16	—.0081	Upper[1]	.226	1.009	.053
2(c)	2	16	—.1533	Lower[1]	—.311	.997	.027
2(d)	8	64	—.0095	Upper[1]	.212	1.011	.062
2(d)	8	64	—.0381	Upper	.045	.983	.054
2(d)	8	64	—.0667	Upper	.005	.984	.044
2(d)	8	64	—.0956	Lower	—.026	.974	.039
2(d)	8	64	—.1243	Lower	—.082	.972	.033
2(d)	8	64	—.1532	Lower[1]	—.308	.997	.022
2(e)	32	256	—.0140	Upper[1]	.196	1.015	.083
2(e)	32	256	—.0410	Upper	.041	.980	.066
2(e)	32	256	—.0683	Upper	.003	.969	.052
2(e)	32	256	—.0958	Lower	—.026	.970	.038
2(e)	32	256	—.1232	Lower	—.078	.975	.024
2(e)	32	256	—.1508	Lower[1]	—.295	.995	.013
2(f)	128	1024	—.0214	Upper[1]	.168	1.021	.126
2(f)	128	1024	—.0464	Upper	.034	.958	.100
2(f)	128	1024	—.0721	Upper	.002	.941	.063
2(f)	128	1024	—.0977	Lower	—.027	.939	.032
2(f)	128	1024	—.1231	Lower	—.079	.955	.004
2(f)	128	1024	—.1488	Lower[1]	—.265	.992	—.008
2(g)	16	16	—.0435	Upper[1]	.149	1.010	.160
2(g)	16	16	—.1598	Lower[1]	—.245	.984	—.023
2(h)	64	64	—.0493	Upper[1]	.128	1.012	.202
2(h)	64	64	—.0705	Upper	.027	.908	.140
2(h)	64	64	—.0902	Lower	—.001	.881	.083
2(h)	64	64	—.1130	Lower	—.027	.881	.033
2(h)	64	64	—.1345	Lower	—.071	.921	—.013
2(h)	64	64	—.1558	Lower[1]	—.225	.983	—.052
2(i)	256	256	—.0587	Upper[1]	.100	.999	.283
2(i)	256	256	—.0763	Upper	.022	.852	.189
2(i)	256	256	—.0940	Lower	—.002	.827	.103
2(i)	256	256	—.1118	Lower	—.023	.815	.015

[1]Denotes tangential trajectories.

TABLE II.— CONCLUDED

Figure number	ψ	R_V	y_0	Surface	s/c	u_d/V	v_d/V
2(i)	256	256	-0.1298	Lower	-0.058	0.863	-0.050
2(i)	256	256	-.1475	Lower[1]	-.177	.963	-.105
2(j)	1024	1024	-.0743	Upper[1]	.063	.914	.424
2(j)	1024	1024	-.1360	Lower[1]	-.118	.902	-.195
2(k)	128	16	-.0955	Upper[1]	.055	.881	.472
2(k)	128	16	-.1065	Upper	.009	.640	.235
2(k)	128	16	-.1160	Lower	-.004	.637	.113
2(k)	128	16	-.1250	Lower	-.017	.642	-.006
2(k)	128	16	-.1335	Lower	-.036	.685	-.109
2(k)	128	16	-.1430	Lower[1]	-.098	.854	-.246
2(l)	512	64	-.1005	Upper[1]	.038	.767	.528
2(l)	512	64	-.1080	Upper	.009	.560	.270
2(l)	512	64	-.1155	Lower	-.004	.542	.132
2(l)	512	64	-.1230	Lower	-.016	.535	-.011
2(l)	512	64	-.1310	Lower	-.03	.611	-.140
2(l)	512	64	-.1382	Lower[1]	-.079	.813	-.300
2(m)	2048	256	-.1085	Upper[1]	.028	.562	.611
2(m)	2048	256	-.1130	Upper	.004	.394	.255
2(m)	2048	256	-.1182	Lower	-.005	.379	.118
2(m)	2048	256	-.1228	Lower	-.014	.377	-.050
2(m)	2048	256	-.1275	Lower	-.029	.500	-.235
2(m)	2048	256	-.1325	Lower[1]	-.055	.688	-.356
2(n)	8192	1024	-.1165	Upper[1]	.015	.210	.514
2(n)	8192	1024	-.1190	- - -	0	.270	.230
2(n)	8192	1024	-.1218	Lower	-.004	.260	.085
2(n)	8192	1024	-.1250	Lower	-.012	.273	-.110
2(n)	8192	1024	-.1275	Lower[1]	-.031	.520	-.390
2(o)	1024	16	-.1232	Upper[1]	.008	.186	.610
2(o)	1024	16	-.1262	Lower[1]	-.015	.100	-.243
2(p)	4096	64	-.1243	Upper[1]	.003	.090	.434
2(p)	4096	64	-.1278	Lower[1]	-.015	.246	-.235
2(q)	16384	256	-.1254	Upper[1]	.002	.103	.506
2(q)	16384	256	-.1275	Lower[1]	-.014	.175	.295

[1]Denotes tangential trajectories.

NACA

TABLE III.— RESULTS FROM DIFFERENTIAL ANALYZER STUDIES OF WATER-DROP
IMPINGEMENT ON A 15—PERCENT—THICK SYMMETRICAL JOUKOWSKI AIRFOIL

$[c_l=0.44; \alpha=4°]$

Figure number	ψ	R_V	y_0	Surface	s/c	u_d/V	v_d/V
3(a)	4	256	−0.1682	Upper[1]	0.204	0.9996	0.0785
3(a)	4	256	−.3215	Lower[1]	−.408	.9946	.0705
3(b)	16	1024	−.1692	Upper[1]	.194	1.0086	.1005
3(b)	16	1024	−.3223	Lower[1]	−.400	.9976	.0705
3(c)	2	16	−.1818	Upper[1]	.192	1.0034	.0962
3(c)	2	16	−.3330	Lower[1]	−.409	.9891	.0688
3(d)	8	64	−.1837	Upper[1]	.170	1.0055	.1032
3(d)	8	64	−.3073	Lower	−.135	.9802	.0728
3(d)	8	64	−.2824	Lower	−.064	.9782	.0789
3(d)	8	64	−.2577	Lower	−.024	.9663	.1120
3(d)	8	64	−.2330	Upper	.004	.9793	.0940
3(d)	8	64	−.2083	Upper	.037	.9854	.1011
3(d)	8	64	−.3320	Lower[1]	−.400	.9930	.0638
3(e)	32	256	−.1881	Upper[1]	.148	1.0174	.1381
3(e)	32	256	−.2121	Upper	.034	.9764	.1221
3(e)	32	256	−.2358	Upper	.002	.9653	.1050
3(e)	32	256	−.2594	Lower	−.024	− − −	− − −
3(e)	32	256	−.2832	Lower	−.062	− − −	− − −
3(e)	32	256	−.3068	Lower	−.124	.9652	.0628
3(e)	32	256	−.3316	Lower[1]	−.379	.9831	.0618
3(f)	128	1024	−.1994	Upper[1]	.127	1.0294	.2031
3(f)	128	1024	−.2074	Upper	.062	.9804	.0931
3(f)	128	1024	−.2205	Upper	.028	.9514	.1670
3(f)	128	1024	−.2386	Upper·	.004	.9304	.1410
3(f)	128	1024	−.2748	Lower	−.041	.9273	.0869
3(f)	128	1024	−.3077	Lower	−.125	.9433	.0519
3(f)	128	1024	−.3316	Lower[1]	−.350	1.0200	.0468
3(g)	16	16	−.2403	Upper[1]	.121	1.0116	.2241
3(g)	16	16	−.3665	Lower[1]	−.336	.9628	.0415
3(h)	64	64	−.2472	Upper[1]	.100	1.0133	.2881
3(h)	64	64	−.3422	Lower	−.113	.8940	.0448
3(h)	64	64	−.3231	Lower	−.060	.8712	.0731
3(h)	64	64	−.3043	Lower	−.028	.8694	.1147
3(h)	64	64	−.2853	Lower	−.004	.8638	.1675
3(h)	64	64	−.2665	Upper	.018	.8990	.2148
3(h)	64	64	−.3606	Lower[1]	−.286	.9578	.0135
3(i)	256	256	−.2622	Upper[1]	.068	1.0121	.4088
3(i)	256	256	−.2775	Upper	.012	.8138	.2746
3(i)	256	256	−.2925	Lower	−.008	.7827	.1843

[1]Denotes tangential trajectories.

NACA

TABLE III.— CONCLUDED

Figure number	ψ	R_V	y_o	Surface	s/c	u_d/V	v_d/V
3(i)	256	256	−0.3078	Lower	−0.028	0.7864	0.1092
3(i)	256	256	−.3353	Lower	−.084	.8281	.0149
3(i)	256	256	−.3444	Lower	−.125	.8660	.0142
3(i)	256	256	−.3537	Lower[1]	−.247	.9558	−.0313
3(j)	1024	1024	−.2782	Upper[1]	.043	.8758	.5817
3(j)	1024	1024	−.3440	Lower[1]	−.155	.8780	−.1212
3(k)	128	16	−.3126	Upper[1]	.042	.8255	.5550
3(k)	128	16	−.3598	Lower	−.067	.7143	.0364
3(k)	128	16	−.3500	Lower	−.040	.6586	.0228
3(k)	128	16	−.3406	Lower	−.022	.6048	.1031
3(k)	128	16	−.3313	Lower	−.006	.615	.2444
3(k)	128	16	−.3220	Upper	−.006	.6562	.3437
3(k)	128	16	−.3688	Lower[1]	−.145	.8632	−.1358
3(l)	512	64	−.3216	Upper[1]	.026	.6392	.7017
3(l)	512	64	−.3303	Lower	−.004	.5021	.3024
3(l)	512	64	−.3383	Lower	−.015	.4678	.1513
3(l)	512	64	−.3441	Lower	−.027	.5197	.0390
3(l)	512	64	−.3500	Lower	−.042	.5566	−.0782
3(l)	512	64	−.3558	Lower	−.062	.6465	−.1363
3(l)	512	64	−.3605	Lower[1]	−.112	.8133	−.2045
3(m)	2048	256	−.3293	Upper[1]	.015	.4240	.7513
3(m)	2048	256	−.3324	Upper	.002	.3300	.4553
3(m)	2048	256	−.3373	Lower	−.008	.2858	.2442
3(m)	2048	256	−.3432	Lower	−.022	.3548	.0060
3(m)	2048	256	−.3471	Lower	−.032	.4137	−.1191
3(m)	2048	256	−.3501	Lower	−.045	.4956	−.1923
3(m)	2048	256	−.3529	Lower[1]	−.072	.6575	−.2912
3(n)	8192	1024	−.3382	Upper[1]	.004	.0918	.7521
3(n)	8192	1024	−.3405	Lower	−.005	.1918	.4371
3(n)	8192	1024	−.3441	Lower	−.012	.1787	.1520
3(n)	8192	1024	−.3458	Lower	−.020	.2767	.0669
3(n)	8192	1024	−.3474	Lower	−.031	.2867	−.2011
3(n)	8192	1024	−.3480	Lower[1]	−.041	.4186	−.2832
3(o)	1024	16	−.3495	Upper[1]	.004	.1147	.6545
3(o)	1024	16	−.3544	Lower[1]	−.035	.3496	−.2808
3(p)	4096	64	−.3495	Upper[1]	.002	.1047	.6945
3(p)	4096	64	−.3530	Lower[1]	−.026	.2146	−.2157
3(q)	16384	256	−.3504	Upper[1]	.002	.1597	.8494
3(q)	16384	256	−.3535	Lower[1]	−.025	.2746	−.2256

[1]Denotes tangential trajectories.

TABLE IV.— RESULTS FROM DIFFERENTIAL ANALYZER STUDIES OF WATER-DROP
IMPINGEMENT ON A 15-PERCENT-THICK CAMBERED JOUKOWSKI AIRFOIL
$[a=1.0$ MEAN LINE; $c_l=0.44$; $\alpha=0°]$

Figure number	ψ	R_V	y_o	Surface	s/c	u_d/V	v_d/V
4(a)	4	256	0.0935	Upper[1]	0.317	1.003	0.007
4(a)	4	256	−.0565	Lower[1]	−.216	.998	−.002
4(b)	16	1024	.0915	Upper[1]	.310	1.008	.013
4(b)	16	1024	−.0565	Lower[1]	−.213	.999	−.006
4(c)	2	16	.0855	Upper[1]	.305	1.009	.022
4(c)	2	16	−.0600	Lower[1]	−.215	.994	−.001
4(d)	8	64	.0818	Upper[1]	.294	1.012	.031
4(d)	8	64	.0536	Upper	.096	.992	.022
4(d)	8	64	.0253	Upper	.038	.988	.020
4(d)	8	64	−.0038	Upper	.002	.985	.011
4(d)	8	64	−.0318	Lower	−.033	.984	.003
4(d)	8	64	−.0610	Lower[1]	−.212	.999	−.008
4(e)	32	256	.0775	Upper[1]	.275	1.022	.050
4(e)	32	256	.0503	Upper	.092	.989	.042
4(e)	32	256	.0225	Upper	.034	.976	.030
4(e)	32	256	−.0045	Upper	.001	.972	.017
4(e)	32	256	−.0325	Lower	−.033	.973	.002
4(e)	32	256	−.0600	Lower[1]	−.199	.990	−.016
4(f)	128	1024	.0660	Upper[1]	.243	1.033	.090
4(f)	128	1024	.0420	Upper	.077	.976	.075
4(f)	128	1024	.0160	Upper	.030	.954	.054
4(f)	128	1024	−.0085	− − −	0	.943	.024
4(f)	128	1024	−.0335	Lower	−.032	.946	−.006
4(f)	128	1024	−.0585	Lower[1]	−.183	.984	−.036
4(g)	16	16	.0377	Upper[1]	.211	1.028	.128
4(g)	16	16	−.0770	Lower[1]	−.180	.978	−.042
4(h)	64	64	.0312	Upper[1]	.192	1.038	.168
4(h)	64	64	.0100	Upper	.061	.936	.131
4(h)	64	64	−.0110	Upper	.022	.898	.095
4(h)	64	64	−.0315	Lower	−.003	.884	.048
4(h)	64	64	−.0525	Lower	−.031	.891	−.007
4(h)	64	64	−.0731	Lower[1]	−.157	.971	−.073
4(i)	256	256	.0180	Upper[1]	.158	1.038	.238
4(i)	256	256	.0010	Upper	.050	.893	.188
4(i)	256	256	−.0165	Upper	.018	.839	.127
4(i)	256	256	−.0340	Lower	−.004	.820	.054
4(i)	256	256	−.0510	Lower	−.028	.838	−.017
4(i)	256	256	−.0680	Lower	−.120	.940	−.129

[1]Denotes tangential trajectories.

TABLE IV.— CONCLUDED

Figure number	ψ	R_V	y_0	Surface	s/c	u_d/V	v_d/V
4(j)	1024	1024	0	Upper[1]	0.109	1.000	0.357
4(j)	1024	1024	−.0620	Lower[1]	−.085	.883	−.220
4(k)	128	16	−.028	Upper[1]	.092	.958	.405
4(k)	128	16	−.0382	Upper	.032	.727	.288
4(k)	128	16	−.0480	Upper	.012	.638	.189
4(k)	128	16	−.0575	Lower	−.004	.649	.060
4(k)	128	16	−.0670	Lower	−.019	.644	−.046
4(k)	128	16	−.0772	Lower[1]	−.068	.838	−.264
4(l)	512	64	−.0347	Upper[1]	.072	.911	.487
4(l)	512	64	−.0425	Upper	.025	.634	.350
4(l)	512	64	−.050	Upper	.010	.535	.208
4(l)	512	64	−.0582	Lower	−.005	.485	.031
4(l)	512	64	−.066	Lower	−.018	.544	−.124
4(l)	512	64	−.0725	Lower[1]	−.053	.754	−.319
4(m)	2048	256	−.0440	Upper[1]	.046	.686	.576
4(m)	2048	256	−.050	Upper	.015	.448	.360
4(m)	2048	256	−.0548	Upper	.005	.381	.192
4(m)	2048	256	−.0594	Lower	−.004	.368	.048
4(m)	2048	256	−.0638	Lower	−.013	.407	−.103
4(m)	2048	256	−.0685	Lower[1]	−.038	.604	−.384
4(n)	8192	1024	−.0548	Upper[1]	.025	.471	.650
4(n)	8192	1024	−.0569	Upper	.007	.258	.308
4(n)	8192	1024	−.0590	Lower	−.001	.178	.082
4(n)	8192	1024	−.0610	Lower	−.008	.184	−.079
4(n)	8192	1024	−.0630	Lower	−.012	.211	−.168
4(n)	8192	1024	−.0650	Lower[1]	−.025	.464	−.428
4(o)	1024	16	−.0604	Upper[1]	.022	.346	.561
4(o)	1024	16	−.0700	Lower[1]	−.018	.317	−.368
4(p)	4096	64	−.0650	Upper[1]	.015	.285	.527
4(p)	4096	64	−.0675	Lower[1]	−.012	.143	−.253
4(q)	16384	256	−.0655	Upper[1]	.006	.113	.391
4(q)	16384	256	−.0670	Lower[1]	−.008	.046	−.118

[1]Denotes tangential trajectories.

TABLE V.— RESULTS FROM DIFFERENTIAL ANALYZER STUDIES OF
WATER-DROP EMPINGEMENT ON AN NACA 65_2-015 AIRFOIL

$[c_l=0.44; \alpha=4^\circ]$

Figure number	ψ	R_V	y_0	Surface	s/c	u_d/V	v_d/V
5(a)	4	256	-0.1281	Upper[1]	0.281	1.0023	0.0814
5(a)	4	256	-.2817	Lower[1]	-.523	.9973	.0704
5(b)	16	1024	-.1298	Upper[1]	.267	1.0073	.0864
5(b)	16	1024	-.2818	Lower[1]	-.514	.9973	.0704
5(c)	2	16	-.1395	Upper[1]	.259	1.0047	.0945
5(c)	2	16	-.1646	Upper	.031	.9881	.0875
5(c)	2	16	-.2026	Lower	-.022	.9847	.0825
5(c)	2	16	-.2246	Lower	-.074	.9867	.0793
5(c)	2	16	-.2467	Lower	-.150	.9857	.0753
5(c)	2	16	-.2687	Lower	-.256	.9847	.0742
5(c)	2	16	-.2909	Lower[1]	-.514	.9927	.0711
5(d)	8	64	-.1424	Upper[1]	.240	1.0107	.1065
5(d)	8	64	-.1719	Upper	.016	.9847	.0935
5(d)	8	64	-.2163	Lower	-.050	.9757	.0824
5(d)	8	64	-.2409	Lower	-.125	.9807	.0743
5(d)	8	64	-.2655	Lower	-.236	.9797	.0712
5(d)	8	64	-.2899	Lower[1]	-.512	.9907	.0641
5(e)	32	256	-.1493	Upper[1]	.209	1.0187	.1326
5(e)	32	256	-.1702	Upper	.023	.9761	.1155
5(e)	32	256	-.2193	Lower	-.052	.9617	.0874
5(e)	32	256	-.2437	Lower	-.131	.9647	.0743
5(e)	32	256	-.2685	Lower	-.249	.9717	.0632
5(e)	32	256	-.2894	Lower[1]	-.506	1.0057	.0531
5(f)	128	1024	-.1603	Upper[1]	.150	1.0207	.1805
5(f)	128	1024	-.1826	Upper	.008	.9517	.1375
5(f)	128	1024	-.2282	Lower	-.068	.9427	.0853
5(f)	128	1024	-.2505	Lower	-.145	.9407	.0642
5(f)	128	1024	-.2726	Lower	-.267	.9557	.0462
5(f)	128	1024	-.2878	Lower[1]	-.485	.9837	.0382
5(g)	16	16	-.1951	Upper[1]	.128	1.0015	.2008
5(g)	16	16	-.3202	Lower[1]	-.481	.9776	.0383
5(h)	64	64	-.2030	Upper[1]	.092	.9956	.2597
5(h)	64	64	-.2136	Upper	.012	.9155	.2055
5(h)	64	64	-.2535	Lower	-.048	.8795	.1092
5(h)	64	64	-.2787	Lower	-.127	.8975	.0609
5(h)	64	64	-.3013	Lower	-.247	.9255	.0227
5(h)	64	64	-.3111	Lower[1]	-.417	.9756	.0074
5(i)	256	256	-.2143	Upper[1]	.047	.9416	.3416
5(i)	256	256	-.2343	Lower	-.007	.8256	.1964

[1]Denotes tangential trajectories.

TABLE V.— CONTINUED

Figure number	ψ	R_V	y_0	Surface	s/c	u_d/V	v_d/V
5(i)	256	256	-0.2543	Lower	-0.040	0.8086	0.1102
5(i)	256	256	-.2717	Lower	-.093	.8316	.0410
5(i)	256	256	-.2892	Lower	-.184	- - -	- - -
5(i)	256	256	-.2983	Lower[1]	-.355	.9686	-.0443
5(j)	1024	1024	-.2267	Upper[1]	.026	.8575	.4614
5(j)	1024	1024	-.2313	Upper	.010	.7726	.3935
5(j)	1024	1024	-.2492	Lower	-.015	.6715	.1972
5(j)	1024	1024	-.2692	Lower	-.060	.6295	.0300
5(j)	1024	1024	-.2782	Lower	-.104	.7875	-.0251
5(j)	1024	1024	-.2853	Lower	-.166	.7495	-.0692
5(j)	1024	1024	-.2883	Lower[1]	-.245	.9175	.0942
5(k)	128	16	-.2633	Upper[1]	.021	.7926	.4950
5(k)	128	16	-.2798	Lower	-.012	.6436	.2336
5(k)	128	16	-.2945	Lower	-.042	.6395	.1003
5(k)	128	16	-.3028	Lower	-.080	.7194	-.0500
5(k)	128	16	-.3059	Lower	-.104	.7634	-.0860
5(k)	128	16	-.3091	Lower[1]	-.185	.8804	-.1302
5(l)	512	64	-.2676	Upper[1]	.018	.7536	.5779
5(l)	512	64	-.2719	Upper	.005	.6496	.4378
5(l)	512	64	-.2857	Lower	-.020	.4935	.1605
5(l)	512	64	-.2926	Lower	-.034	.5504	.0403
5(l)	512	64	-.3015	Lower	-.079	.6954	-.0989
5(l)	512	64	-.3035	Lower[1]	-.145	.8284	-.1540
5(m)	2048	256	-.2737	Upper[1]	.014	.6606	.6718
5(m)	2048	256	-.2748	Upper	.007	.5986	.5868
5(m)	2048	256	-.2781	- - -	0	.5216	.4106
5(m)	2048	256	-.2861	Lower	-.012	.4085	.2245
5(m)	2048	256	-.2906	Lower	-.022	.3905	.0604
5(m)	2048	256	-.2965	Lower	-.048	.5485	-.0967
5(m)	2048	256	-.2989	Lower[1]	-.100	.7584	-.1768
5(n)	8192	1024	-.2798	Upper[1]	.010	.5976	.7847
5(n)	8192	1024	-.2801	Upper	.005	- - -	- - -
5(n)	8192	1024	-.2850	Lower	-.004	- - -	- - -
5(n)	8192	1024	-.2886	Lower	-.010	.3035	.2454
5(n)	8192	1024	-.2932	Lower	-.022	.2124	.0033
5(n)	8192	1024	-.2945	Lower	-.030	.3423	-.0863
5(n)	8192	1024	-.2958	Lower	-.033	.3983	-.1068
5(n)	8192	1024	-.2971	Lower[1]	-.065	.6765	-.1867
5(o)	1024	16	-.2933	Upper[1]	.008	.4372	.8238
5(o)	1024	16	-.3037	Lower[1]	-.040	.4891	-.1997

[1]Denotes tangential trajectories.

TABLE V.— CONCLUDED

Figure number	ψ	R_V	y_0	Surface	s/c	u_d/V	v_d/V
5(p)	4096	64	-0.2947	Upper[1]	0.008	0.5712	0.8627
5(p)	4096	64	-.3026	Lower[1]	-.024	.2221	-.1126
5(q)	16384	256	-.2952	Upper[1]	.008	.5730	.9007
5(q)	16384	256	-.3028	Lower[1]	-.019	.1099	-.0525

[1]Denotes tangential trajectories.

TABLE VI.— VALUES OF $c_d R/24$ AS A FUNCTION OF R

R	$c_d R/24$	R	$c_d R/24$
0.00	1.000	500	11.46
.05	1.009	600	12.97
.1	1.018	800	15.81
.2	1.037	1,000	18.62
.4	1.073	1,200	21.3
.6	1.108	1,400	24.0
.8	1.142	1,600	26.9
1.0	1.176	1,800	29.8
1.2	1.201	2,000	32.7
1.4	1.225	2,500	40.4
1.6	1.248	3,000	47.8
1.8	1.267	3,500	55.6
2.0	1.285	4,000	63.7
2.5	1.332	5,000	80.0
3.0	1.374	6,000	96.8
3.5	1.412	8,000	130.6
4.0	1.447	10,000	166.3
5.0	1.513	12,000	204
6.0	1.572	14,000	243
8.0	1.678	16,000	285
10.0	1.782	18,000	325
12	1.901	20,000	365
14	2.008	25,000	470
16	2.109	30,000	574
18	2.198	35,000	674
20	2.291	40,000	778
25	2.489	50,000	980
30	2.673	60,000	1175
35	2.851	80,000	1552
40	3.013	100,000	1905
50	3.327	1.2×10^5	2234
60	3.60	1.4×10^5	2549
80	4.11	1.6×10^5	2851
100	4.59		
120	5.01		
140	5.40		
160	5.76		
180	6.16		
200	6.52		
250	7.38		
300	8.26		
350	9.00		
400	9.82		

TABLE VII.— COMPARISON OF PRODUCTS OF SCALE MODULUS AND DROP DRAG COEFFICIENT FOR THE UPPER AND LOWER SURFACES OF A 15–PERCENT–THICK SYMMETRICAL JOUKOWSKI AIRFOIL

$$[\alpha=0°; \quad c_l=0]$$

s/c	R_{V_1}	ψ_1	R_{V_2}	ψ_2	R_{V_3}	ψ_3	R_{V_4}	ψ_4	R_{V_5}	ψ_5	$c_{d_1}\psi_1$	$c_{d_2}\psi_2$	$c_{d_3}\psi_3$	$c_{d_4}\psi_4$	$c_{d_5}\psi_5$
0.197	8	8.0	32	24.5	128	52.0	512	105.0	2048	210.0	122.3	122.2	106.0	101.4	113.6
.078	8	64.0	32	220.0	128	500.0	512	1000.0	2048	1810.0	831.9	953.9	914.6	874.0	921.7
.023	8	512.0	32	1700.0	128	4250.0	512	9700.0	2048	13500.0	7650.5	8302.2	8535.7	9705.8	7253.0
.273	8	---	32	4.0	128	5.0	512	8.8	2048	15.6	---	24.1	11.8	9.6	9.1
.185	8	9.8	32	32.0	128	65.5	512	132.0	2048	260.0	146.5	157.1	132.0	125.9	139.8
.073	8	73.5	32	256.0	128	560.0	512	1100.0	2048	2030.0	977.8	1133.3	1041.2	978.5	1044.2
.265	8	---	32	4.3	128	2.0	512	14.7	2048	27.5	---	27.7	29.4	16.5	164.2
.244	8	3.1	32	8.3	128	16.0	512	42.2	2048	64.0	57.2	49.0	37.3	45.6	37.3
.150	8	17.3	32	58.5	128	128.0	512	250.0	2048	460.0	239.6	267.6	244.6	229.4	240.5
.052	8	140.0	32	475.0	128	1024.0	512	2250.0	2048	3860.0	1944.9	2180.9	1962.7	2079.6	2017.2
.015	8	1130.0	32	3400.0	128	8192.0	512	27000.0	2048	37000.0	16884.8	16604.4	16452.8	27016.2	19878.6
.273	8	---	32	2.9	128	5.0	512	8.0	2048	15.6	---	18.3	12.2	10.0	9.3
.225	8	4.7	32	13.4	128	27.3	512	64.0	2048	112.0	77.7	72.3	59.3	64.7	62.5
.108	8	35.5	32	122.0	128	260.0	512	512.0	2048	940.0	470.9	538.0	482.6	415.0	483.0
.038	8	220.0	32	730.0	128	1720.0	512	4096.0	2048	6000.0	3096.5	3385.0	3319.8	3760.8	3147.6
.016	8	1085.0	32	3300.0	128	8250.0	512	32768.0	2048	26500.0	13930.5	14157.2	14931.5	28546.2	13440.0
.262	8	2.0	32	4.9	128	9.0	512	17.0	2048	32.0	37.6	29.4	21.3	18.5	18.7
.188	8	9.2	32	29.0	128	60.0	512	124.0	2048	256.0	137.8	141.9	120.8	118.0	137.6
.072	8	76.0	32	265.0	128	575.0	512	1170.0	2048	2048.0	1002.1	660.3	1063.1	945.6	1048.5
.022	8	580.0	32	1860.0	128	4900.0	512	11200.0	2048	16348.0	8683.2	9113.1	9872.0	10682.5	8814.1

TABLE VIII.— COMPARISON OF PRODUCTS OF SCALE MODULUS AND DROP DRAG COEFFICIENT
FOR A 15—PERCENT—THICK JOUKOWSKI AIRFOIL

$[\alpha=2^o; \quad c_l=0.22]$

(a) Upper Surface

s/c	R_{V_1}	ψ_1	R_{V_2}	ψ_2	R_{V_3}	ψ_3	R_{V_4}	ψ_4	$c_{d_1}\psi_1$	$c_{d_2}\psi_2$	$c_{d_3}\psi_3$	$c_{d_4}\psi_4$
0.226	16	2.0	64	4.2	256	9.6	1024	17.0	14.2	11.1	11.6	10.8
.149	16	16.0	64	40.0	256	95.0	1024	185.0	106.8	102.3	110.8	113.1
.055	16	128.0	64	325.0	256	700.0	1024	1310.0	826.0	808.1	796.8	788.5
.008	16	1024.0	64	2380.0	256	6200.0	1024	9700.0	9450.0	7893.9	10258.8	7026.6
.212	16	3.7	64	8.0	256	18.4	1024	35.0	26.1	21.4	22.3	22.1
.128	16	24.5	64	64.0	256	140.0	1024	276.0	161.1	162.2	161.7	168.1
.038	16	220.0	64	512.0	256	1155.0	1024	2150.0	1449.0	1300.0	1334.3	1310.4
.003	16	1700.0	64	4096.0	256	12500.0	1024	— — —	13430.6	11462.5	16280.6	— — —
.236	16	— — —	64	— — —	256	4.0	1024	8.0	— — — —	— — — —	4.9	5.1
.196	16	5.8	64	12.9	256	32.0	1024	61.0	40.2	34.1	38.2	38.1
.100	16	45.0	64	115.0	256	256.0	1024	475.0	286.5	284.3	290.1	284.2
.024	16	372.0	64	930.0	256	2048.0	1024	3700.0	2534.9	2919.6	2424.0	2289.5
.002	16	2300.0	64	5300.0	256	16384.0	1024	— — —	26270.1	20785.4	27433.4	— — —
.223	16	2.4	64	4.7	256	11.0	1024	16.0	16.9	12.6	13.4	10.2
.168	16	10.7	64	25.6	256	62.0	1024	128.0	71.8	63.6	72.8	78.8
.063	16	106.0	64	263.0	256	560.0	1024	1024.0	670.2	648.5	630.8	630.3
.010	16	850.0	64	2100.0	256	5400.0	1024	8192.0	6679.1	6121.9	7023.0	5454.7

TABLE VIII.— CONCLUDED

(b) Lower Surface

s/c	R_{V_1}	ψ_1	R_{V_2}	ψ_2	R_{V_3}	ψ_3	R_{V_4}	ψ_4	$c_{d_1}\psi_1$	$c_{d_2}\psi_2$	$c_{d_3}\psi_3$	$c_{d_4}\psi_4$
−0.311	16	2.0	64	6.0	256	10.0	1024	17.2	25.2	25.7	18.1	14.9
−.245	16	16.0	64	45.5	256	89.0	1024	170.0	195.0	187.0	155.9	143.9
−.098	16	128.0	64	370.0	256	780.0	1024	1440.0	1372.0	1385.1	1253.7	1131.4
−.015	16	1024.0	64	4000.0	256	13000.0	1024	21200.0	19660.0	24463.4	31159.7	23460.3
−.308	16	2.5	64	8.0	256	12.4	1024	21.6	31.8	34.0	22.3	18.7
−.225	16	22.1	64	64.0	256	121.0	1024	237.0	257.2	249.3	205.0	194.6
−.079	16	163.0	64	512.0	256	1130.0	1024	2100.0	1748.2	1843.4	1815.8	1652.5
−.015	16	1000.0	64	4096.0	256	13200.0	1024	21100.0	14382.4	19346.4	25814.3	19672.2
−.316	16	---	64	---	256	4.0	1024	---	---	---	7.1	---
−.295	16	5.2	64	14.3	256	32.0	1024	52.5	64.9	60.1	57.2	45.3
−.177	16	43.0	64	121.0	256	256.0	1024	490.0	482.2	454.7	422.7	554.5
−.055	16	265.0	64	850.0	256	2048.0	1024	3750.0	2804.8	3024.9	3263.0	2923.7
−.014	16	1100.0	64	4250.0	256	16384.0	1024	---	19103.7	23730.3	35962.1	---
−.310	16	2.0	64	6.2	256	11.0	1024	16.0	25.5	26.4	19.8	13.9
−.265	16	11.1	64	31.3	256	62.5	1024	128.0	137.0	129.0	110.2	108.6
−.118	16	91.0	64	272.0	256	560.0	1024	1024.0	993.8	996.3	909.4	811.4
−.031	16	480.0	64	1600.0	256	3900.0	1024	8192.0	6575.0	7249.8	7381.0	7400.0

NACA

TABLE IX.— COMPARISON OF PRODUCTS OF SCALE MODULUS AND DROP DRAG COEFFICIENT FOR A 15—PERCENT—THICK SYMMETRICAL JOUKOWSKI AIRFOIL

$$[\alpha=4°; \quad c_l=0.44]$$

(a) Upper Surface

s/c	R_{V_1}	ψ_1	R_{V_2}	ψ_2	R_{V_3}	ψ_3	R_{V_4}	ψ_4	$c_{d_1}\psi_1$	$c_{d_2}\psi_2$	$c_{d_3}\psi_3$	$c_{d_4}\psi_4$
0.192	16	2.0	64	3.6	256	7.6	1024	16.5	11.3	8.1	7.9	9.4
.121	16	16.0	64	34.3	256	64.5	1024	137.0	87.2	74.3	65.5	76.2
.042	16	128.0	64	335.0	256	520.0	1024	1000.0	635.0	680.2	2274.9	540.7
.004	16	1024.0	64	3000.0	256	7400.0	1024	– – –	8740.0	9352.9	10161.2	– – –
.170	16	4.4	64	8.0	256	17.0	1024	36.0	24.8	18.0	17.8	20.7
.100	16	27.5	64	64.0	256	112.0	1024	230.0	147.4	138.3	114.3	116.9
.026	16	230.0	64	512.0	256	970.0	1024	1680.0	1117.3	1023.0	919.8	896.5
.002	16	– – –	64	4096.0	256	13000.0	1024	– – –	– – –	13065.4	18246.3	– – –
.204	16	– – –	64	– – –	256	4.0	1024	9.0	– – –	– – –	4.1	5.1
.148	16	8.0	64	15.5	256	32.0	1024	68.0	44.5	34.5	33.1	38.4
.068	16	63.0	64	150.0	256	256.0	1024	490.0	328.7	317.2	255.1	270.4
.015	16	370.0	64	990.0	256	2048.0	1024	2850.0	2203.4	2320.8	2225.7	1661.6
.002	16	– – –	64	– – –	256	16384.0	1024	– – –	– – –	22147.7	– – –	– – –
.194	16	– – –	64	3.3	256	6.8	1024	16.0	– – –	7.4	7.1	9.1
.127	16	13.6	64	29.0	256	55.0	1024	128.0	74.9	64.0	56.6	72.2
.043	16	130.0	64	320.0	256	500.0	1024	1024.0	542.1	544.0	477.9	552.7
.004	16	– – –	64	2900.0	256	7400.0	1024	8192.0	– – –	10190.8	11236.8	6156.6

TABLE IX.— CONCLUDED

(b) Lower Surface

s/c	Rv₁	ψ₁	Rv₂	ψ₂	Rv₃	ψ₃	Rv₄	ψ₄	$c_{d_1}\psi_1$	$c_{d_2}\psi_2$	$c_{d_3}\psi_3$	$c_{d_4}\psi_4$
−0.409	16	2.0	64	2.0	256	− −	1024	7.0	39.8	10.6	− − −	8.7
−.336	16	16.0	64	35.0	256	84.0	1024	152.0	254.6	150.4	201.2	168.6
−.145	16	128.0	64	330.0	256	740.0	1024	1150.0	1220.6	1372.5	1297.1	971.9
−.035	16	1024.0	64	2400.0	256	6600.0	1024	11500.0	10233.0	10232.0	11898.0	999.1
−.400	16	3.7	64	8.0	256	9.5	1024	20.0	72.9	41.5	26.7	24.5
−.286	16	20.8	64	64.0	256	170.0	1024	280.0	285.2	239.8	369.8	288.6
−.112	16	187.0	64	512.0	256	1100.0	1024	1700.0	1847.1	2161.5	1968.5	1460.9
−.026	16	1670.0	64	4096.0	256	12000.0	1024	27000.0	20155.0	13461.0	24002.1	25598.0
−.408	16	2.3	64	2.5	256	4.0	1024	7.0	45.2	13.1	10.9	8.6
−.379	16	7.4	64	16.0	256	32.0	1024	60.0	133.8	77.5	86.6	70.6
−.247	16	42.5	64	102.0	256	256.0	1024	420.0	520.5	344.6	519.6	405.3
−.072	16	350.0	64	900.0	256	2048.0	1024	3400.0	3890.6	2792.0	3948.3	3119.2
−.025	16	1700.0	64	4500.0	256	16384.0	1024	28000.0	20822.0	15201.0	33260.0	27025.0
−.400	16	3.8	64	6.2	256	9.5	1024	16.0	72.9	32.1	26.7	19.6
−.350	16	12.5	64	28.0	256	65.0	1024	128.0	204.8	123.7	158.8	143.6
−.155	16	114.0	64	295.0	256	6500.0	1024	1024.0	1087.1	1227.0	1139.4	865.4
−.041	16	760.0	64	1950.0	256	4700.0	1024	8192.0	7987.6	5727.3	8729.8	7280.3

TABLE X.— COMPARISON OF PRODUCTS OF SCALE MODULUS AND DROP DRAG COEFFICIENT FOR A
15-PERCENT-THICK CAMBERED JOUKOWSKI AIRFOIL

[$\alpha=0°$; $c_l=0.44$; a=1.0 MEAN LINE]

(a) Upper Surface

s/c	RV_1	ψ_1	RV_2	ψ_2	RV_3	ψ_3	RV_4	ψ_4	$C_{d_1}\psi_1$	$C_{d_2}\psi_2$	$C_{d_3}\psi_3$	$C_{d_4}\psi_4$
0.305	16	2.0	64	5.0	256	10.7	1024	21.5	15.0	13.9	13.5	13.9
.211	16	16.0	64	47.0	256	112.5	1024	222.0	122.9	134.0	143.9	146.5
.092	16	128.0	64	338.0	256	730.0	1024	1380.0	1116.0	1074.3	1017.2	971.6
.022	16	1024.0	64	2550.0	256	5100.0	1024	9300.0	14170.0	11670.1	9747.6	8457.7
.294	16	3.1	64	8.0	256	17.5	1024	34.2	22.9	22.4	22.0	22.2
.192	16	22.0	64	64.0	256	152.0	1024	292.0	172.4	185.9	197.0	194.5
.072	16	203.0	64	512.0	256	1070.0	1024	2050.0	1900.4	1697.8	1563.6	1496.0
.015	16	1510.0	64	4096.0	256	7400.0	1024	13000.0	20354.5	18122.2	13735.2	11553.5
.317	16	– – –	64	– – –	256	4.0	1024	8.4	– – – –	– – – –	5.1	5.5
.275	16	5.1	64	13.5	256	32.0	1024	63.0	37.4	37.2	39.3	40.5
.158	16	38.5	64	107.0	256	256.0	1024	475.0	304.2	313.9	333.6	317.7
.046	16	305.0	64	1000.0	256	2048.0	1024	3850.0	3619.9	4035.1	3533.4	3208.3
.006	16	3500.0	64	9600.0	256	16384.0	1024	29000.0	41119.9	38413.8	27985.0	24083.6
.310	16	– – –	64	3.4	256	7.9	1024	16.0	– – – –	9.6	10.1	10.6
.243	16	9.4	64	26.2	256	64.7	1024	128.0	70.3	73.6	81.4	83.2
.109	16	92.0	64	245.0	256	540.0	1024	1024.0	771.4	753.3	730.9	706.2
.025	16	870.0	64	2120.0	256	4300.0	1024	8192.0	12211.0	9806.6	8287.0	7515.4

TABLE X.— CONCLUDED

(b) Lower Surface

s/c	R_{V_1}	ψ_1	R_{V_2}	ψ_2	R_{V_3}	ψ_3	R_{V_4}	ψ_4	$c_{d_1}\psi_1$	$c_{d_2}\psi_2$	$c_{d_3}\psi_3$	$c_{d_4}\psi_4$
-0.215	16	2.0	64	6.6	256	8.0	1024	12.0	22.6	25.6	13.3	9.7
-.180	16	16.0	64	36.5	256	67.8	1024	140.0	162.0	130.3	104.6	106.3
-.068	16	128.0	64	345.0	256	740.0	1024	1520.0	988.0	993.3	952.5	1005.8
-.018	16	1024.0	64	225.0	256	6300.0	1024	12500.0	9680.0	7605.0	9266.1	9154.0
-.212	16	3.2	64	8.0	256	10.0	1024	19.0	36.1	31.0	16.6	15.4
-.157	16	26.5	64	64.0	256	122.0	1024	250.0	257.1	221.2	182.6	186.3
-.053	16	183.0	64	512.0	256	1430.0	1024	2400.0	1410.4	1469.8	1449.5	1580.8
-.012	16	1700.0	64	4096.0	256	11000.0	1024	22000.0	15049.1	13150.4	15489.9	15616.7
-.216	16	---	64	---	256	4.0	1024	10.0	---	---	9.5	8.1
-.199	16	8.3	64	19.0	256	32.0	1024	58.0	89.4	71.0	53.6	45.5
-.120	16	49.0	64	129.0	256	256.0	1024	508.0	435.3	414.9	361.5	360.1
-.038	16	320.0	64	840.0	256	2048.0	1024	4200.0	2643.6	2554.3	2748.6	2882.8
-.008	16	2500.0	64	6400.0	256	16384.0	1024	28500.0	18407.6	17738.0	20373.0	18450.6
-.213	16	2.6	64	5.6	256	6.0	1024	16.0	29.8	22.1	10.1	13.0
-.183	16	14.3	64	33.0	256	62.0	1024	128.0	147.9	119.8	96.9	98.5
-.085	16	89.0	64	245.0	256	508.0	1024	1024.0	714.4	725.7	668.6	692.2
-.025	16	610.0	64	1500.0	256	4000.0	1024	8192.0	5854.3	5121.0	5952.4	6055.4

NACA

TABLE XI.— COMPARISON OF PRODUCTS OF SCALE MODULUS AND DROP DRAG COEFFICIENT FOR
AN NACA 65_2–015 AIRFOIL

$[\alpha=0^\circ;\ c_l=0.44]$

(a) Upper Surface

s/c	R_{V_1}	ψ_1	R_{V_2}	ψ_2	R_{V_3}	ψ_3	R_{V_4}	ψ_4	$c_{d_1}\psi_1$	$c_{d_2}\psi_2$	$c_{d_3}\psi_3$	$c_{d_4}\psi_4$
0.259	16	2.0	64	5.0	256	10.0	1024	20.5	13.3	12.8	11.6	12.5
.128	16	16.0	64	41.0	256	92.0	1024	161.0	106.8	104.9	107.3	98.7
.021	16	128.0	64	390.0	256	760.0	1024	1400.0	859.0	1004.2	892.1	861.6
.008	16	1024.0	64	3000.0	256	9000.0	1024	– – –	9973.3	10410.1	13503.7	– – –
.240	16	3.5	64	8.0	256	17.1	1024	33.7	23.4	20.6	19.9	20.7
.092	16	25.0	64	64.0	256	137.0	1024	248.0	165.9	163.7	159.3	151.6
.018	16	160.0	64	512.0	256	1050.0	1024	1800.0	1102.3	1349.7	1249.6	1121.6
.008	16	– – –	64	4096.0	256	– – –	1024	– – –	– – –	12800.0	– – –	– – –
.281	16	– – –	64	– – –	256	4.0	1024	7.6	– – –	– – –	4.7	4.6
.209	16	5.9	64	14.4	256	32.0	1024	59.0	39.3	36.9	37.2	36.1
.047	16	52.0	64	128.0	256	256.0	1024	500.0	342.0	324.3	295.6	303.9
.014	16	260.0	64	890.0	256	2048.0	1024	3500.0	1980.5	2534.9	2612.2	2304.7
.008	16	– – –	64	– – –	256	16384.0	1024	– – –	– – –	– – –	25005.3	– – –
.267	16	– – –	64	3.7	256	7.6	1024	16.0	– – –	9.4	8.8	9.8
.150	16	12.2	64	32.0	256	71.0	1024	128.0	81.7	82.4	82.8	78.6
.026	16	97.0	64	270.0	256	530.0	1024	1024.0	641.1	687.5	614.6	624.5
.010	16	540.0	64	2100.0	256	5000.0	1024	8192.0	4657.4	6593.7	6910.3	5729.5

TABLE XI.— CONCLUDED

(b) Lower Surface

s/c	R_{V_1}	ψ_1	R_{V_2}	ψ_2	R_{V_3}	ψ_3	R_{V_4}	ψ_4	$c_{d_1}\psi_1$	$c_{d_2}\psi_2$	$c_{d_3}\psi_3$	$c_{d_4}\psi_4$
−0.514	16	2.0	64	5.0	256	10.0	1024	16.0	27.2	21.9	18.4	13.2
−.481	16	16.0	64	31.0	256	74.0	1024	135.0	213.0	137.2	132.4	119.9
−.185	16	128.0	64	345.0	256	900.0	1024	1620.0	2330.0	2013.4	2079.1	1732.5
−.040	16	1024.0	64	2400.0	256	5800.0	1024	15800.0	17910.0	13499.9	12989.4	15734.6
−.512	16	2.7	64	8.0	256	13.5	1024	21.0	36.5	34.9	24.8	18.5
−.417	16	28.0	64	64.0	256	160.0	1024	275.0	396.1	289.8	303.3	226.5
−.145	16	172.0	64	512.0	256	1250.0	1024	2360.0	3275.0	3107.2	2975.1	2587.9
−.024	16	1200.0	64	4096.0	256	10800.0	1024	− − −	20475.7	18420.0	18749.1	− − −
−.523	16	− − −	64	− − −	256	4.0	1024	− − −	− − −	− − −	7.4	− − −
−.506	16	6.0	64	12.3	256	32.0	1024	52.0	82.9	54.6	59.7	46.3
−.355	16	42.0	64	98.0	256	256.0	1024	448.0	623.7	476.3	512.2	396.7
−.100	16	282.0	64	780.0	256	2048.0	1024	4000.0	5617.2	4927.4	5051.8	4516.0
−.019	16	− − −	64	− − −	256	16384.0	1024	− − −	− − −	− − −	19462.9	− − −
−.514	16	2.0	64	5.0	256	10.0	1024	16.0	27.4	22.0	18.5	14.2
−.485	16	14.8	64	29.5	256	70.0	1024	128.0	205.8	131.7	130.9	114.5
−.245	16	83.5	64	215.0	256	570.0	1024	1024.0	1316.1	1101.6	1188.3	952.1
−.065	16	500.0	64	1330.0	256	3280.0	1024	8192.0	9869.7	8340.7	8014.6	9250.3
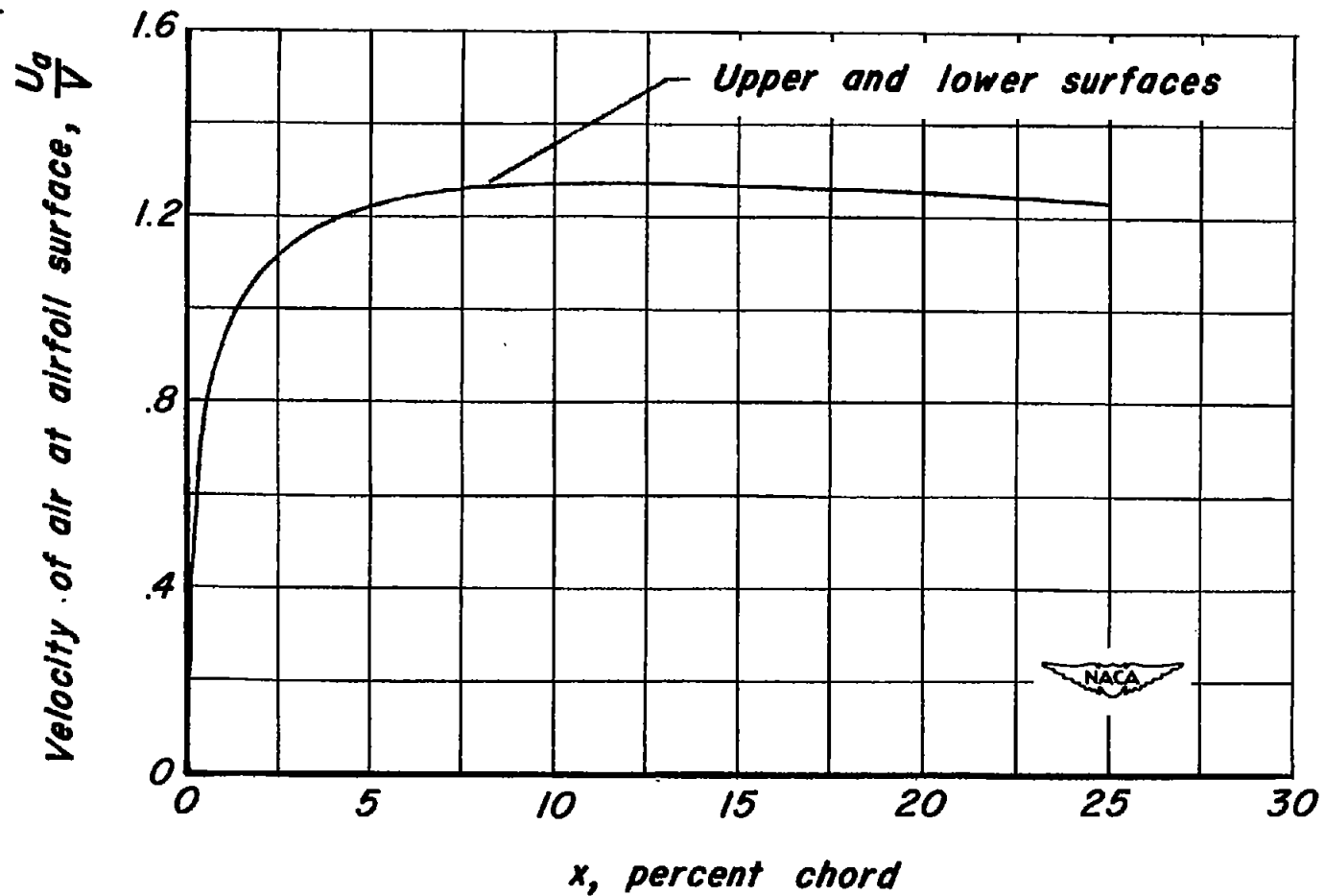
(a) 15 - percent - thick symmetrical Joukowski; $a = 0°$.

Figure 1.- Airfoil velocity distributions for the five airfoil cases comprising the differential analyzer study.
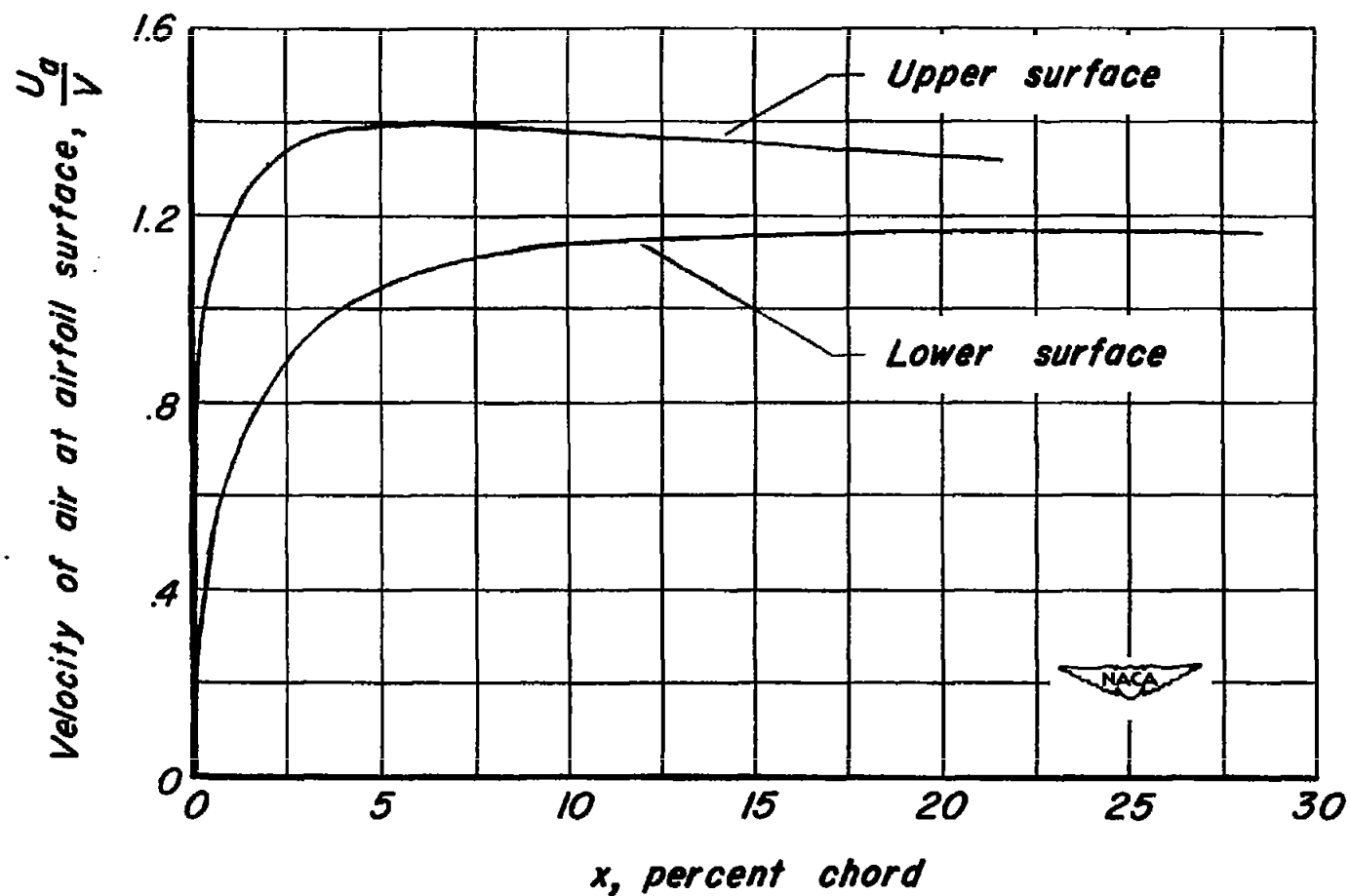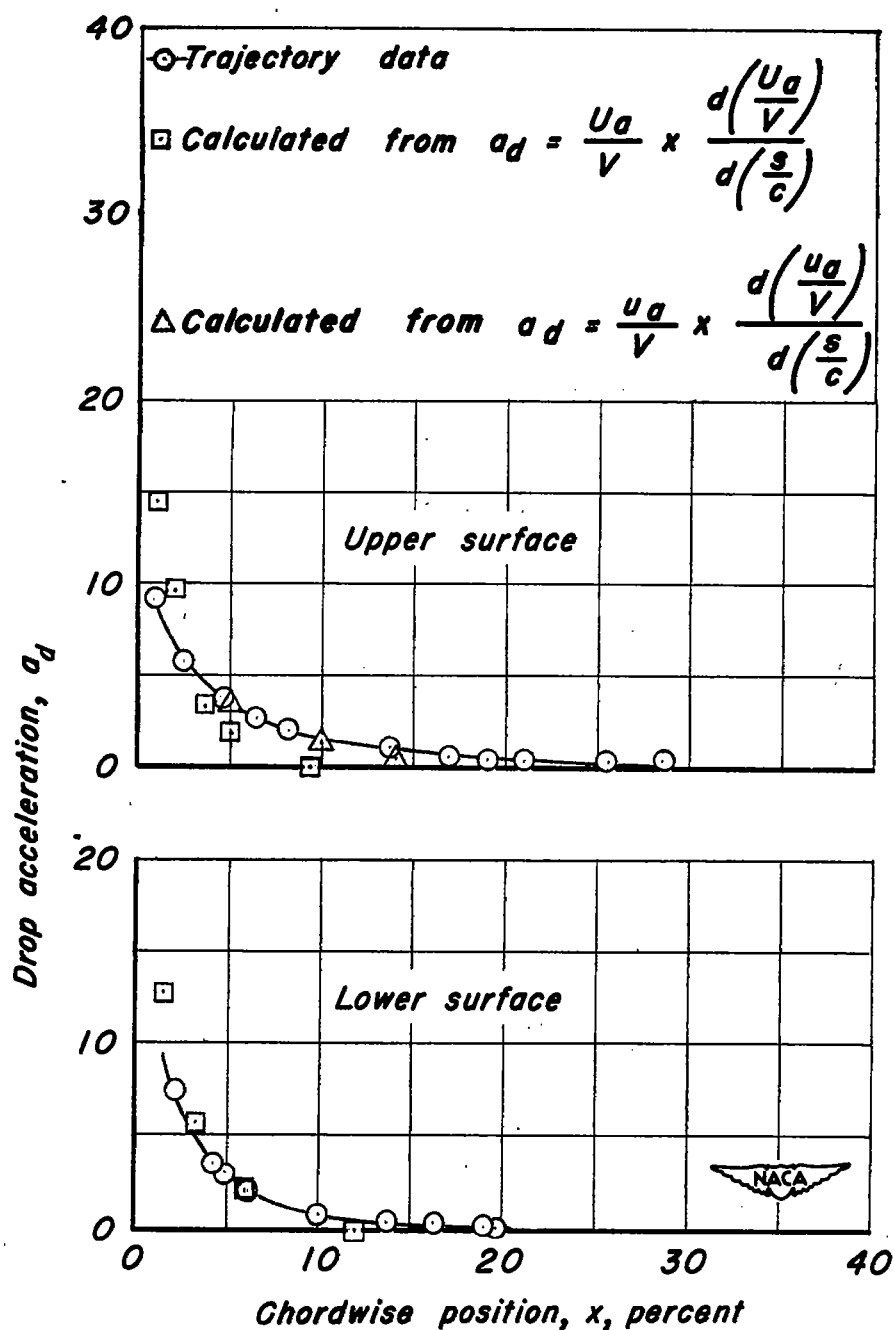
(b) 15 - percent - thick symmetrical Joukowski; a = 2°.

Figure I.- Continued.
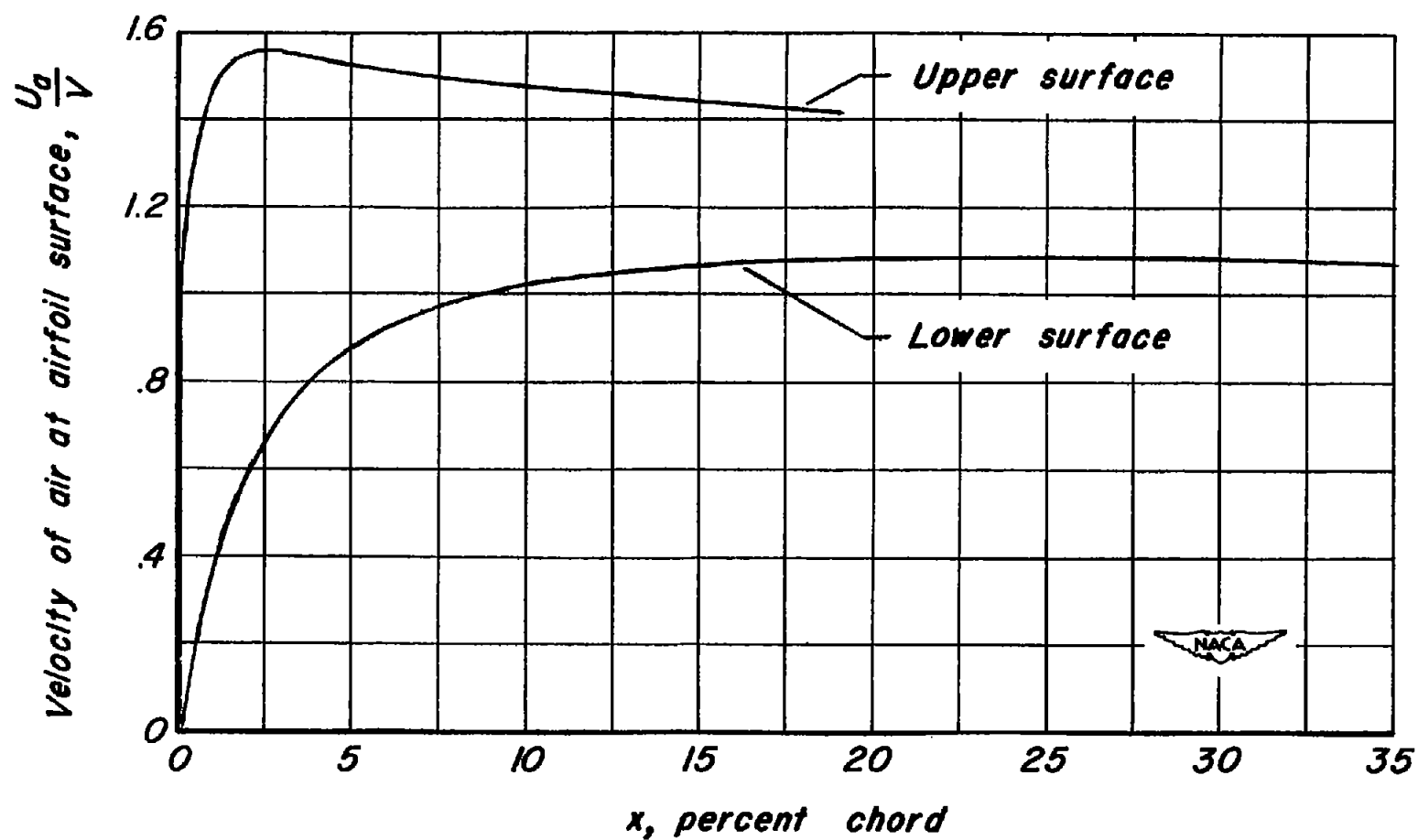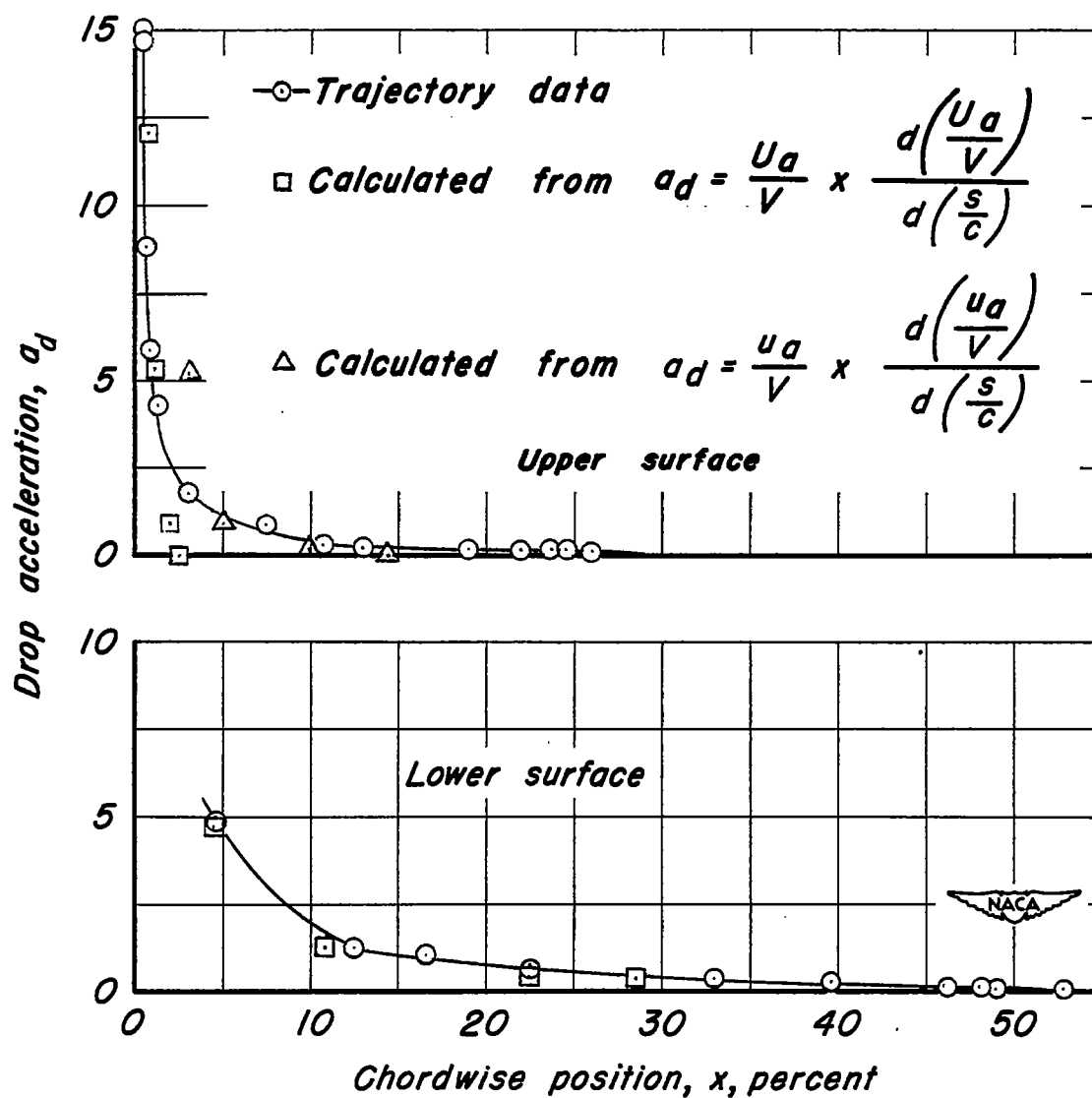
(c) 15 - percent - thick symmetrical Joukowski; $a = 4°$.

Figure 1.- Continued.
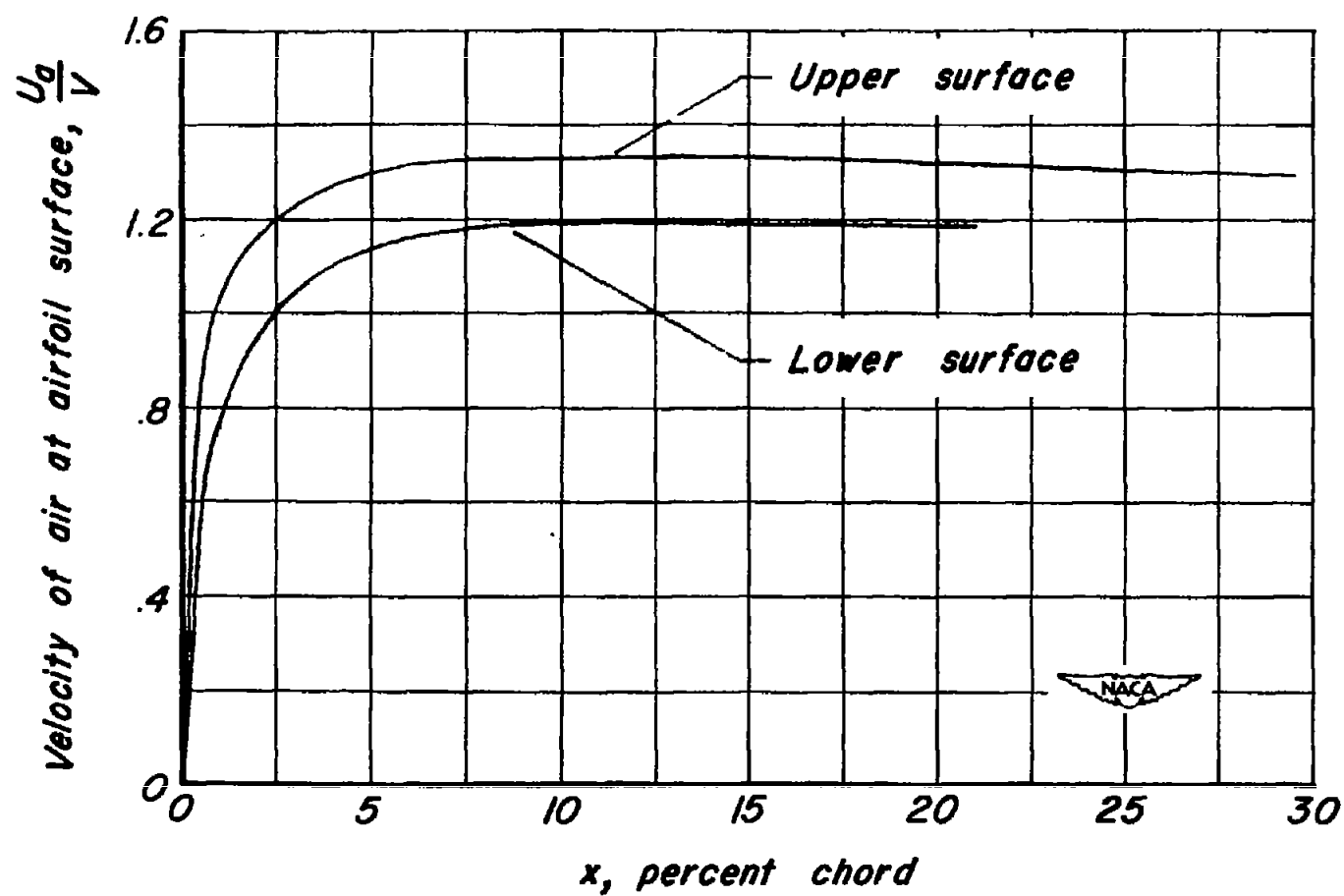
(d) 15-percent-thick cambered Joukowski; $c_l = 0.44$; $a = 0°$; $a = 1.0$ mean line.

Figure 1. – Continued.

(e) NACA 65_2 - 015 airfoil; a = 4°.

Figure 1. - Concluded.

(a) $\psi = 2$; $R_v = 128$

(b) $\psi = 8$; $R_v = 512$

(c) $\psi = 32$; $R_v = 2048$

(d) $\psi = 4$; $R_v = 32$

(e) $\psi = 16$; $R_v = 128$

(f) $\psi = 64$; $R_v = 512$
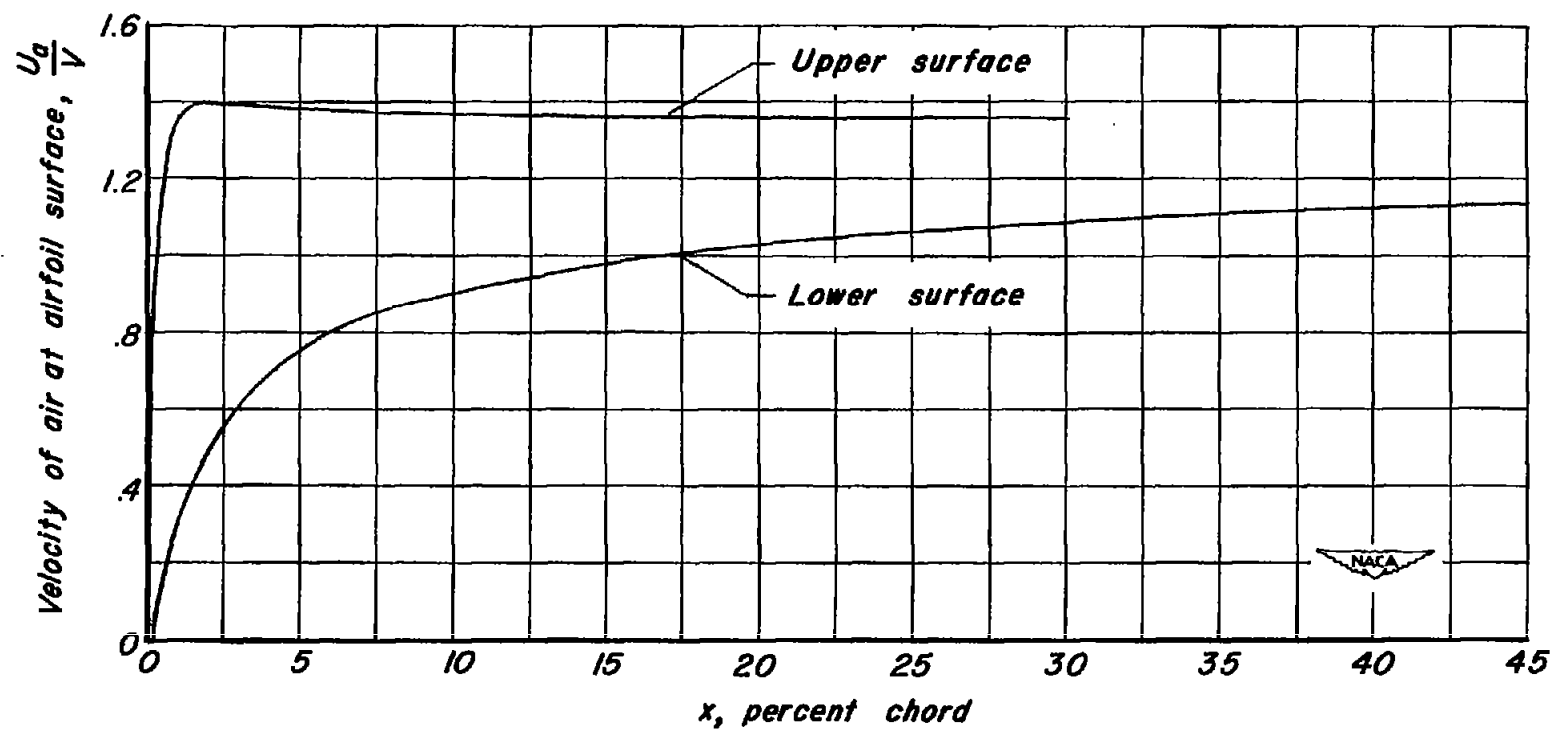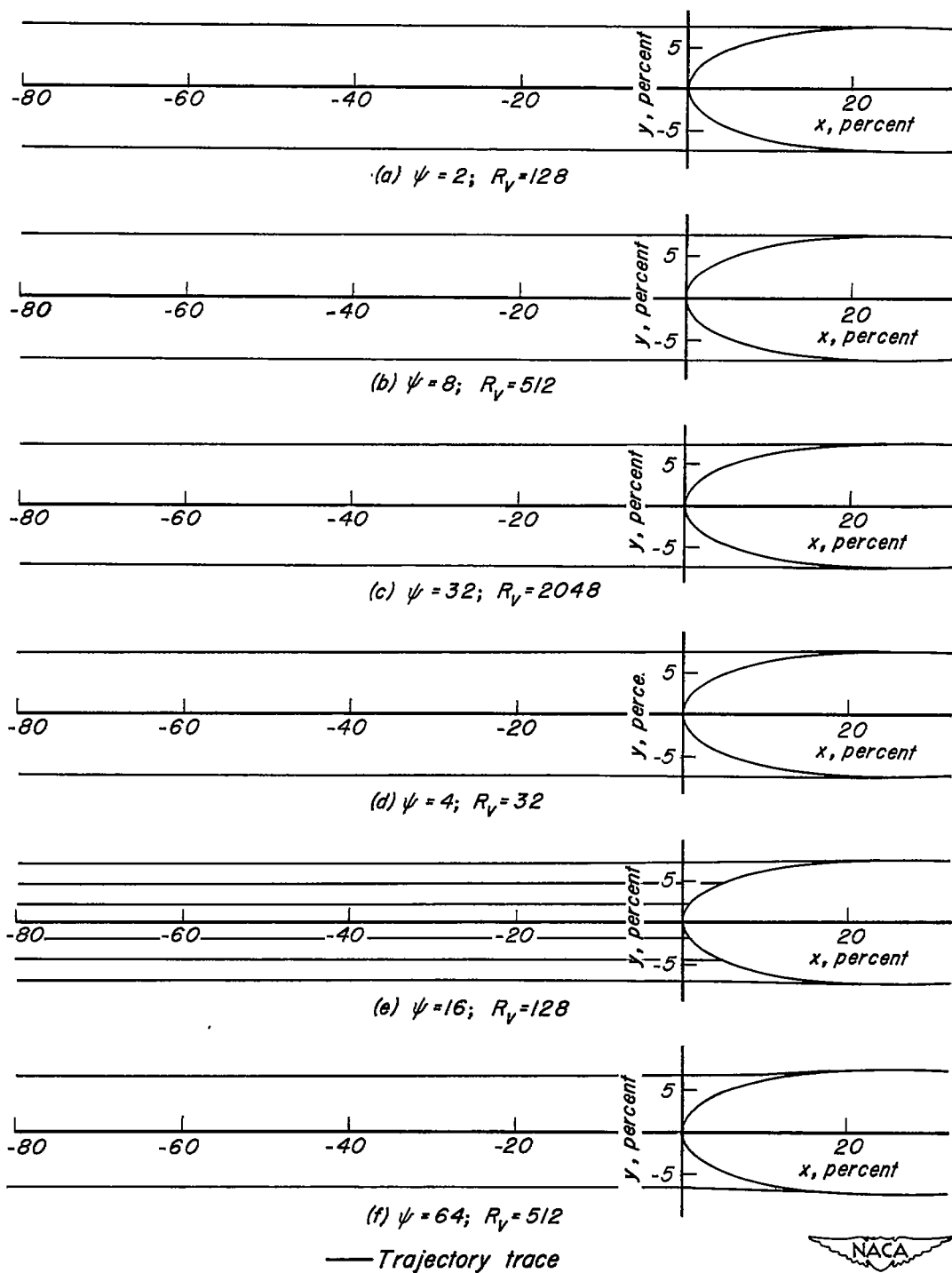
——— Trajectory trace

Figure 2.- Water-drop trajectory traces from a differential analyzer for a 15-percent-thick symmetrical Joukowski airfoil; $c_l = 0$; $a = 0°$.

(g) $\psi = 256$; $R_v = 2048$

(h) $\psi = 8$; $R_v = 8$

(i) $\psi = 32$; $R_v = 32$

(j) $\psi = 128$; $R_v = 128$

(k) $\psi = 512$; $R_v = 512$

(l) $\psi = 2048$; $R_v = 2048$

Figure 2.- Continued.

(m) $\psi = 64$; $R_V = 8$

(n) $\psi = 256$; $R_V = 32$

(o) $\psi = 1024$; $R_V = 128$

(p) $\psi = 4096$; $R_V = 512$

(q) $\psi = 16384$; $R_V = 2048$

(r) $\psi = 512$; $R_V = 8$

Figure 2.- Continued.

(s) $\psi = 8192$; $R_v = 128$

(t) $\psi = 32768$; $R_v = 512$

Figure 2.- Concluded.

(a) $\psi = 4$; $R_v = 256$

(b) $\psi = 16$; $R_v = 1024$

(c) $\psi = 2$; $R_v = 16$

(d) $\psi = 8$; $R_v = 64$

(e) $\psi = 32$; $R_v = 256$

(f) $\psi = 128$; $R_v = 1024$
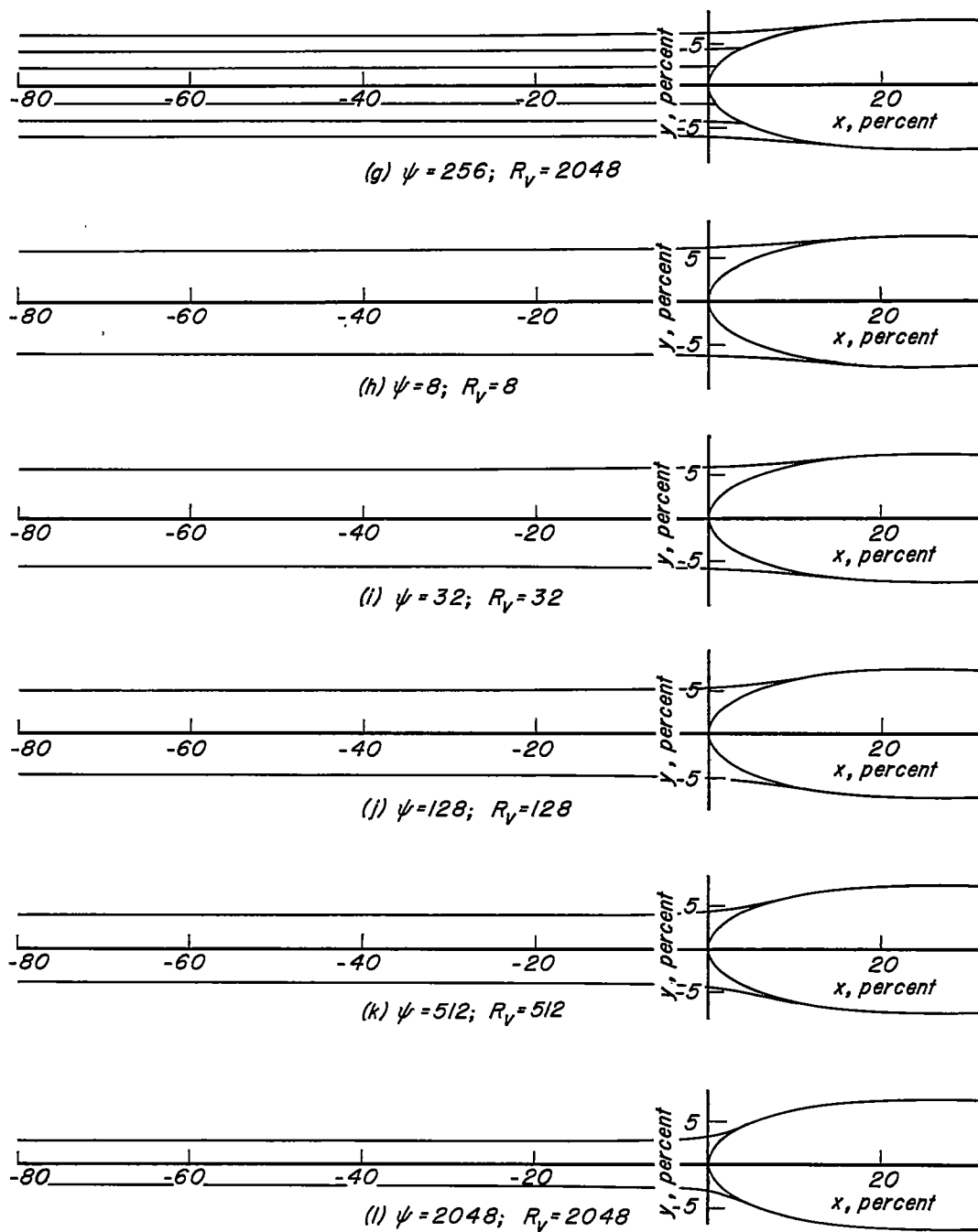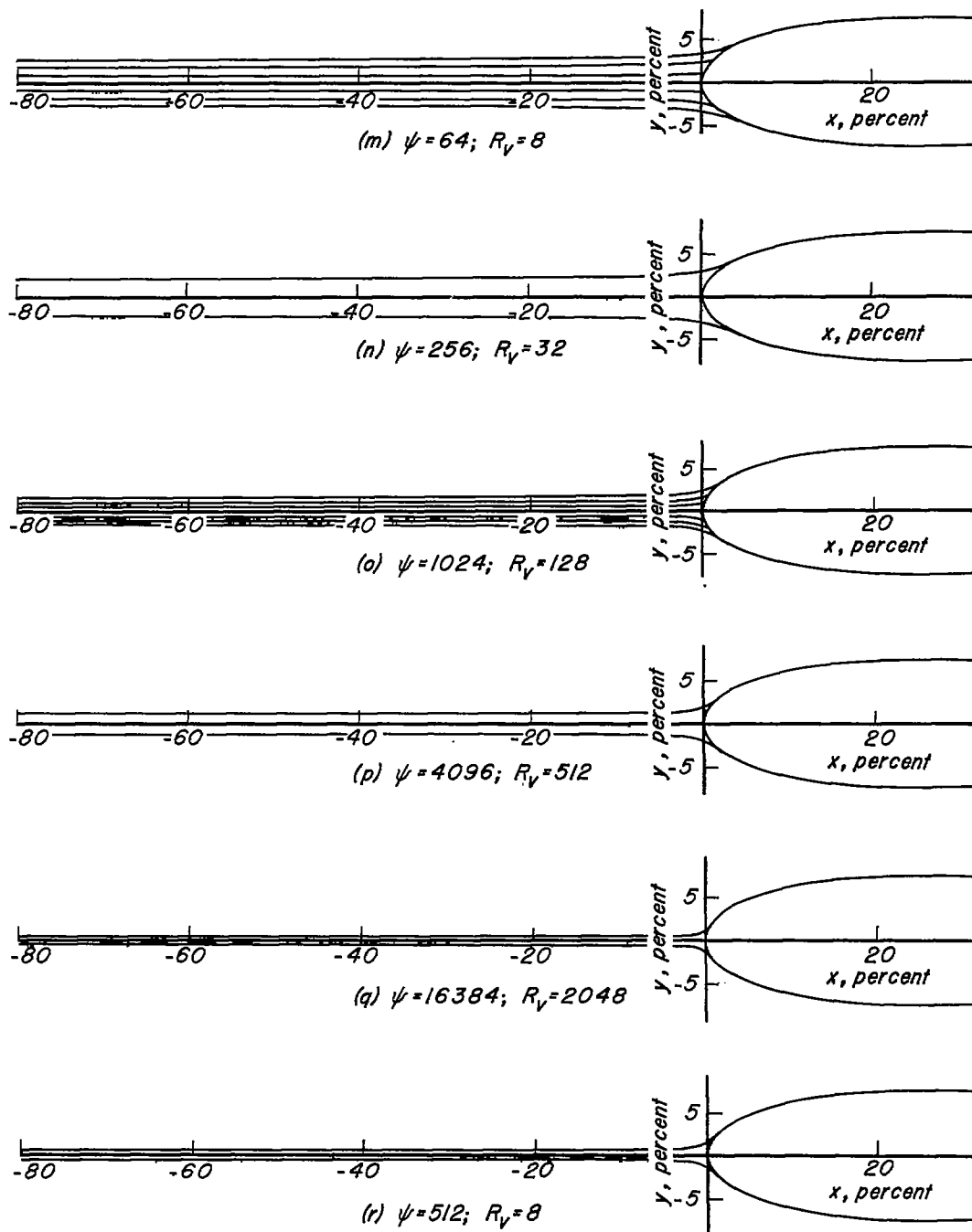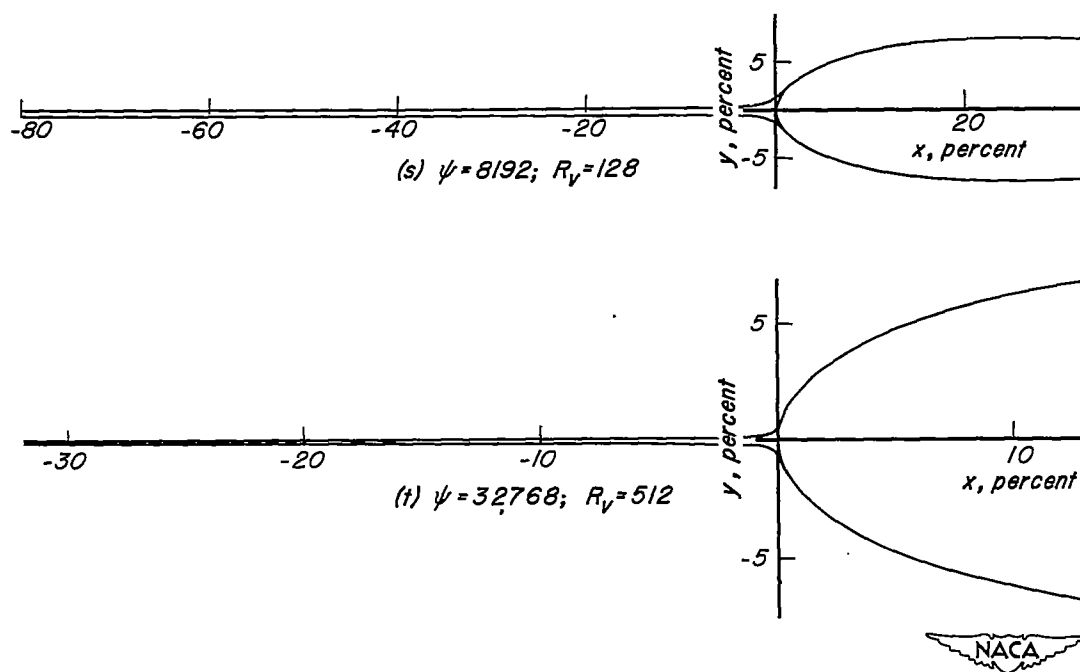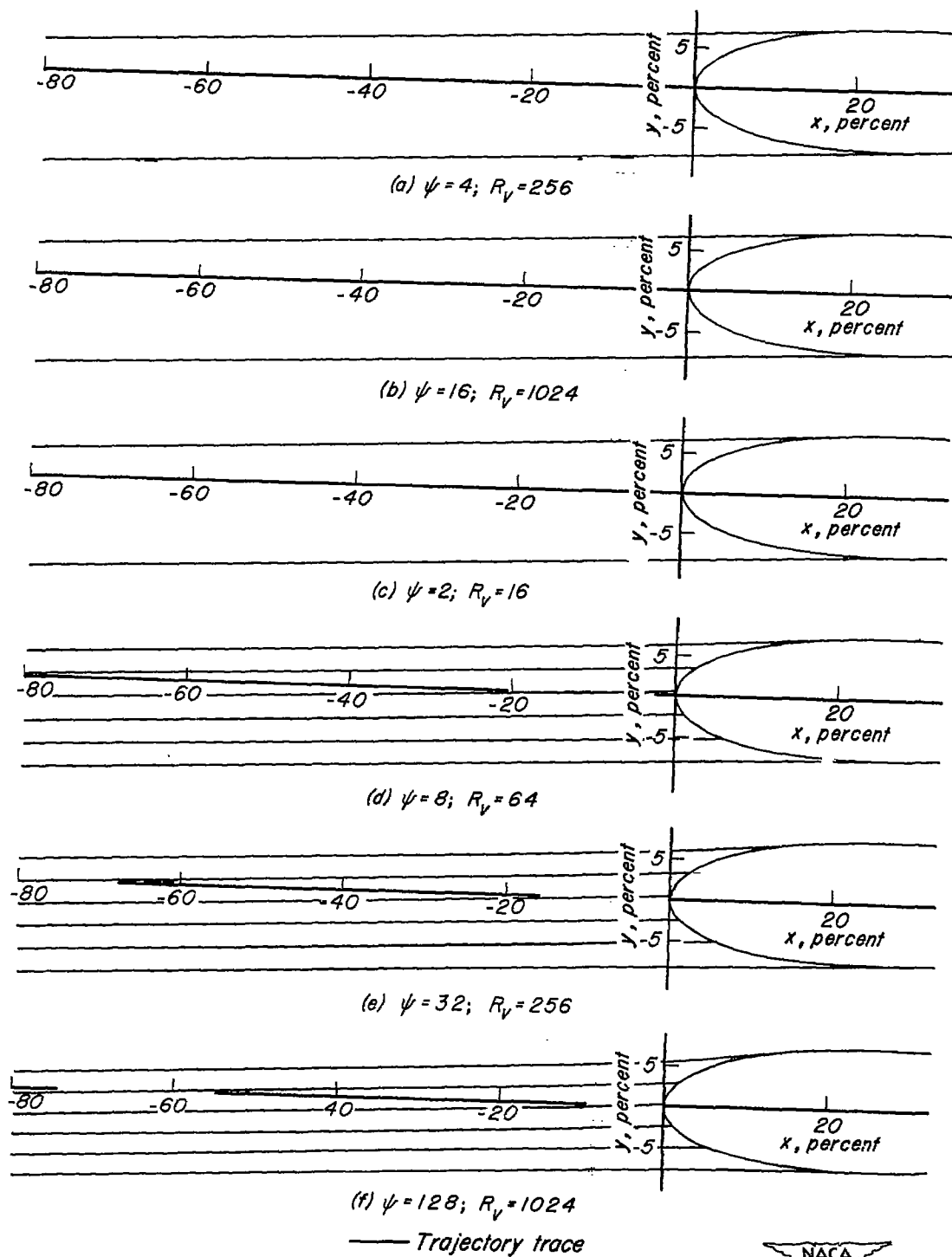
——— Trajectory trace

Figure 3.- Water-drop trajectory traces from a differential analyzer for a 15-percent-thick symmetrical Joukowski airfoil; $c_l = 0.22$; $a = 2°$.

(g) $\psi = 16$; $R_v = 16$

(h) $\psi = 64$; $R_v = 64$

(i) $\psi = 256$; $R_v = 256$

(j) $\psi = 1024$; $R_v = 1024$

(k) $\psi = 128$; $R_v = 16$

(l) $\psi = 512$; $R_v = 64$

Figure 3.- Continued.

(m) $\psi = 2048$; $R_v = 256$

(n) $\psi = 8192$; $R_v = 1024$

(o) $\psi = 1024$; $R_v = 16$

(p) $\psi = 4096$; $R_v = 64$

Figure 3.- Continued.

(q) $\psi = 16384$; $R_v = 256$

Figure 3.- Concluded.

(a) $\psi = 4$; $R_V = 256$

(b) $\psi = 16$; $R_V = 1024$

(c) $\psi = 2$; $R_V = 16$

(d) $\psi = 8$; $R_V = 64$
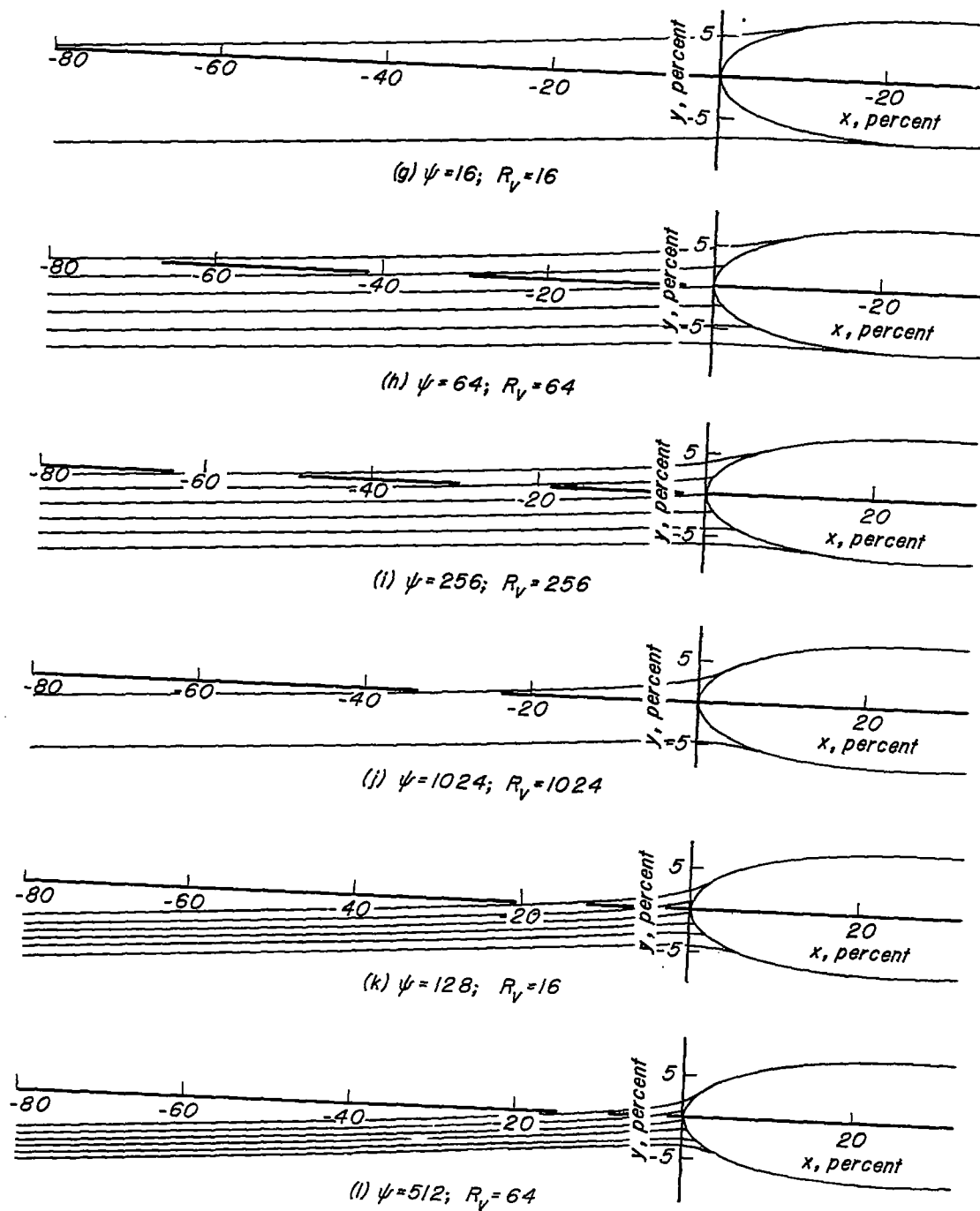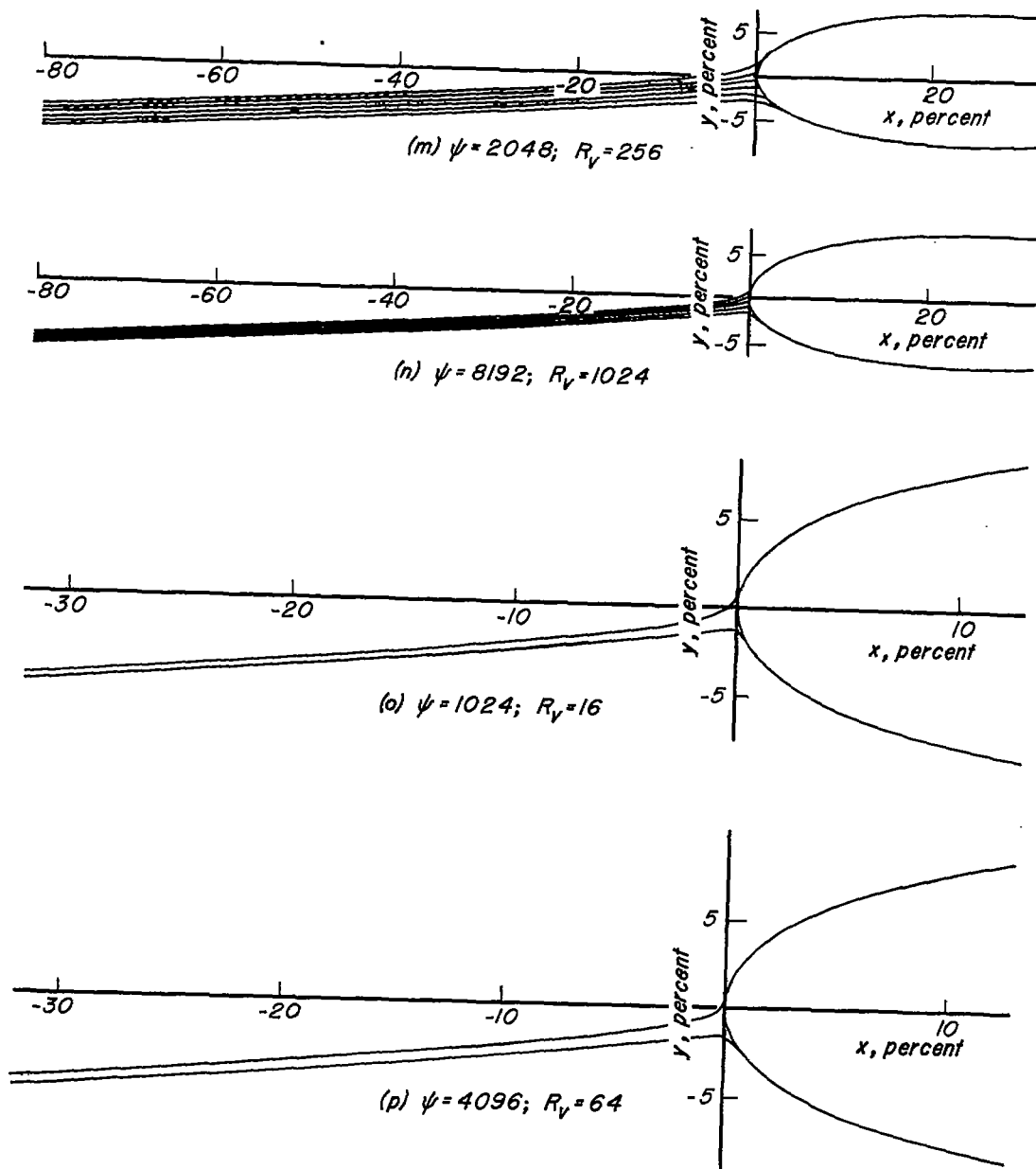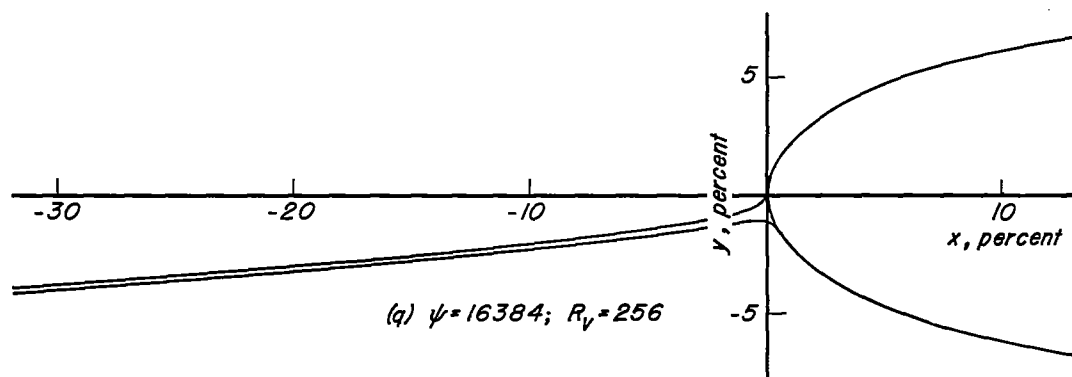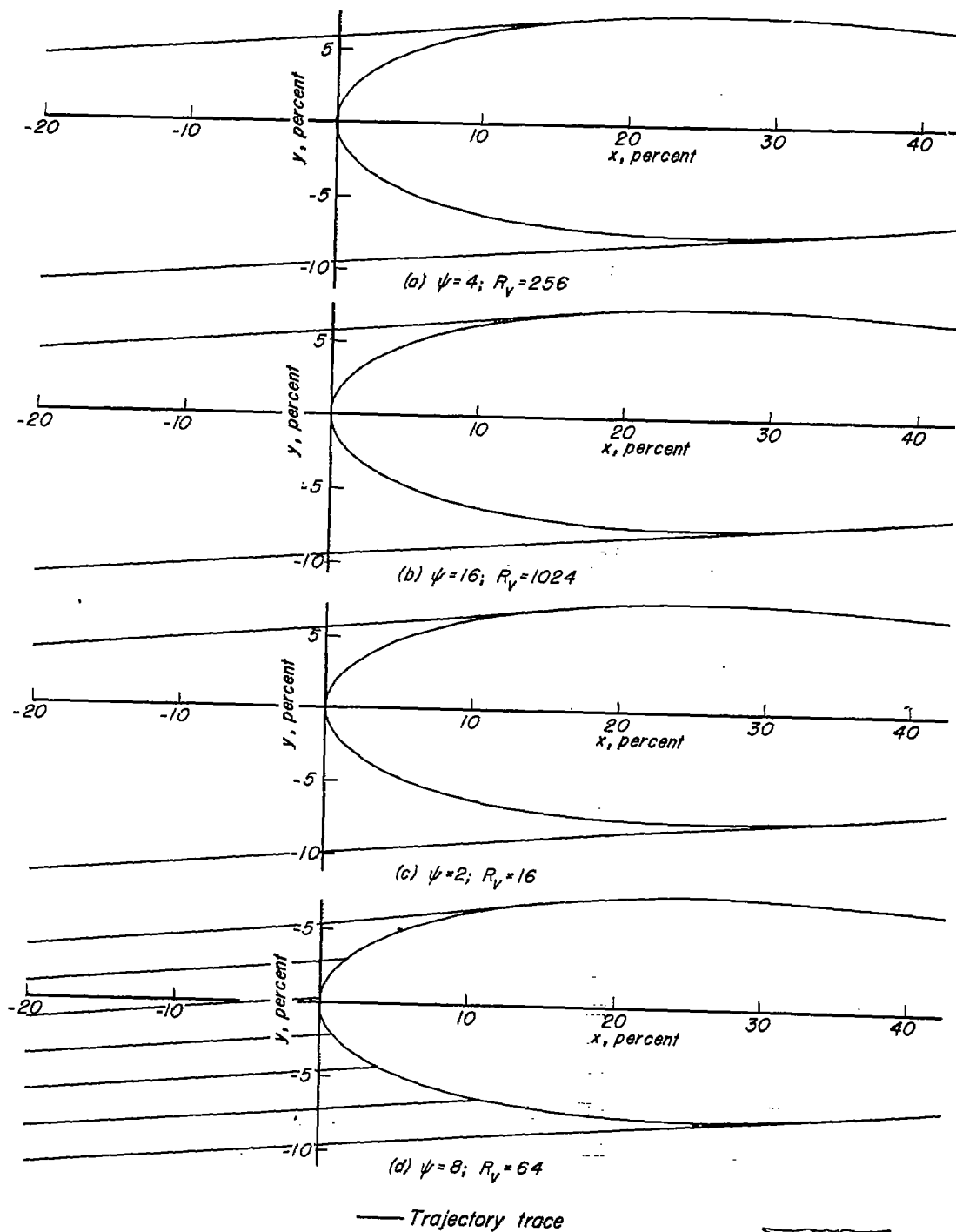
——— Trajectory trace

Figure 4.—Water-drop trajectory traces from a differential analyzer for a 15-percent-thick symmetrical Joukowski airfoil; $c_l = 0.44$; $\alpha = 4°$.

(e) $\psi = 32$; $R_v = 256$

(f) $\psi = 128$; $R_v = 1024$

(g) $\psi = 16$; $R_v = 16$

(h) $\psi = 64$; $R_v = 64$

Figure 4.- Continued.

(i) $\psi = 256$; $R_V = 256$

(j) $\psi = 1024$; $R_V = 1024$

(k) $\psi = 128$; $R_V = 16$

(l) $\psi = 512$; $R_V = 64$

Figure 4.- Continued.

81

(m) $\psi = 2048$; $R_v = 256$

(n) $\psi = 8192$; $R_v = 1024$

(o) $\psi = 1024$; $R_v = 16$

(p) $\psi = 4096$; $R_v = 64$

Figure 4. - Continued.

(q) $\psi = 16384$; $R_v = 256$

Figure 4.- Concluded.

(a) $\psi = 4$; $R_V = 256$

(b) $\psi = 16$; $R_V = 1024$

(c) $\psi = 2$; $R_V = 16$

(d) $\psi = 8$; $R_V = 64$

(e) $\psi = 32$; $R_V = 256$

(f) $\psi = 128$; $R_V = 1024$
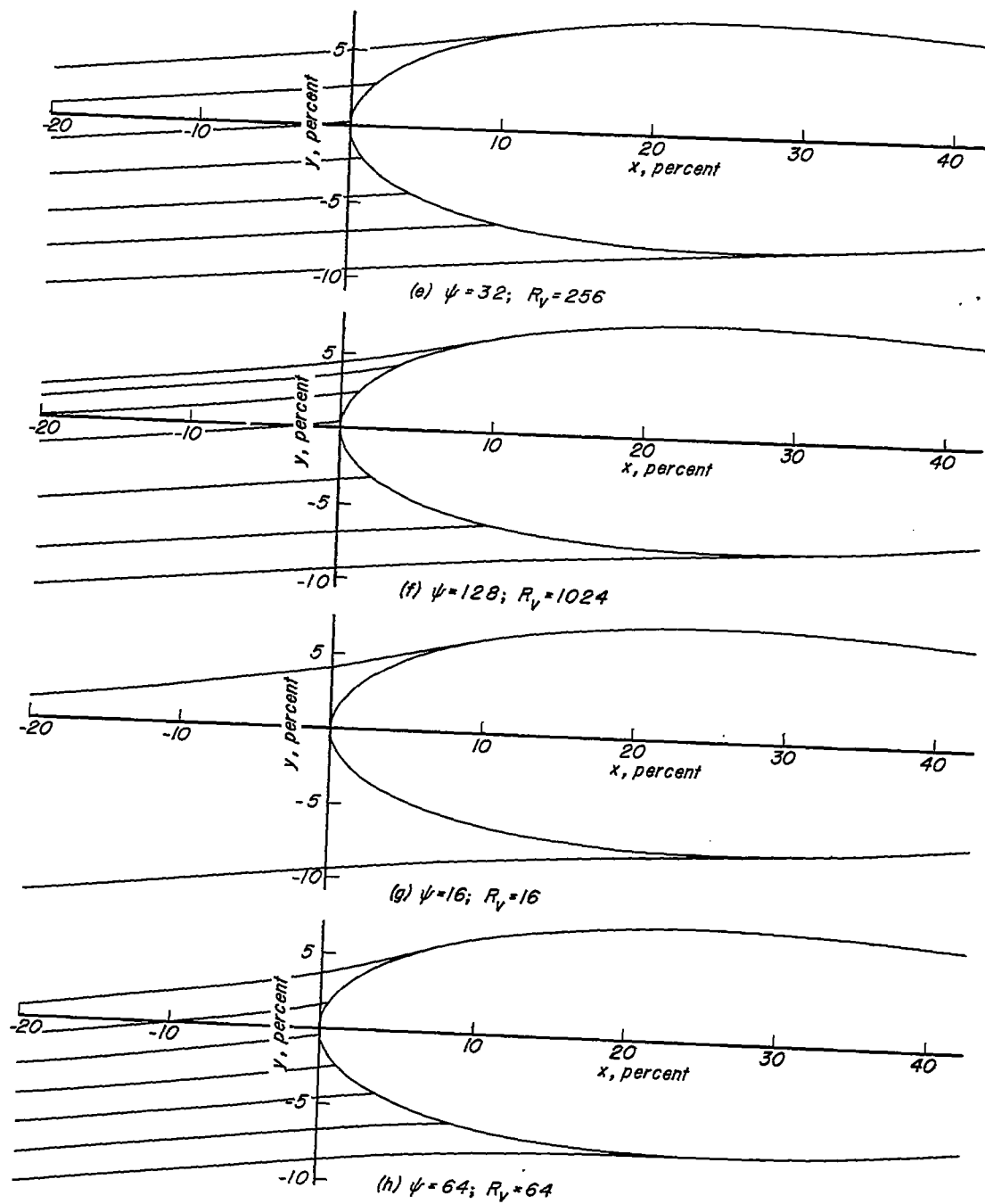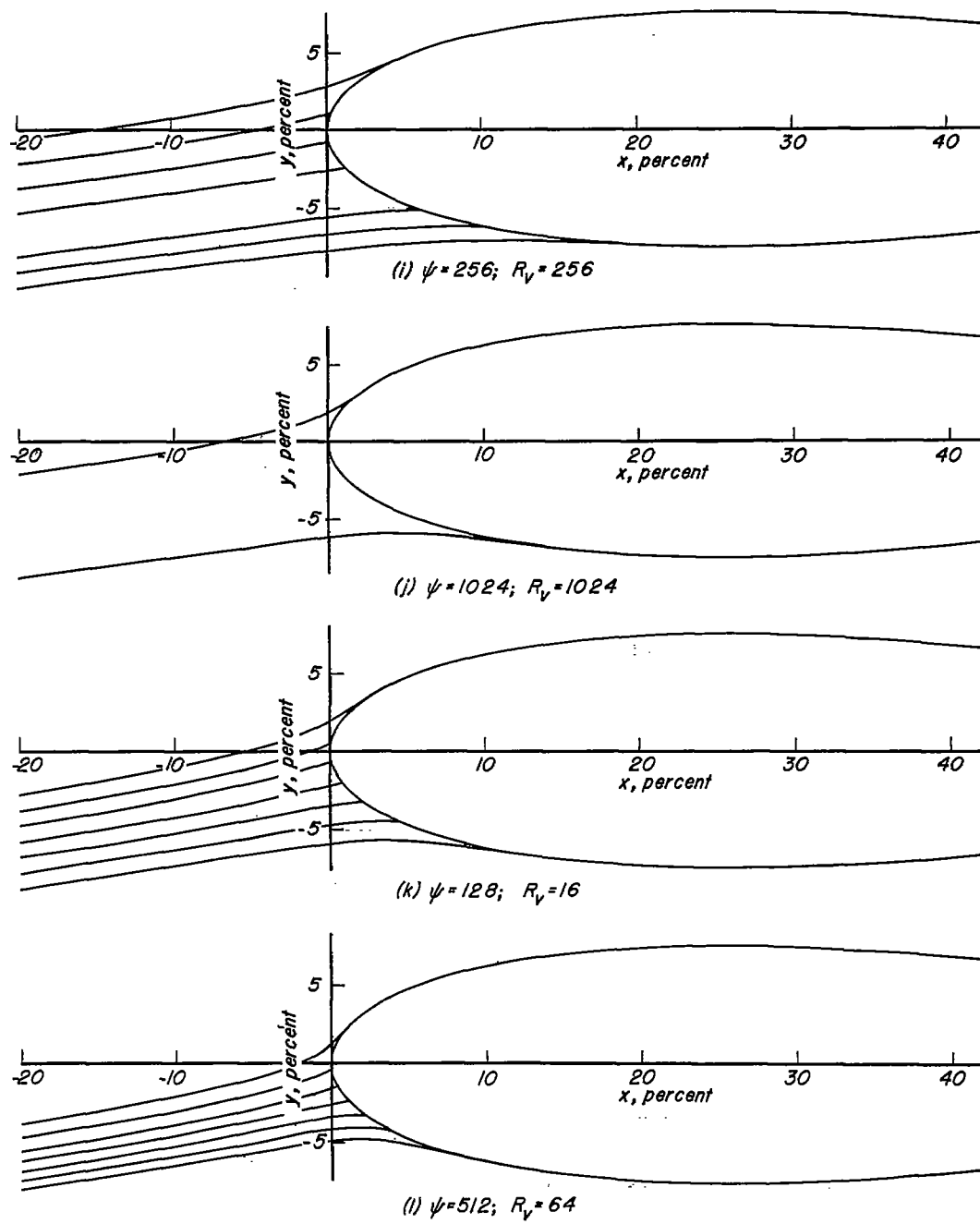
——— Trajectory trace

Figure 5.— Water-drop trajectory traces from a differential analyzer for a 15-percent-thick cambered Joukowski airfoil; a = 1.0 mean line; c_l = 0.44; α = 0°.

-80   -60   -40   -20 y, percent   5   20   x, percent   -5

(g) $\psi = 16$; $R_v = 16$

-80   -60   -40   -20 y, percent   5   20   x, percent   -5

(h) $\psi = 64$; $R_v = 64$

-80   -60   -40   -20 y, percent   -5   20   x, percent   -5

(i) $\psi = 256$; $R_v = 256$

-80   -60   -40   -20 y, percent   5   20   x, percent   -5

(j) $\psi = 1024$; $R_v = 1024$

-80   -60   -40   -20 y, percent   5   20   x, percent   .5

(k) $\psi = 128$; $R_v = 16$

-80   -60   -40   -20 y, percent   5   20   x, percent   .5

(l) $\psi = 512$; $R_v = 64$.

NACA

Figure 5.- Continued.

(m) $\psi = 2048$; $R_v = 256$

(n) $\psi = 8192$; $R_v = 1024$

(o) $\psi = 1024$; $R_v = 16$

(p) $\psi = 4096$; $R_v = 64$

Figure 5.- Continued.

(q) $\psi = 16384$; $R_v = 256$

Figure 5.- Concluded.

(a) $\psi = 4$; $R_V = 256$

(b) $\psi = 16$; $R_V = 1024$

(c) $\psi = 2$; $R_V = 16$

(d) $\psi = 8$; $R_V = 64$

———— Trajectory trace

Figure 6.—Water-drop trajectory traces from a differential analyzer for an NACA 65$_2$-015 airfoil; $c_l = 0.44$; $\alpha = 4°$.

(e) $\psi = 32$; $R_v = 256$

(f) $\psi = 128$; $R_v = 1024$

(g) $\psi = 16$; $R_v = 16$

(h) $\psi = 64$; $R_v = 64$

Figure 6.- Continued.

(i) $\psi = 256$; $R_V = 256$

(j) $\psi = 1024$; $R_V = 1024$

(k) $\psi = 128$; $R_V = 16$

(l) $\psi = 512$; $R_V = 64$
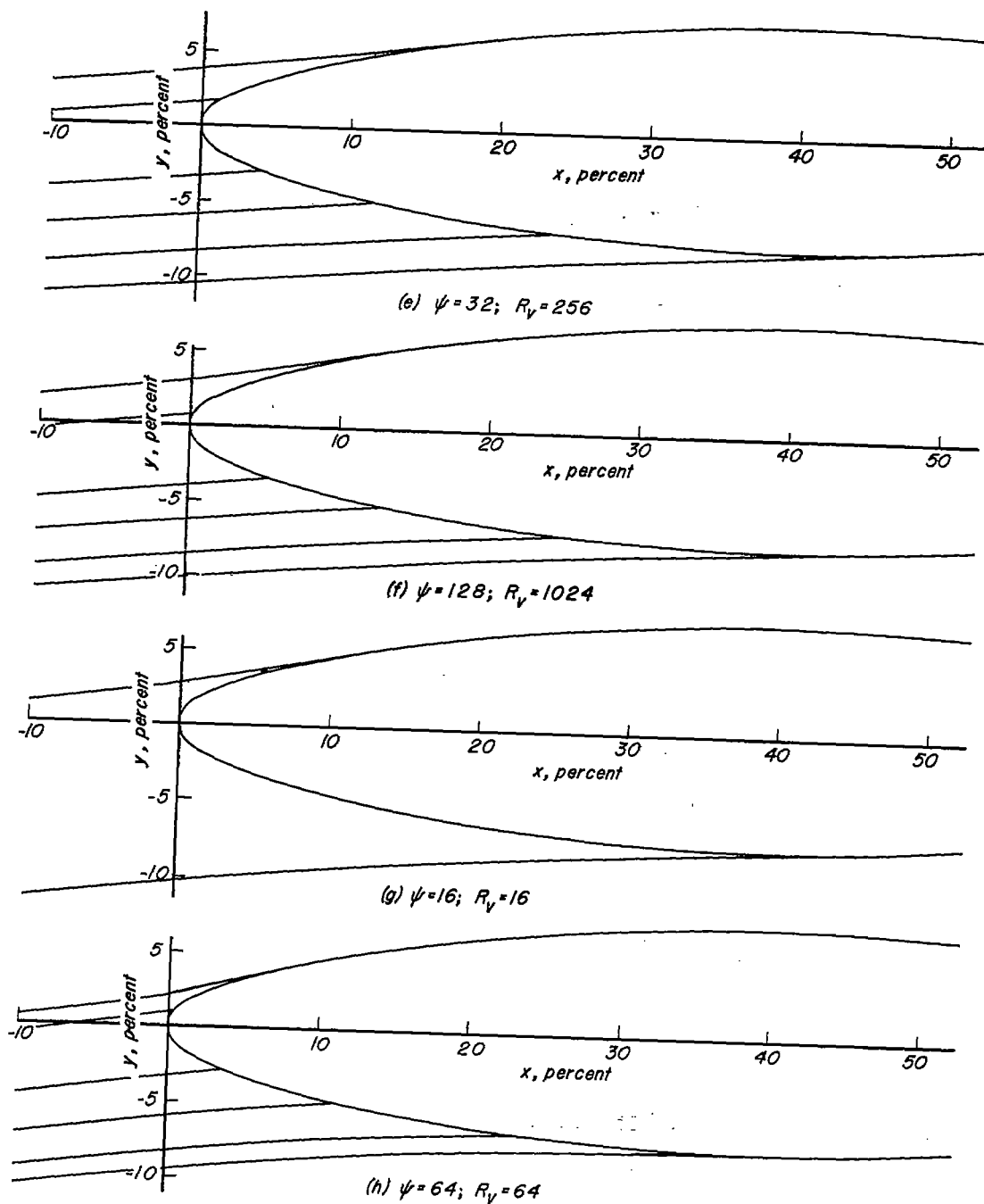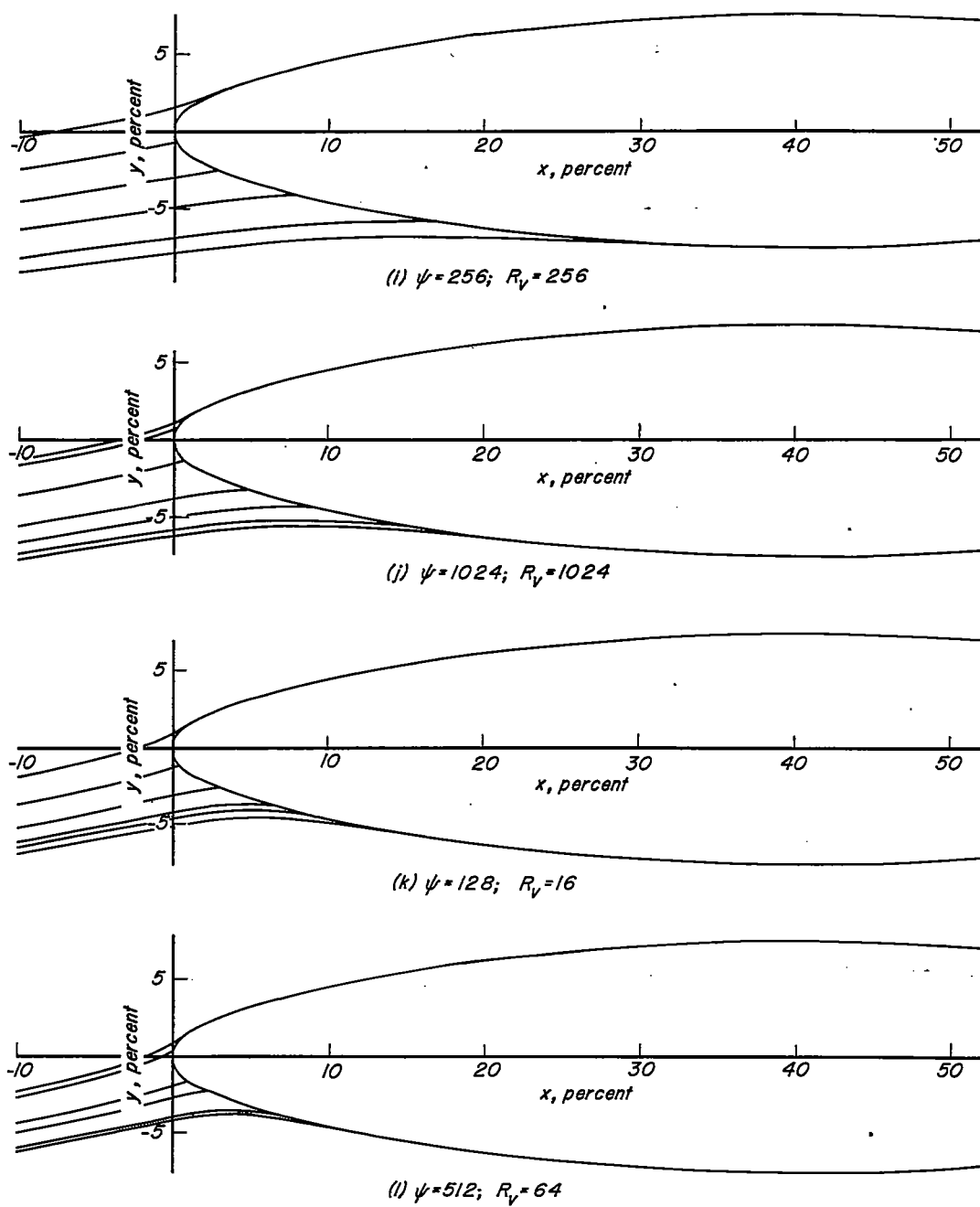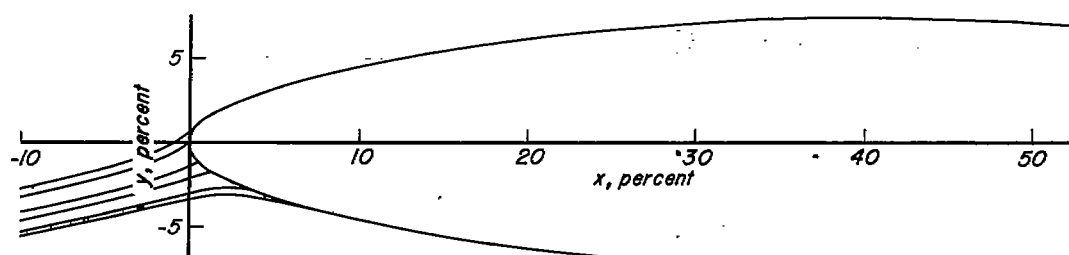
Figure 6.- Continued.

(m) $\psi = 2048$; $R_v = 256$
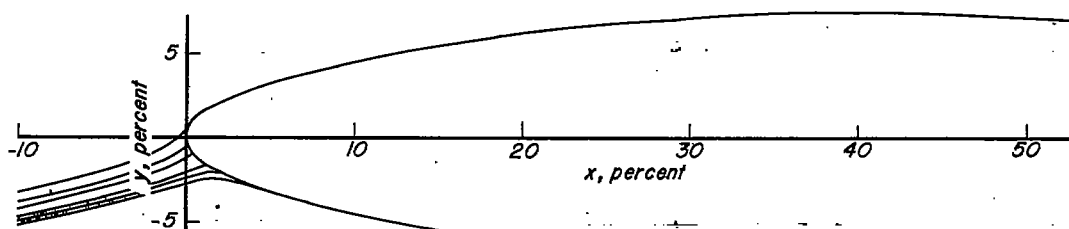
(n) $\psi = 8192$; $R_v = 1024$
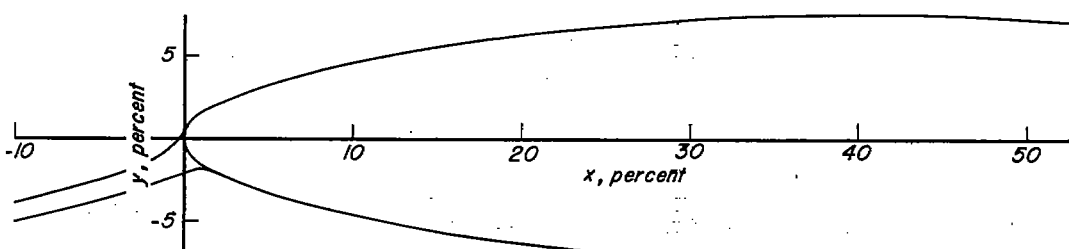
(o) $\psi = 1024$; $R_v = 16$
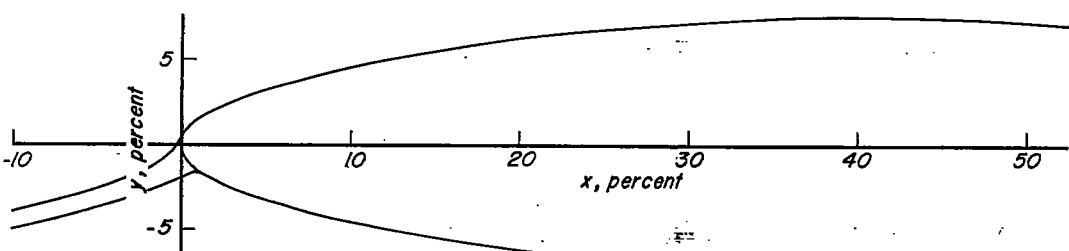
(p) $\psi = 4096$; $R_v = 64$

Figure 6.- Continued.

(q) $\psi = 16384$; $R_V = 256$
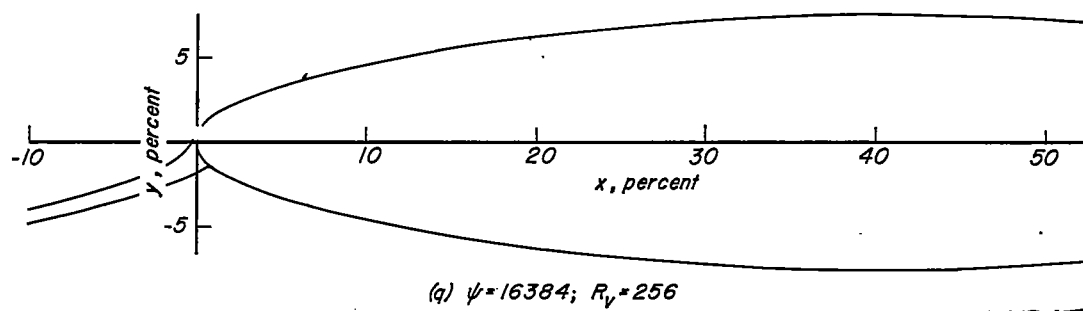
Figure 6.— Concluded.
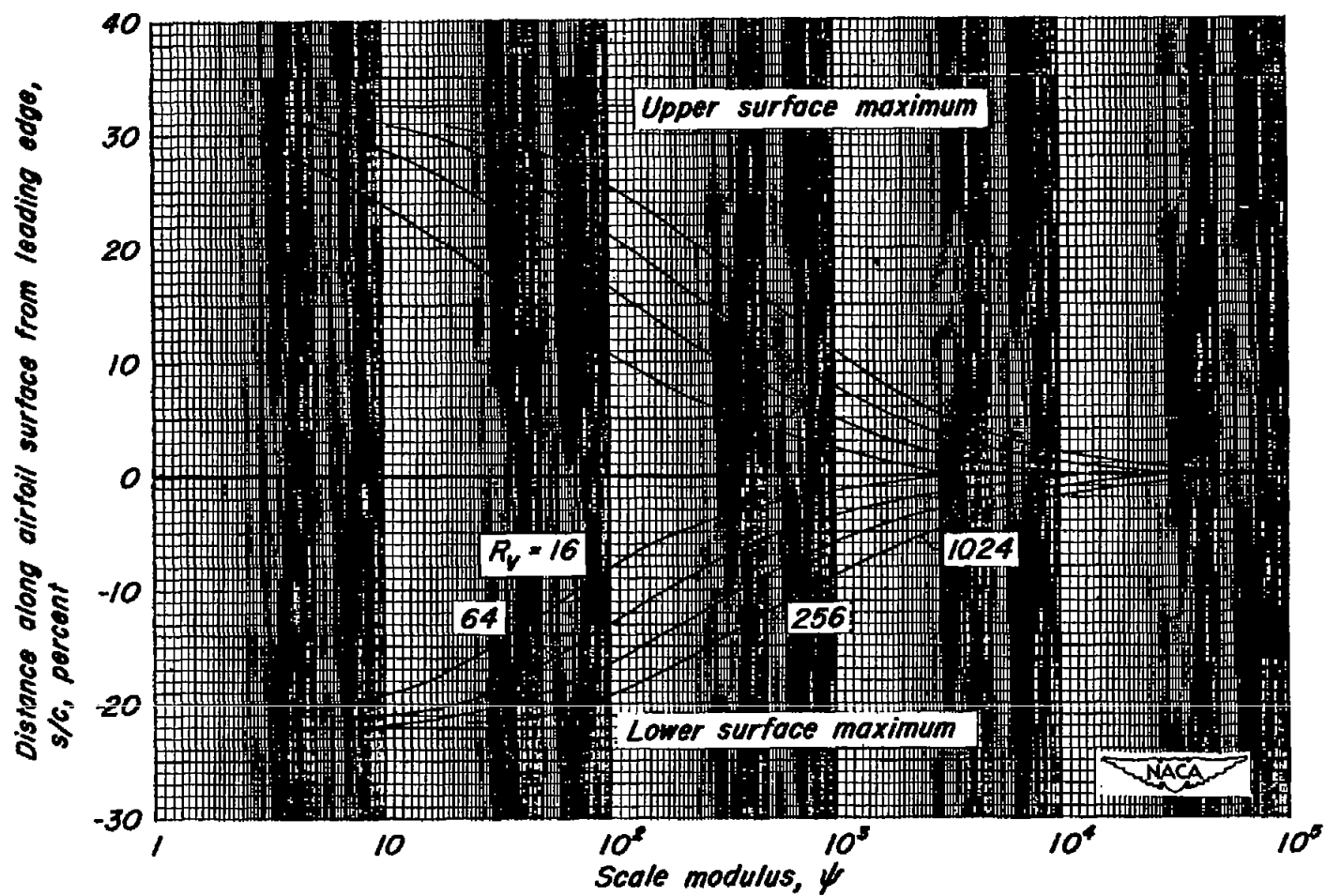
Figure 7.— Typical relation between farthest position of drop impingement, scale modulus, and free-stream drop Reynolds number as exemplified by a 15-percent-thick cambered Joukowski airfoil; $c_l = 0.44$; $a = 0°$; $a = 1.0$ mean line.
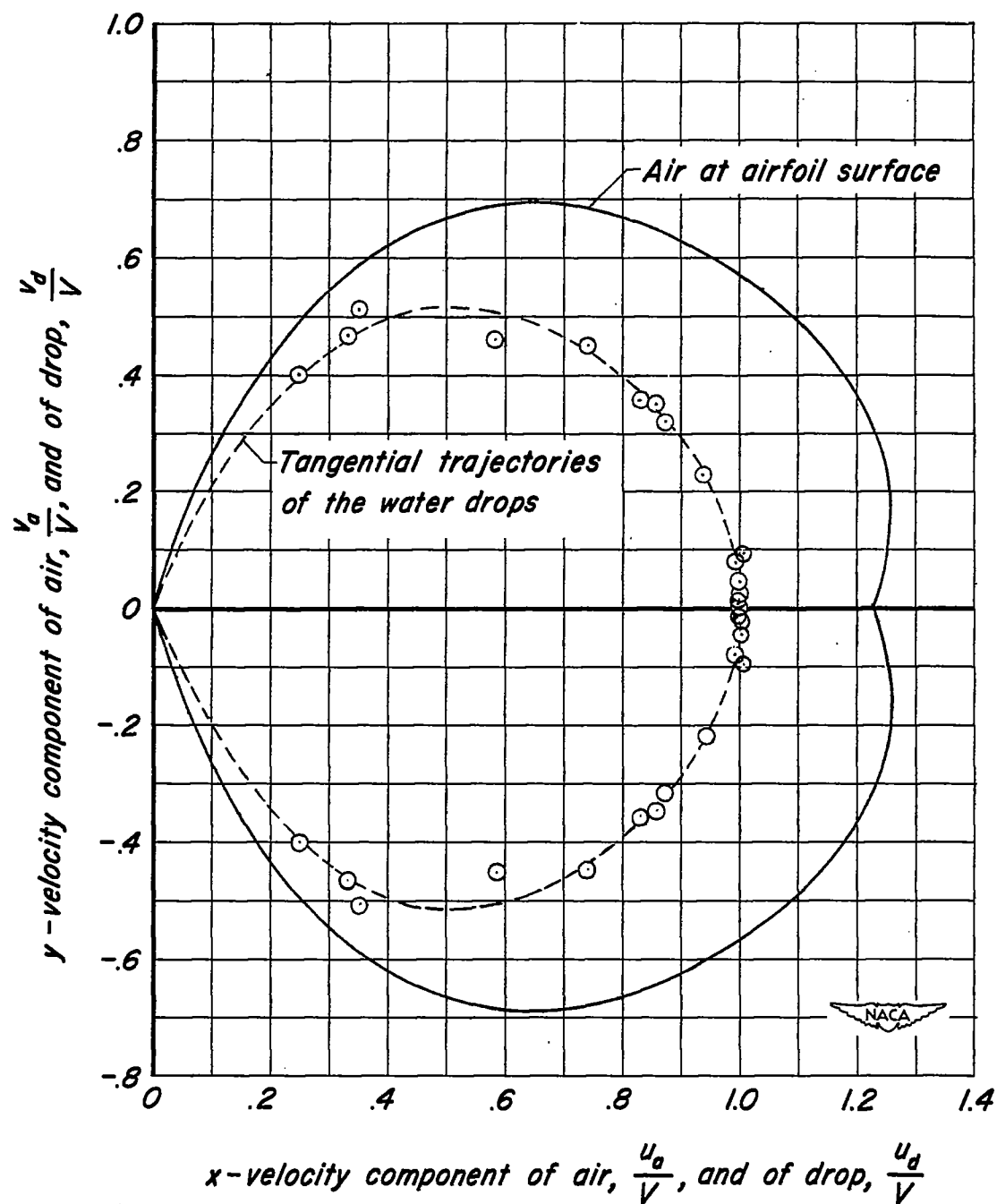
(a) 15-percent-thick symmetrical Joukowski airfoil, $\alpha = 0°$.

Figure 8.— Hodograph of tangential-trajectory, velocities and hodograph of air velocities on the airfoil surface.
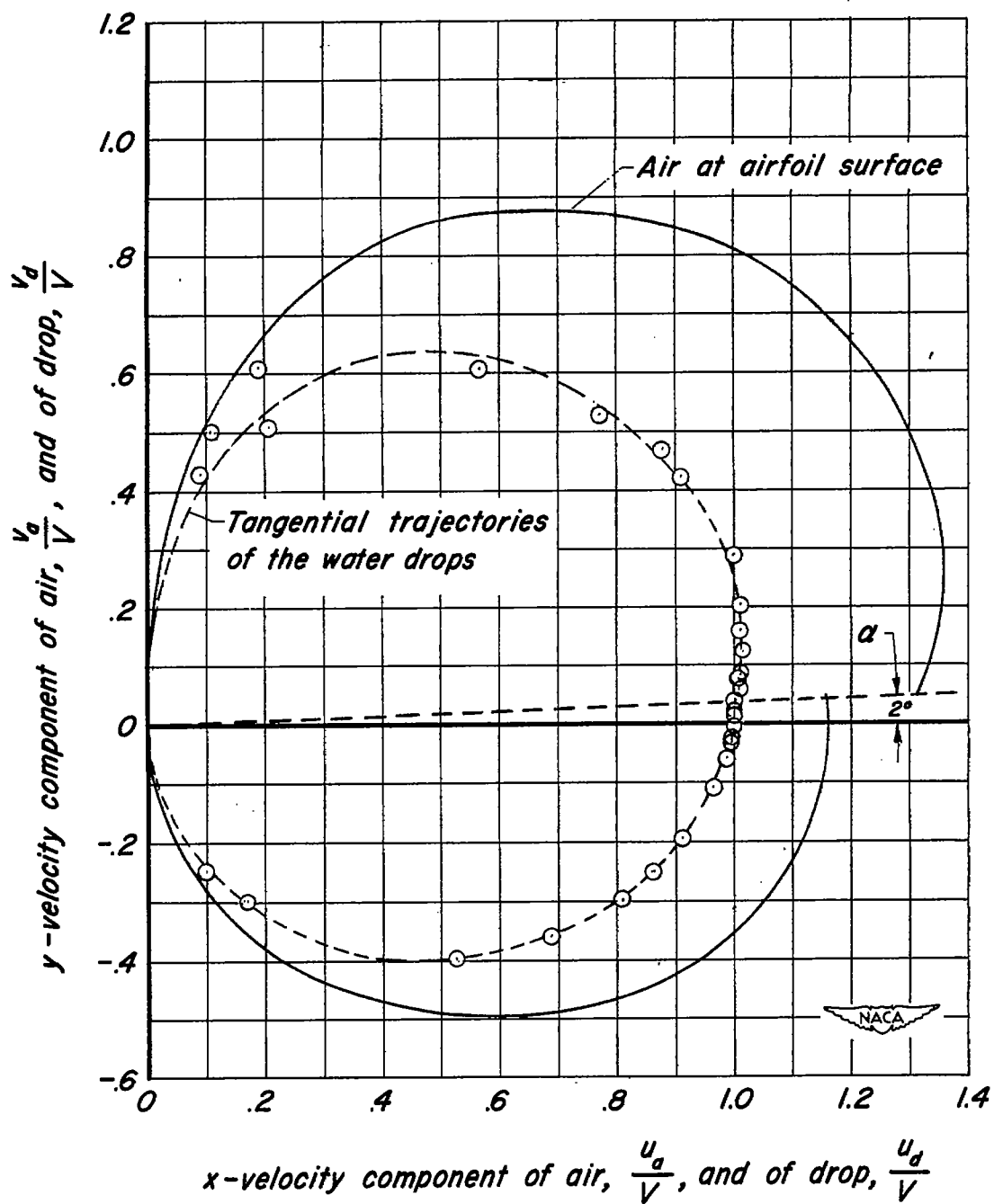
(b) 15-percent-thick symmetrical Joukowski airfoil, $\alpha = 2°$.

Figure 8. — Continued.
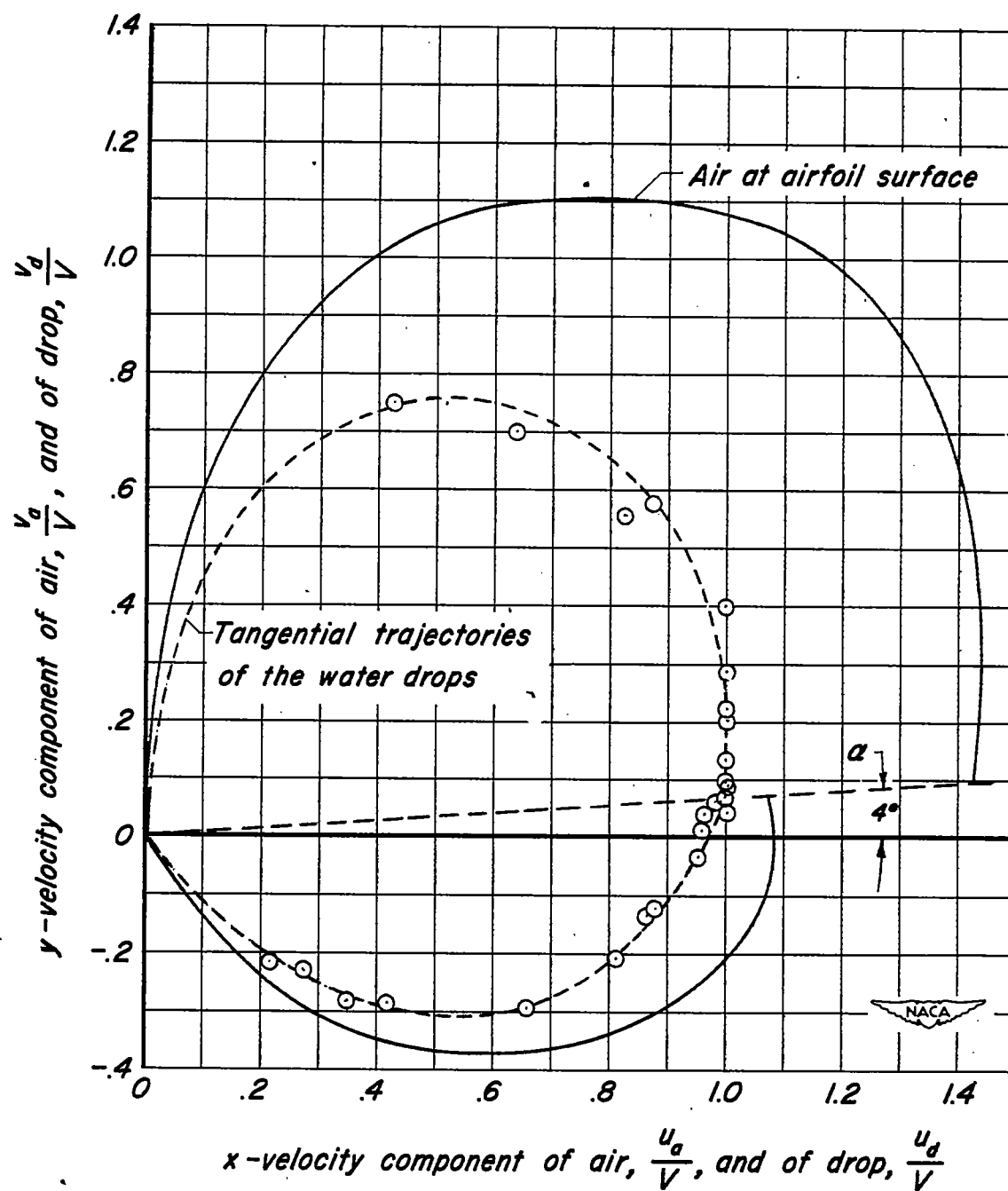
(c) 15-percent-thick symmetrical Joukowski airfoil, α = 4°

Figure 8. — Continued.
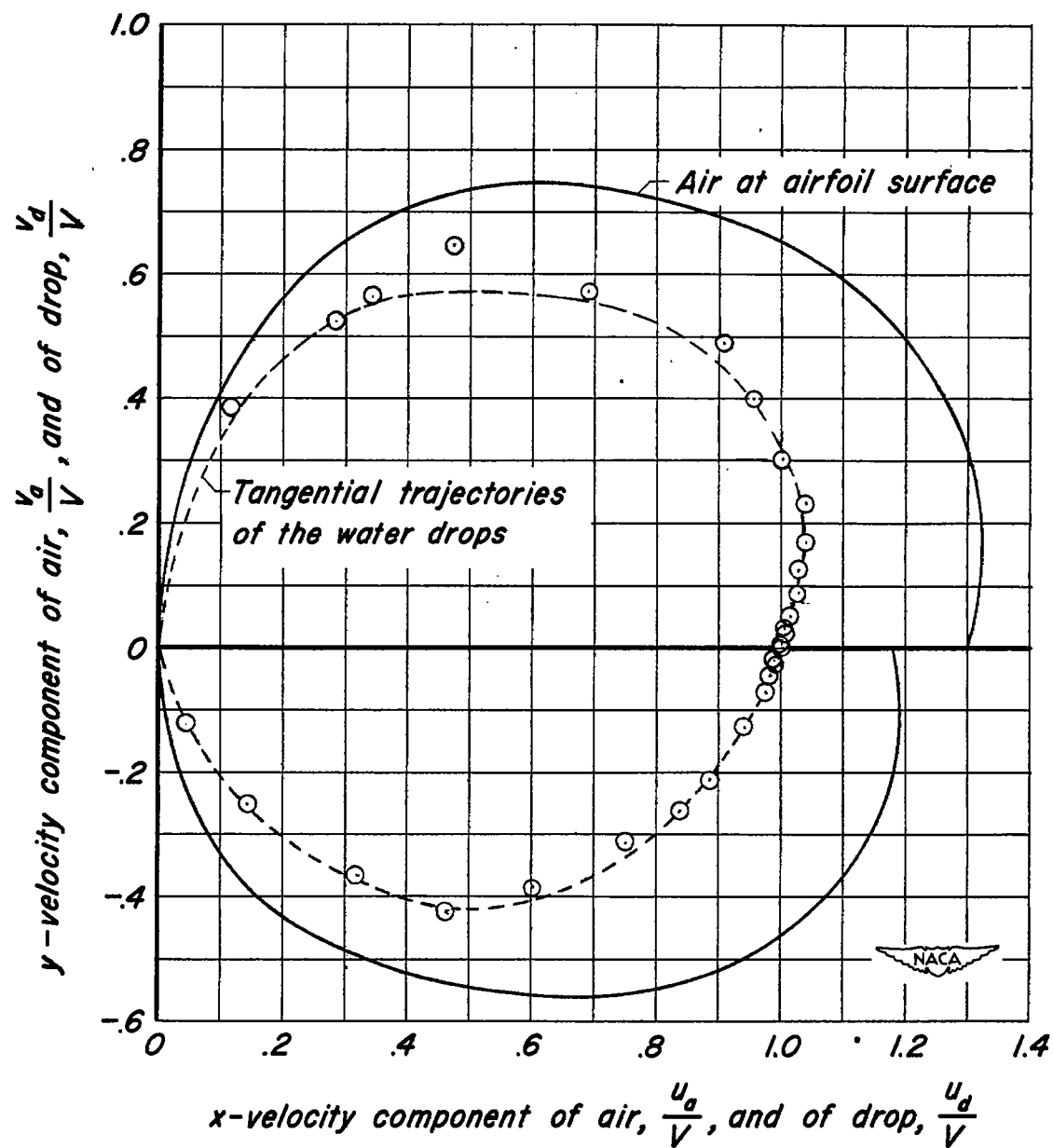
(d) 15-percent-thick cambered Joukowski airfoil; a = 1.0;
α = 0°.

Figure 8.- Continued.

(e) NACA 65_2-015 airfoil, $a = 4°$.

Figure 8.- Concluded.

Several trajectories impinging tangentially at a common point

Point of tangency, $(s/c)_t$

$\frac{U_a}{V}$

$\frac{U_d}{V}$

V

x-axis

a θ

y-axis

(a) Physical plane.

$\frac{v_d}{V}$

y-velocity component of air, $\frac{v_a}{V}$, and of drop, $\frac{v_d}{V}$

$\frac{U_a}{V}$ $\frac{U_d}{V}$

$\left(\frac{R}{R_V}\right)_t = \sqrt{\left(\frac{v_a}{V} - \frac{v_d}{V}\right)^2 + \left(\frac{u_a}{V} - \frac{u_d}{V}\right)^2}$

Tangential trajectories

$(s/c)_t$

Air at airfoil surface

θ a

1.0

x-velocity component of air, $\frac{u_a}{V}$, and of drop, $\frac{u_d}{V}$
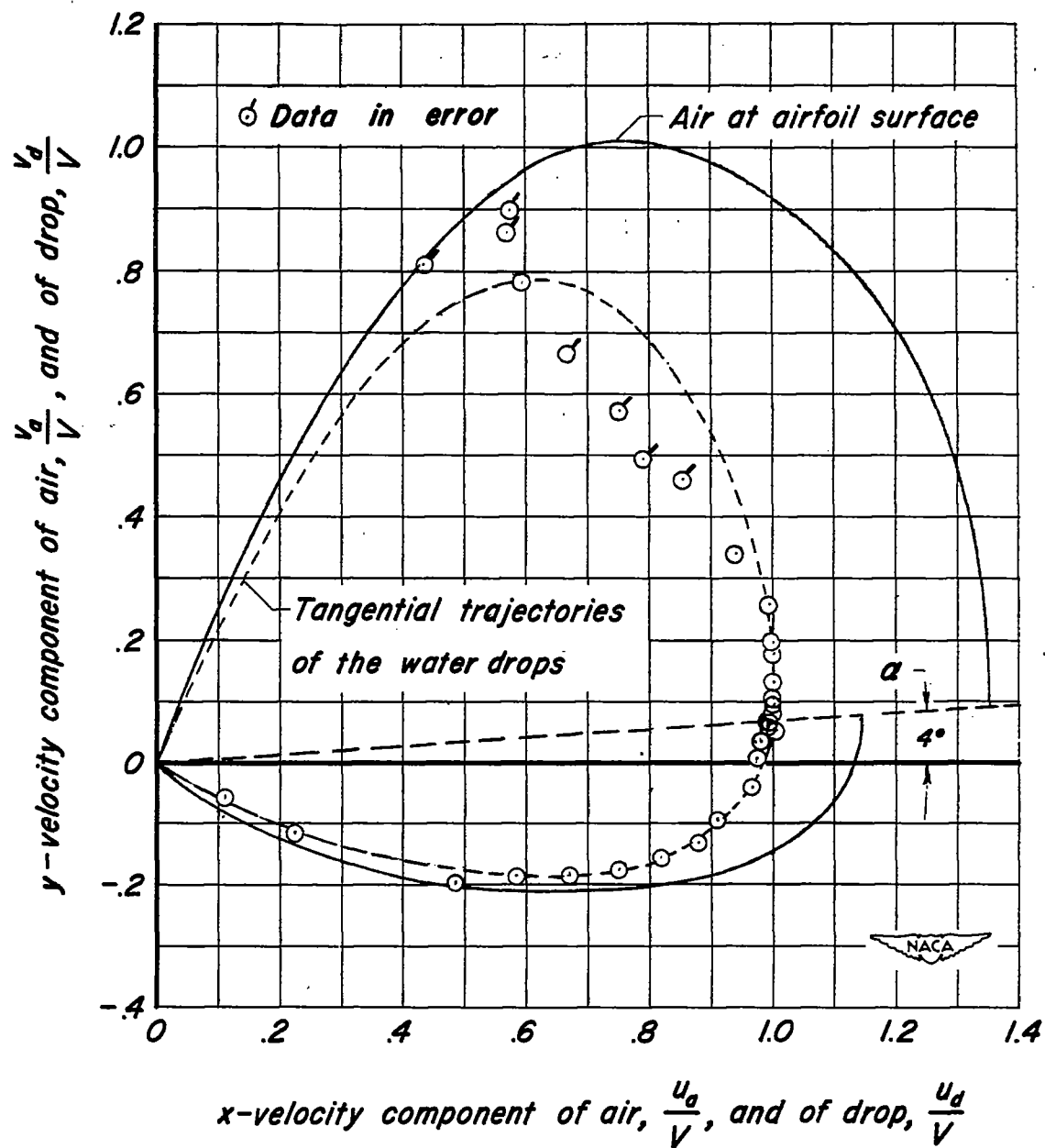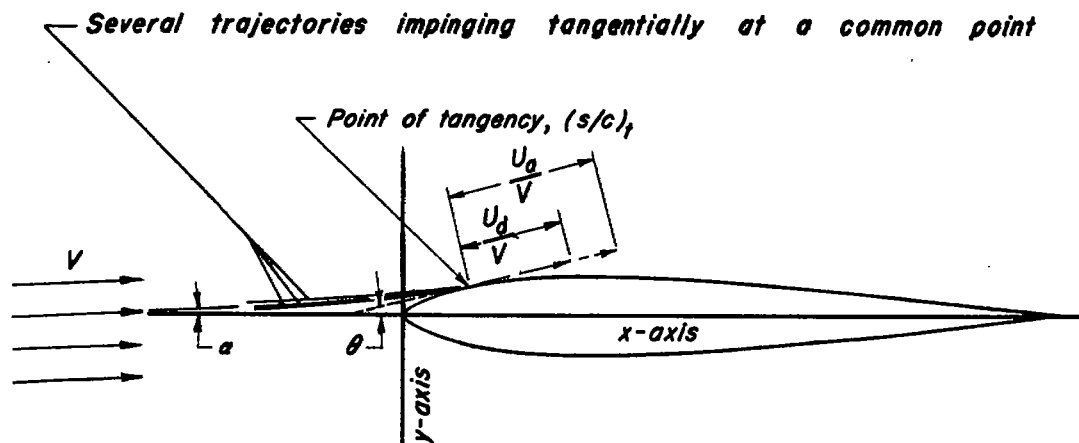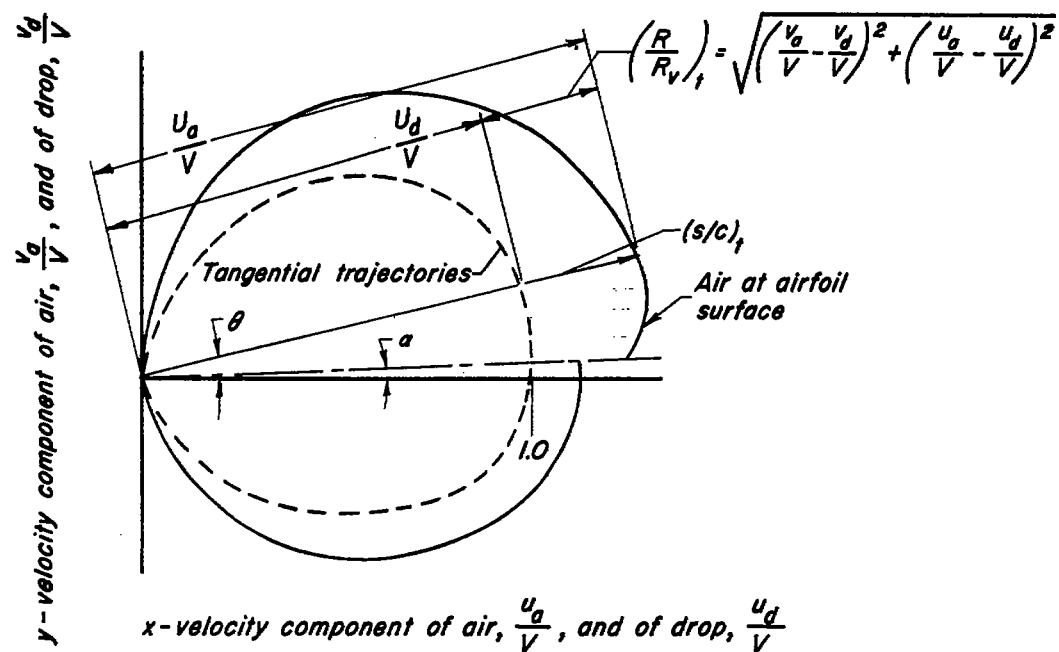
(b) Hodograph plane.

Figure 9.- Relationship between physical and hodograph planes for drop and air velocities at airfoil surface.
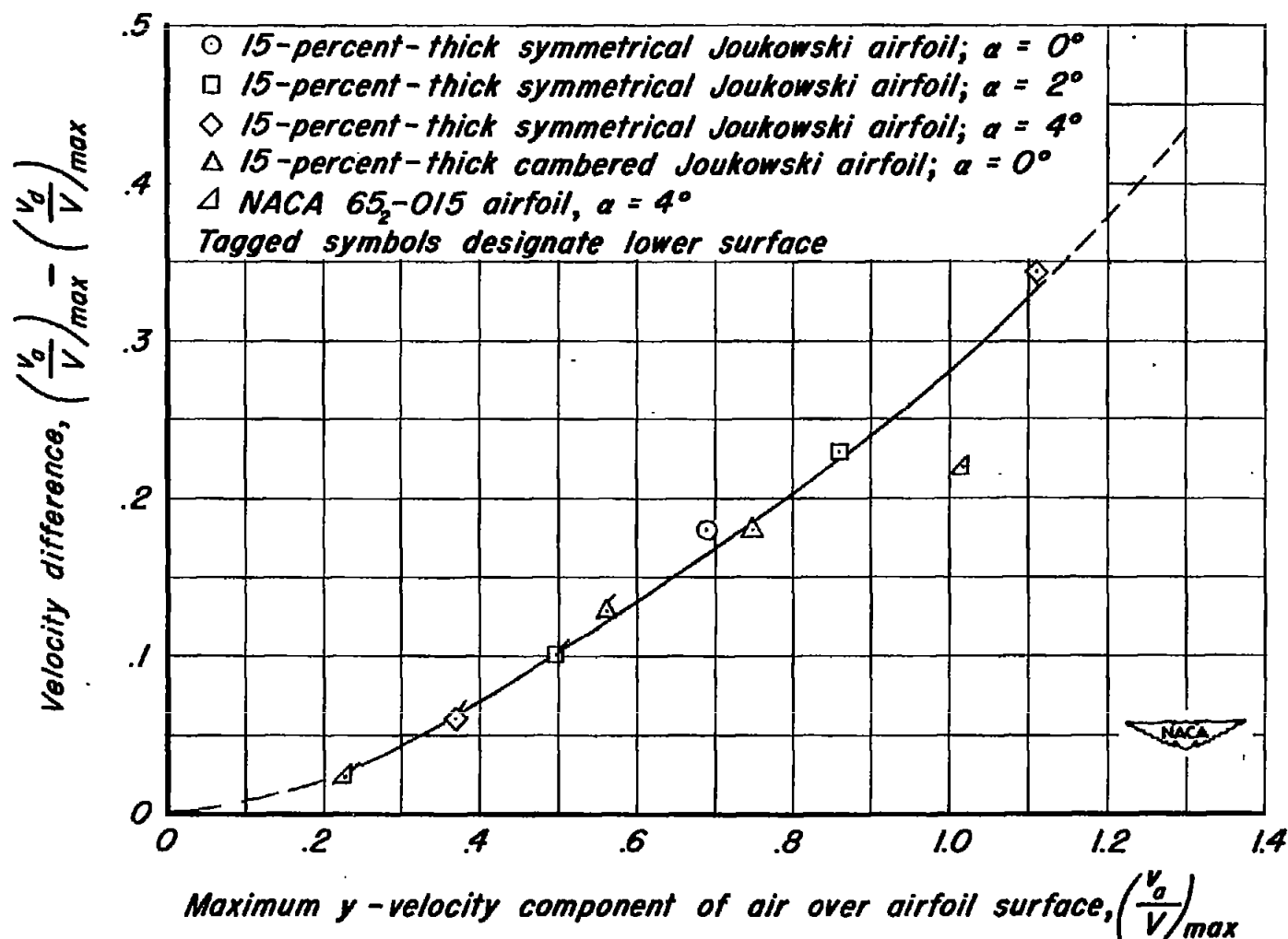
Figure 10.—Variation of velocity difference between drop and air with maximum y-velocity component of air for the five airfoil cases investigated.

Curve A based on $\dfrac{R}{R_V} = \left(\dfrac{R}{R_V}\right)_{v_{a_{max}}} \times \dfrac{\left(\dfrac{U_a}{V}\right)}{\left(\dfrac{U_a}{V}\right)_{v_{a_{max}}}}$

Curve C based on $\dfrac{R}{R_V} = $ constant

Curve D based on $\dfrac{\dfrac{R}{R_V}}{\dfrac{U_a}{V}} = $ constant
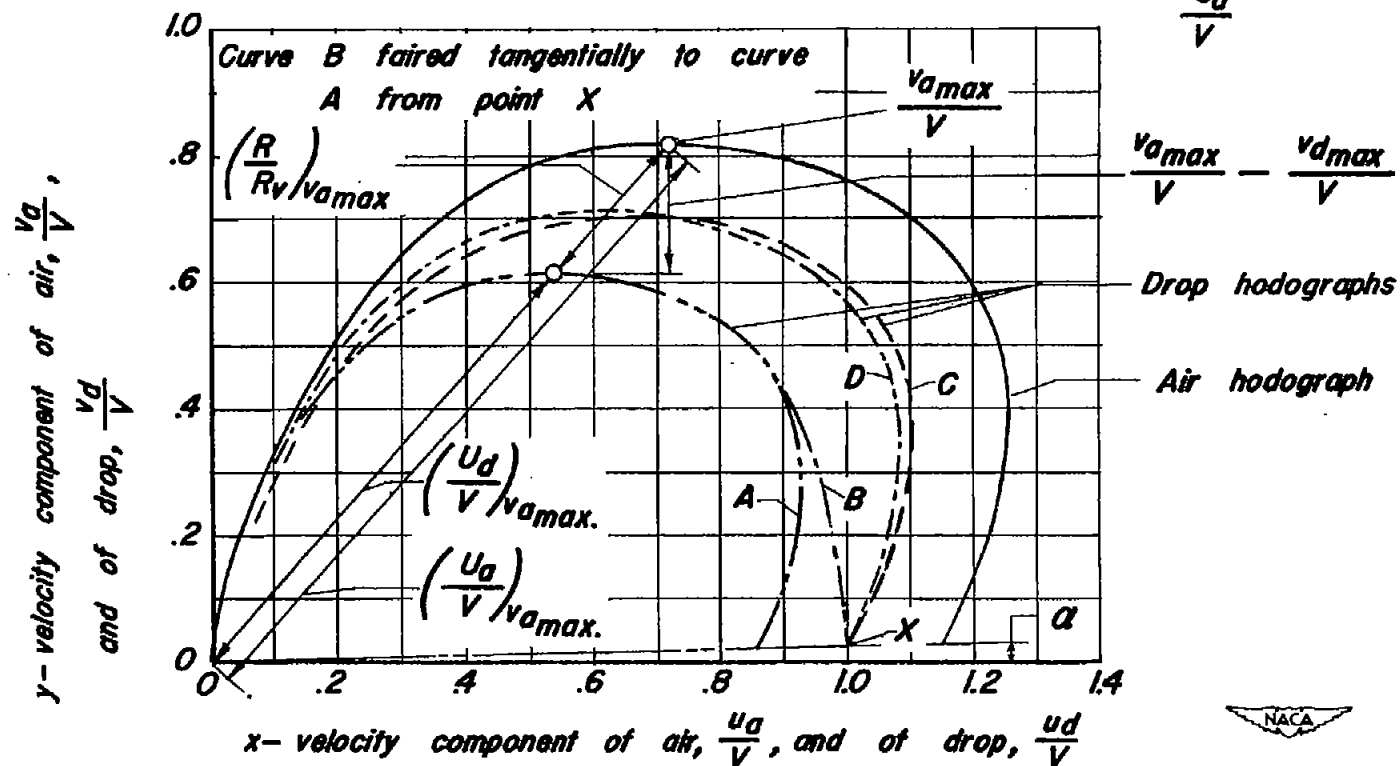
Figure 11.– Illustration of four possible techniques for the construction of a drop hodograph from a specified air hodograph.
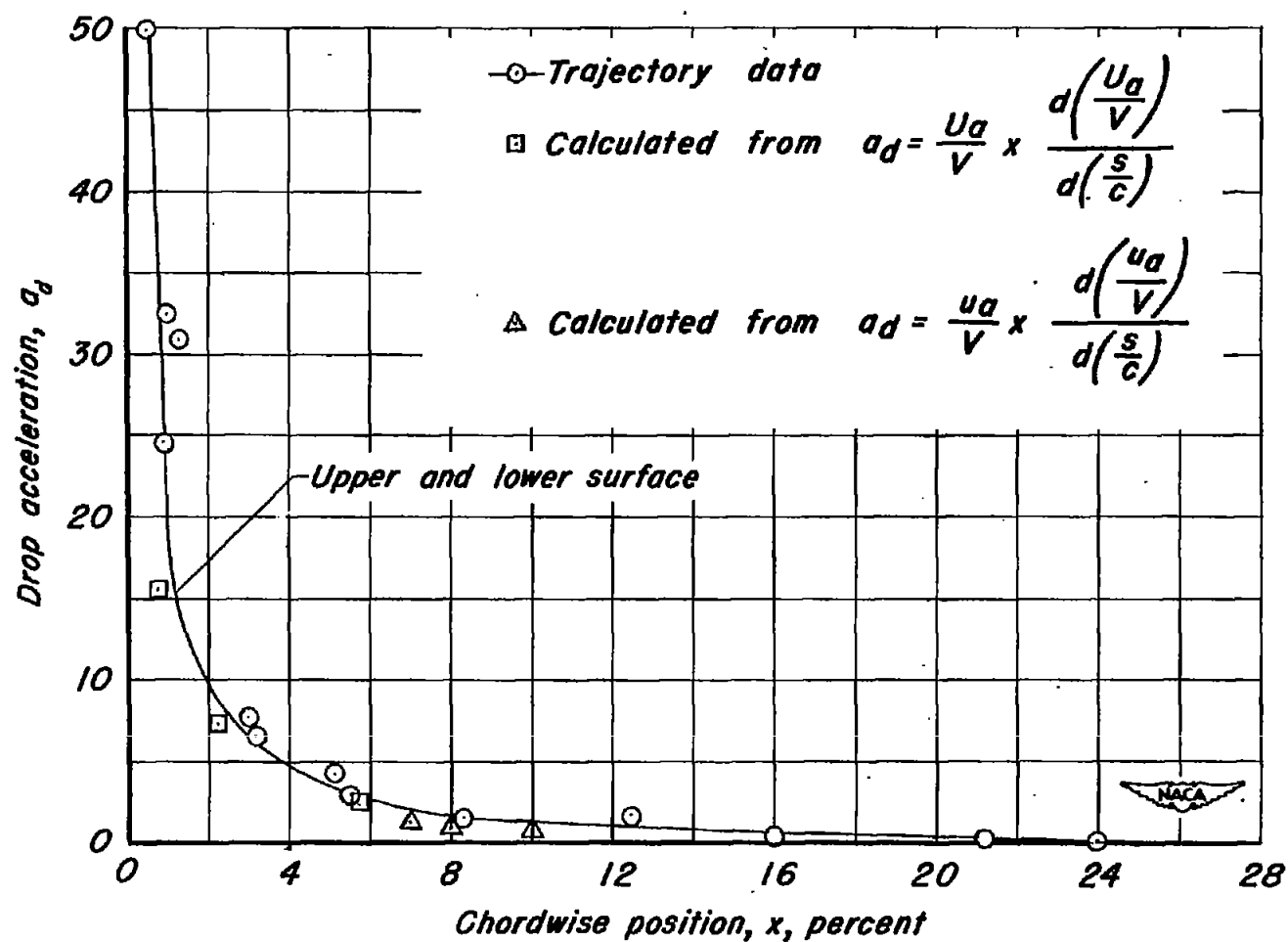
(a) 15-percent-thick symmetrical Joukowski airfoil; $a = 0^\circ$.

Figure 12.- Chordwise distribution of instantaneous drop-acceleration values for tangential trajectories at instant of drop impact.
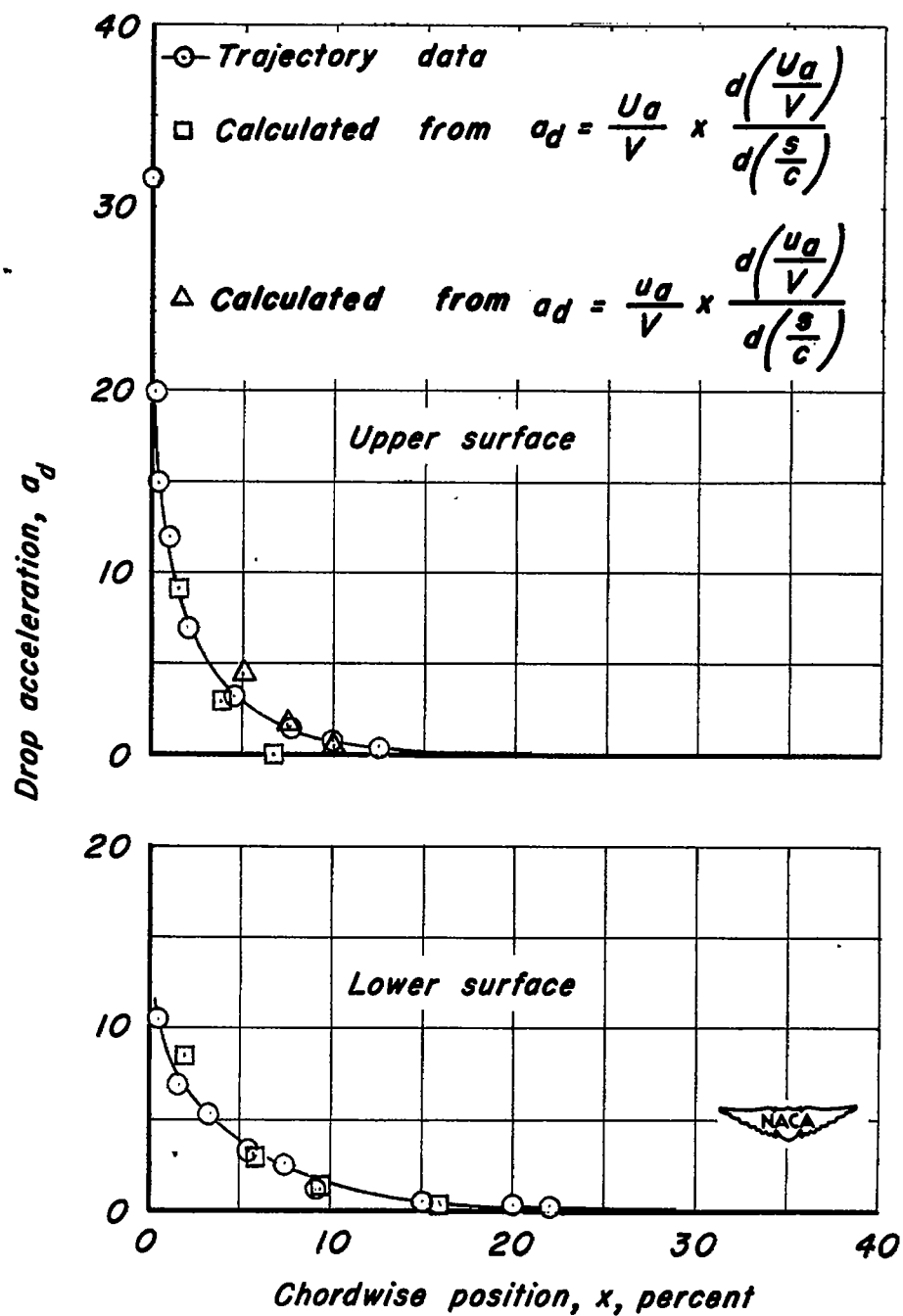
(b) 15-percent-thick symmetrical Joukowski
     airfoil; a = 2°.

Figure 12.- Continued.

$$a_d = \frac{U_a}{V} \times \frac{d\left(\frac{U_a}{V}\right)}{d\left(\frac{s}{c}\right)}$$

$$a_d = \frac{u_a}{V} \times \frac{d\left(\frac{u_a}{V}\right)}{d\left(\frac{s}{c}\right)}$$
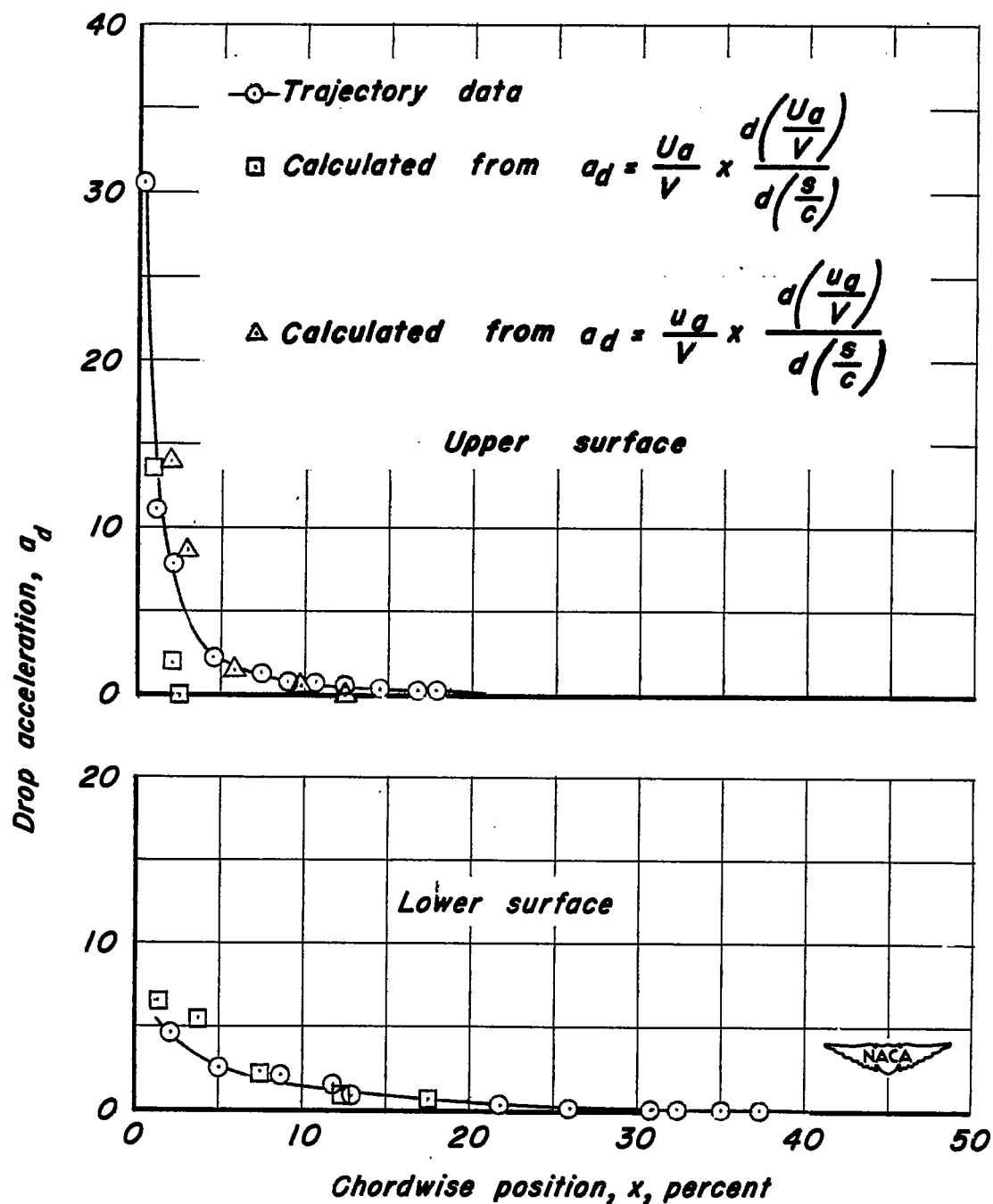
(c) 15-percent-thick symmetrical Joukowski airfoil; $a = 4°$.

Figure 12.— Continued.

(d) 15 - percent - thick cambered Joukowski
airfoil ; $a = 0°$; $a = 1.0$ mean line.

Figure 12.- Continued.

(e) NACA 65$_2$-015 airfoil; a = 4°.

Figure 12.- Concluded.
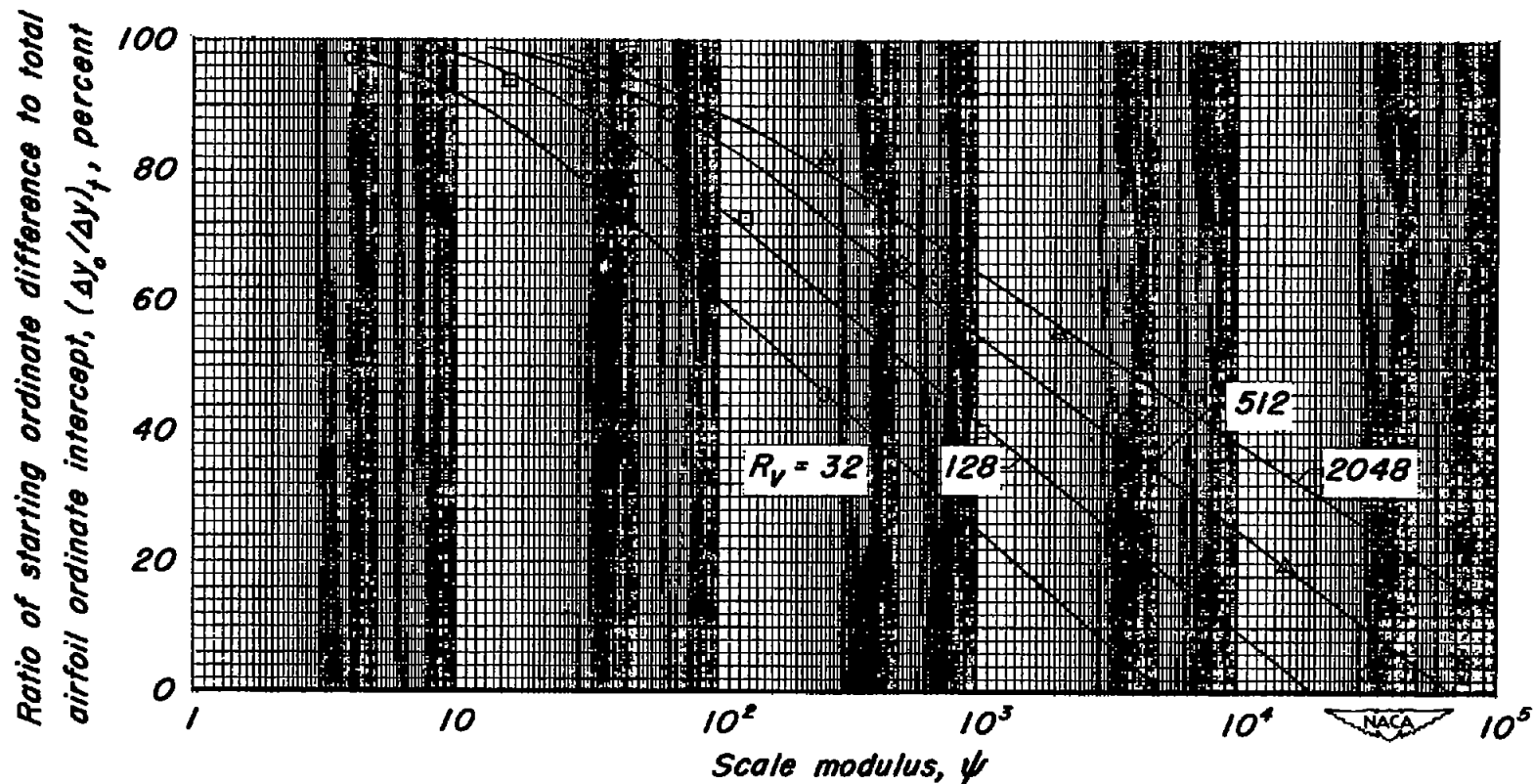
(a) 15-percent-thick symmetrical Joukowski airfoil; α = 0°.

Figure 13.- Ratio of trajectory starting ordinate difference to total airfoil ordinate intercept as a function of scale modulus and free-stream Reynolds number.
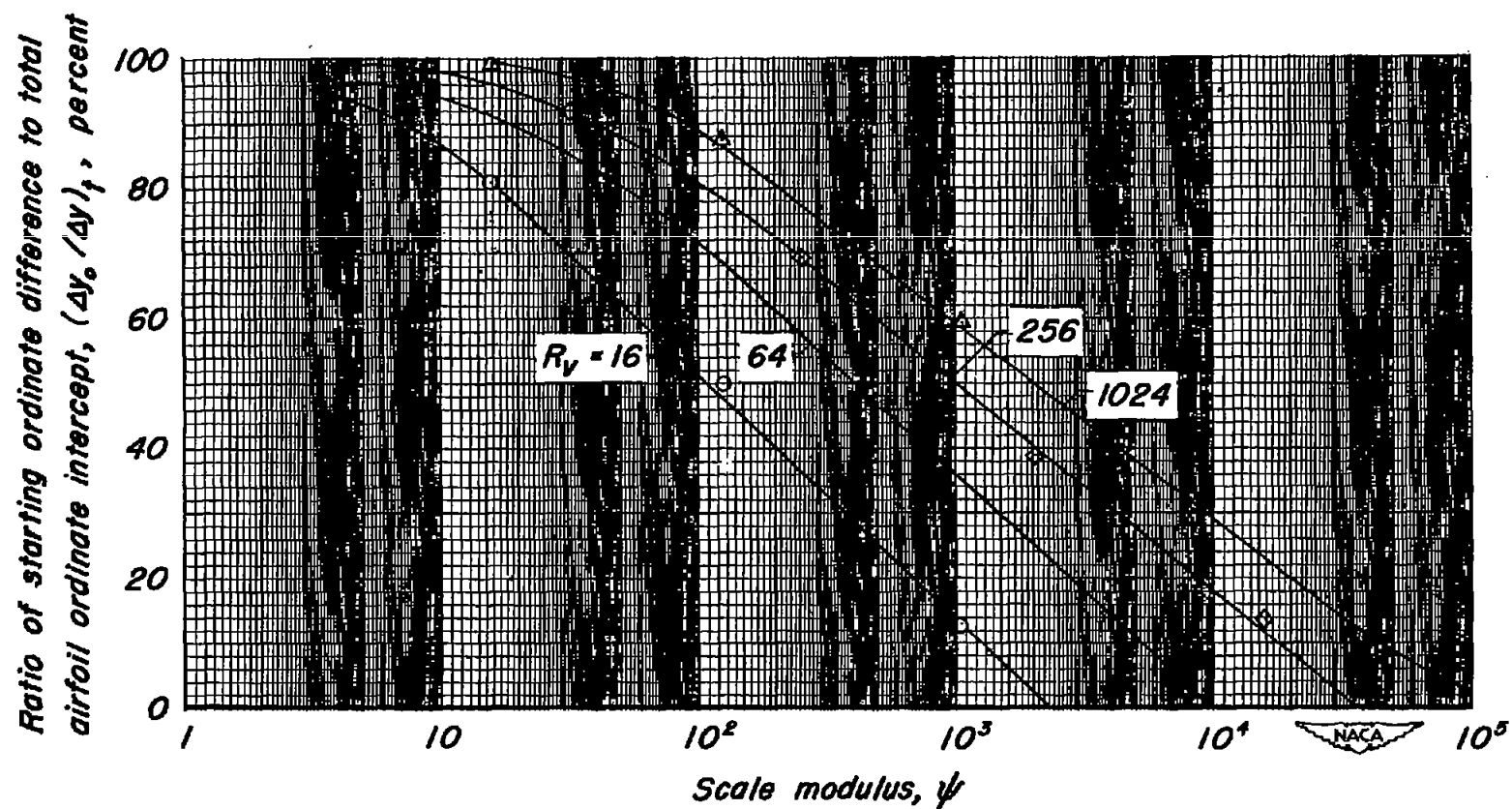
(b) 15-percent-thick symmetrical Joukowski airfoil; $\alpha = 2°$.

Figure 13.- Continued.
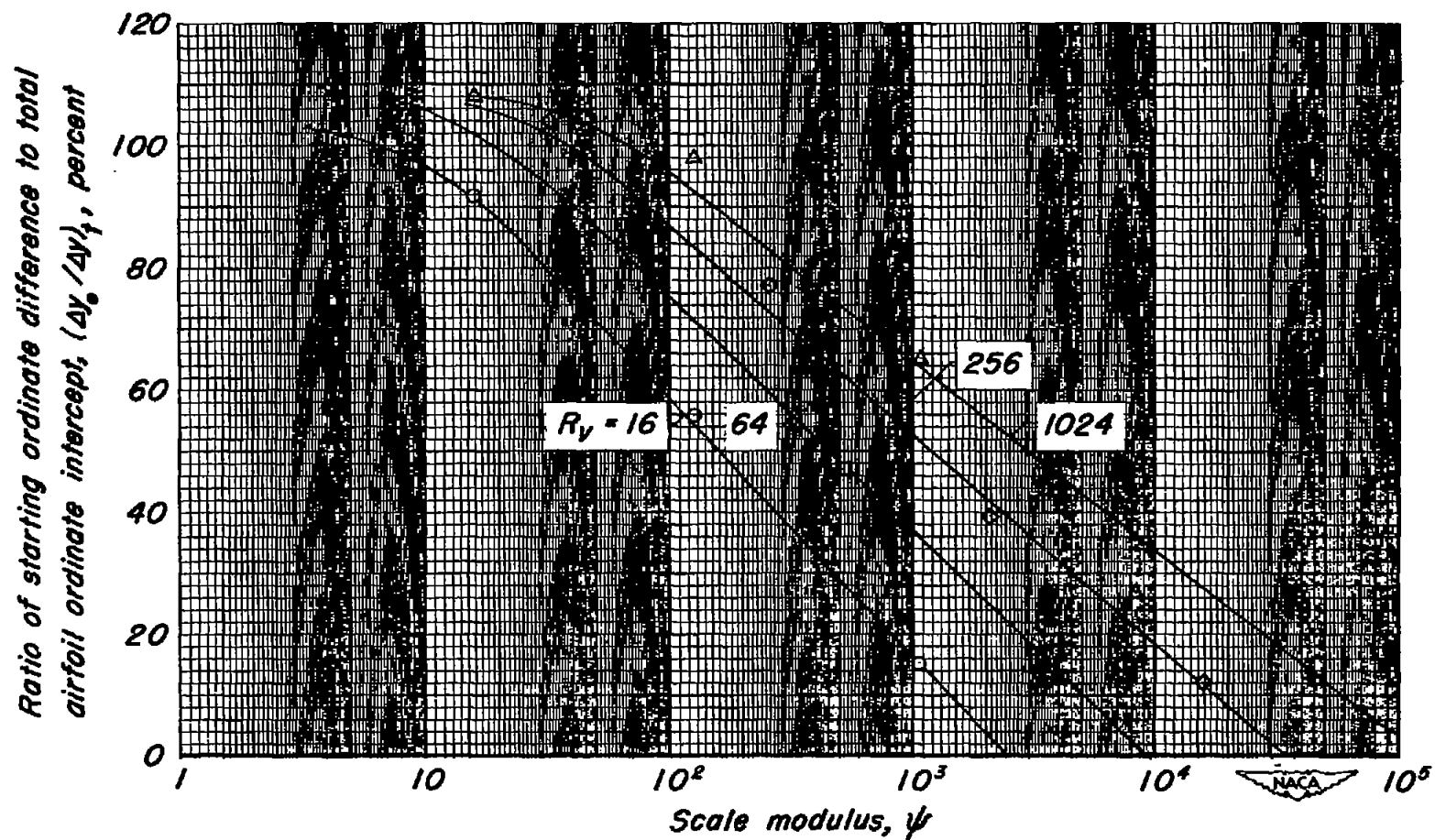
(c) 15-percent-thick symmetrical Joukowski airfoil; $\alpha = 4°$.

Figure 13.—Continued.
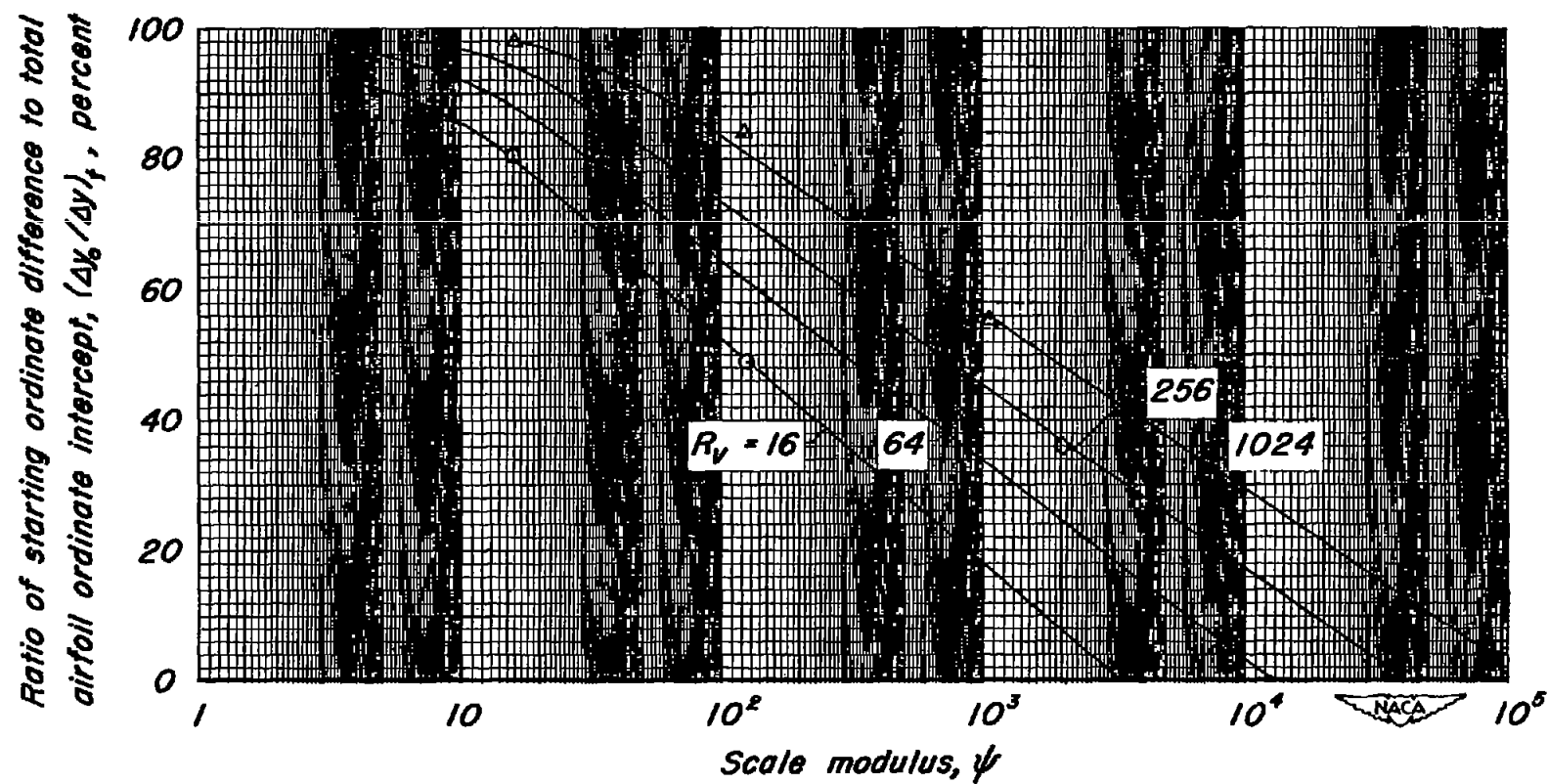
(d) 15-percent-thick cambered Joukowski airfoil; a = 1.0 mean line; α = 0°.

Figure 13.- Continued.
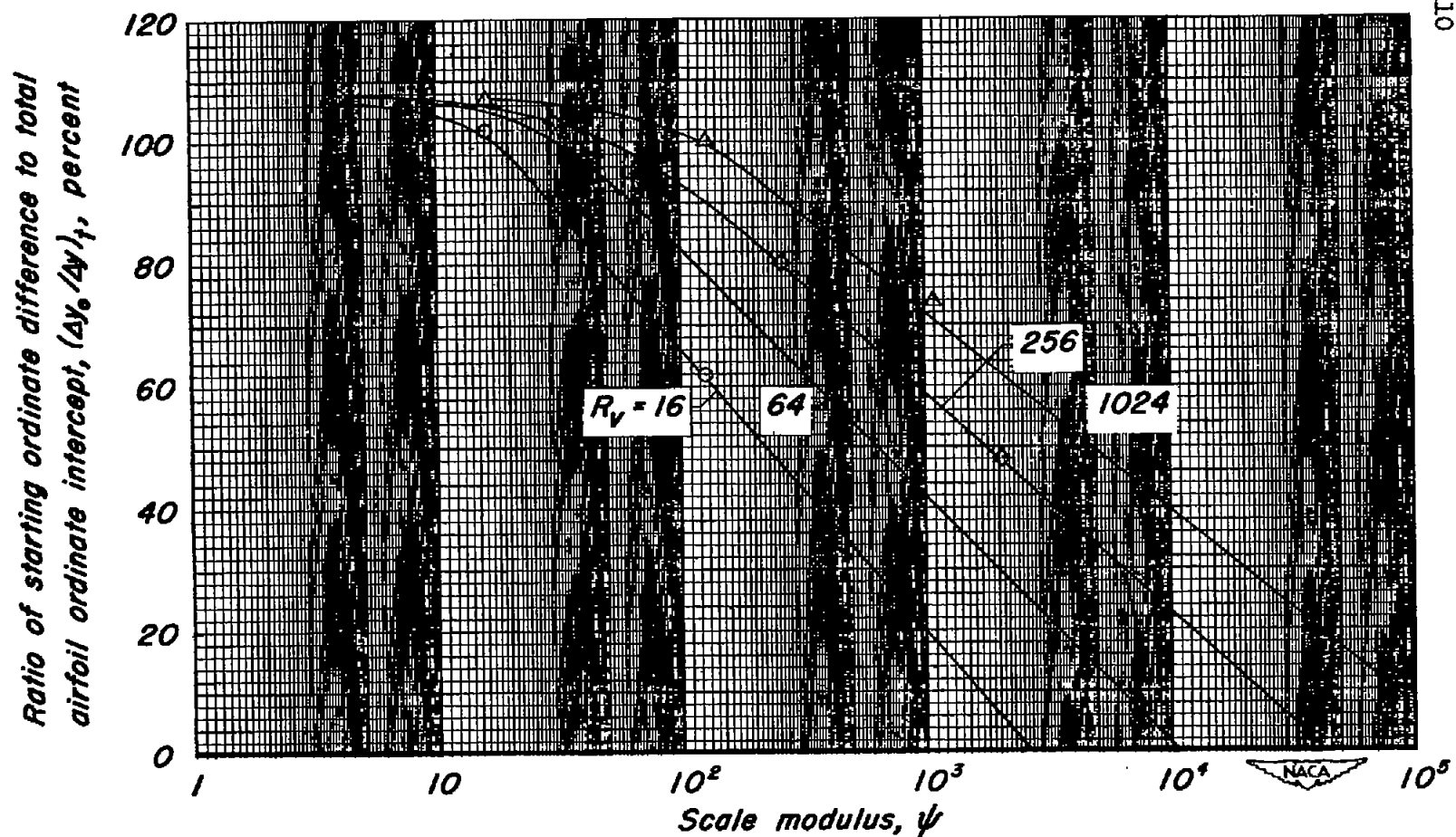
(e) NACA 65_2-015 airfoil; $\alpha = 4°$.

Figure 13.- Concluded.
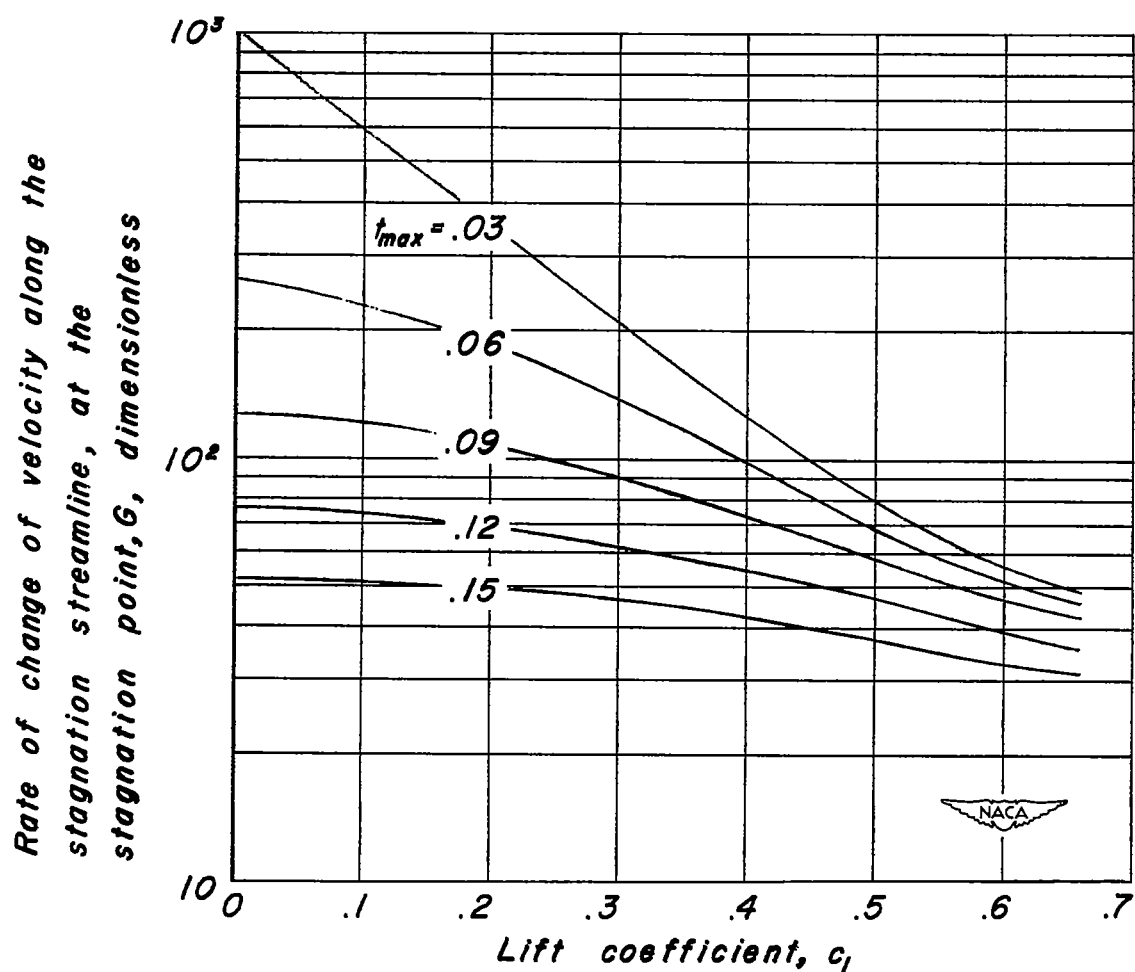
(a) Joukowski airfoil.

Figure 14. Velocity gradient along the stagnation streamline, at
the stagnation point, as a function of lift coefficient and
thickness ratio for two profiles.
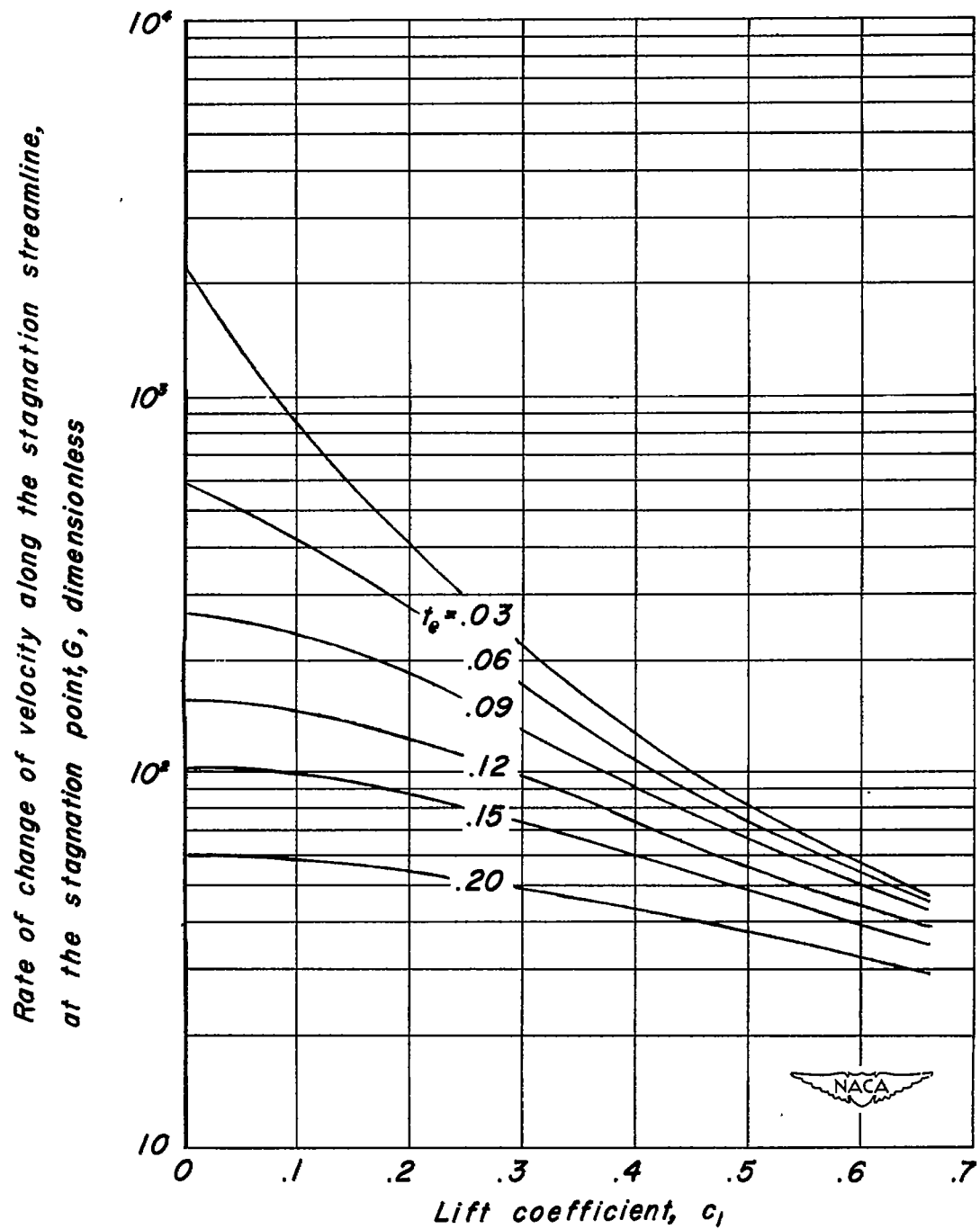
(b) Ellipse.

Figure 14. Concluded.
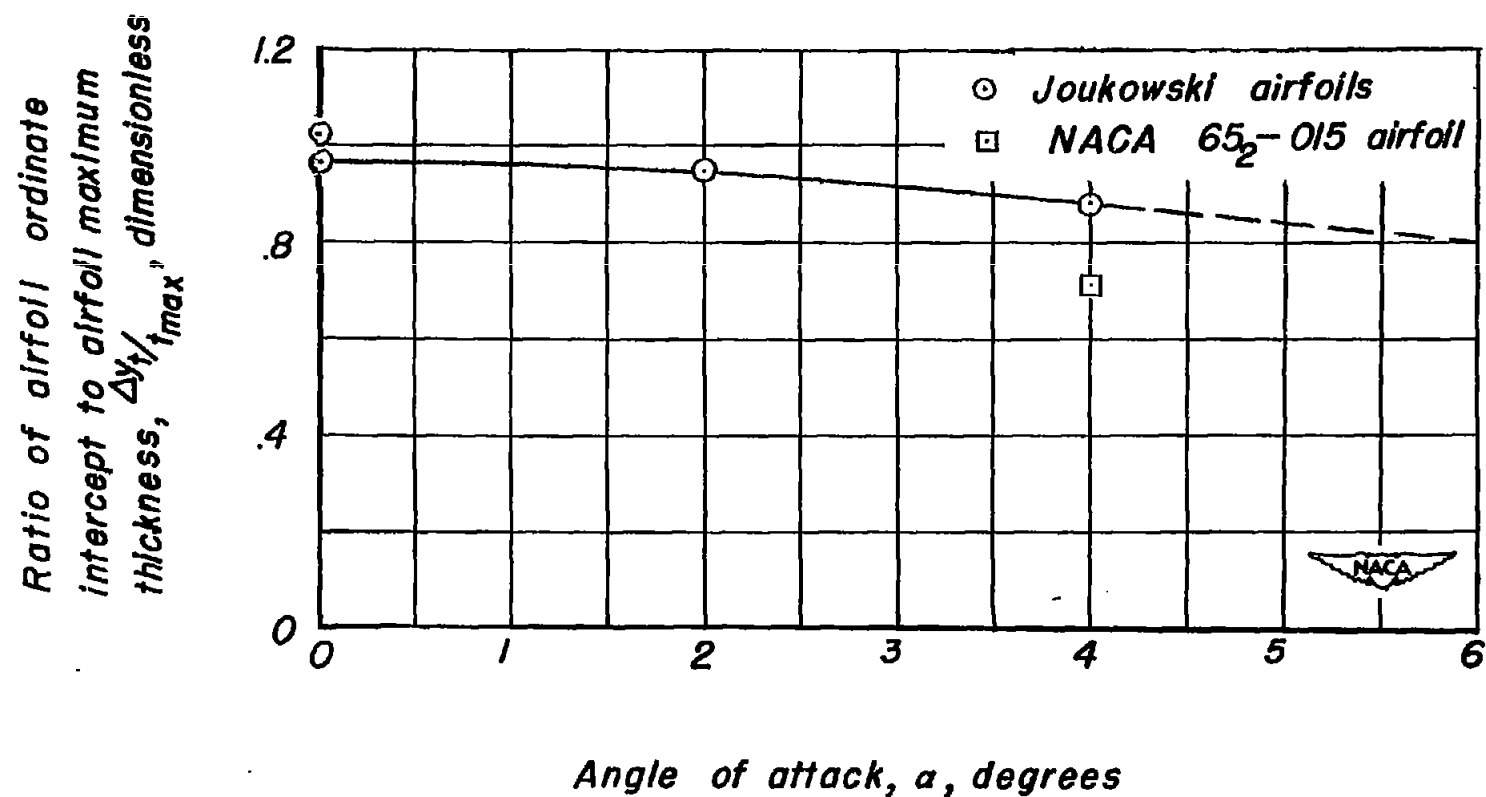
Figure 15.— Ratio of $\Delta y_t/t_{max}$ as a function of angle of attack for $(\Delta y_o/\Delta y)_t = 0.8$

(a) Farthest position of drop impingement

(b) Airfoil ordinate at farthest position of drop impingement

(c) Ordinate-intercept ratio
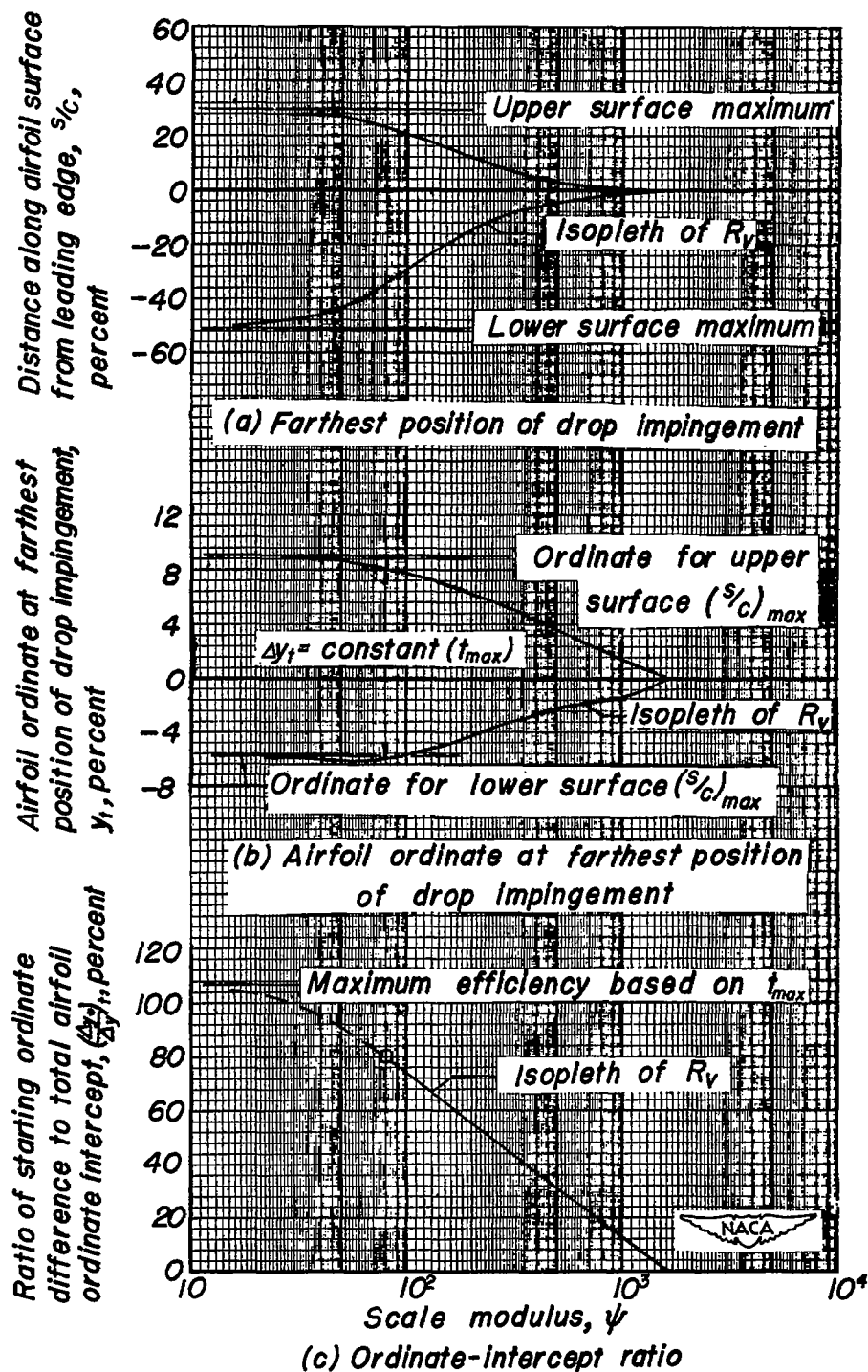
Figure 16.— Graphical representation of the procedure used to obtain a value of ψ corresponding to $\left(\frac{\Delta y_y}{\Delta y}\right)_t = 0.8$
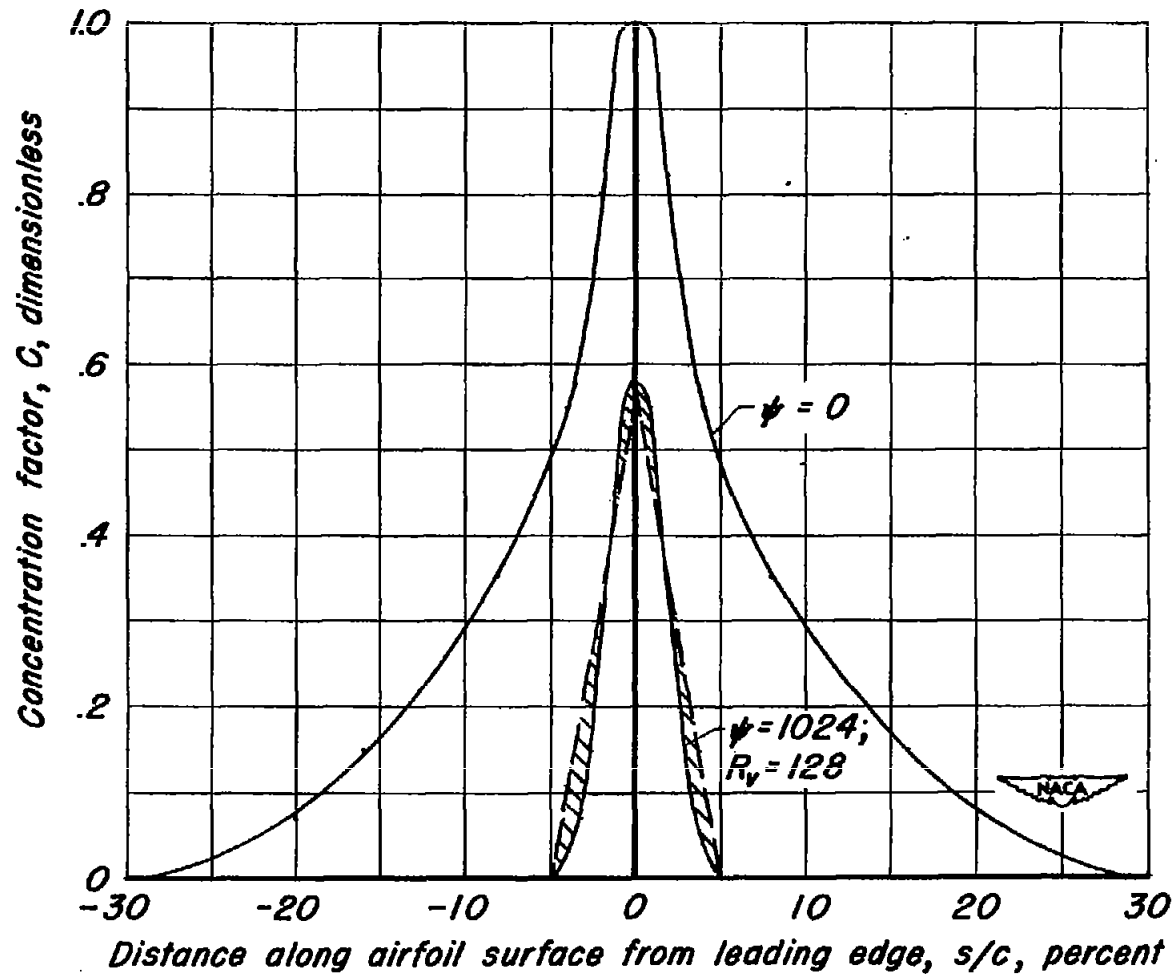
(a) 15 - percent - thick symmetrical Joukowski airfoil; $\alpha = 0°$.

Figure 17. - Surface distribution of water-drop impingement for five airfoils.
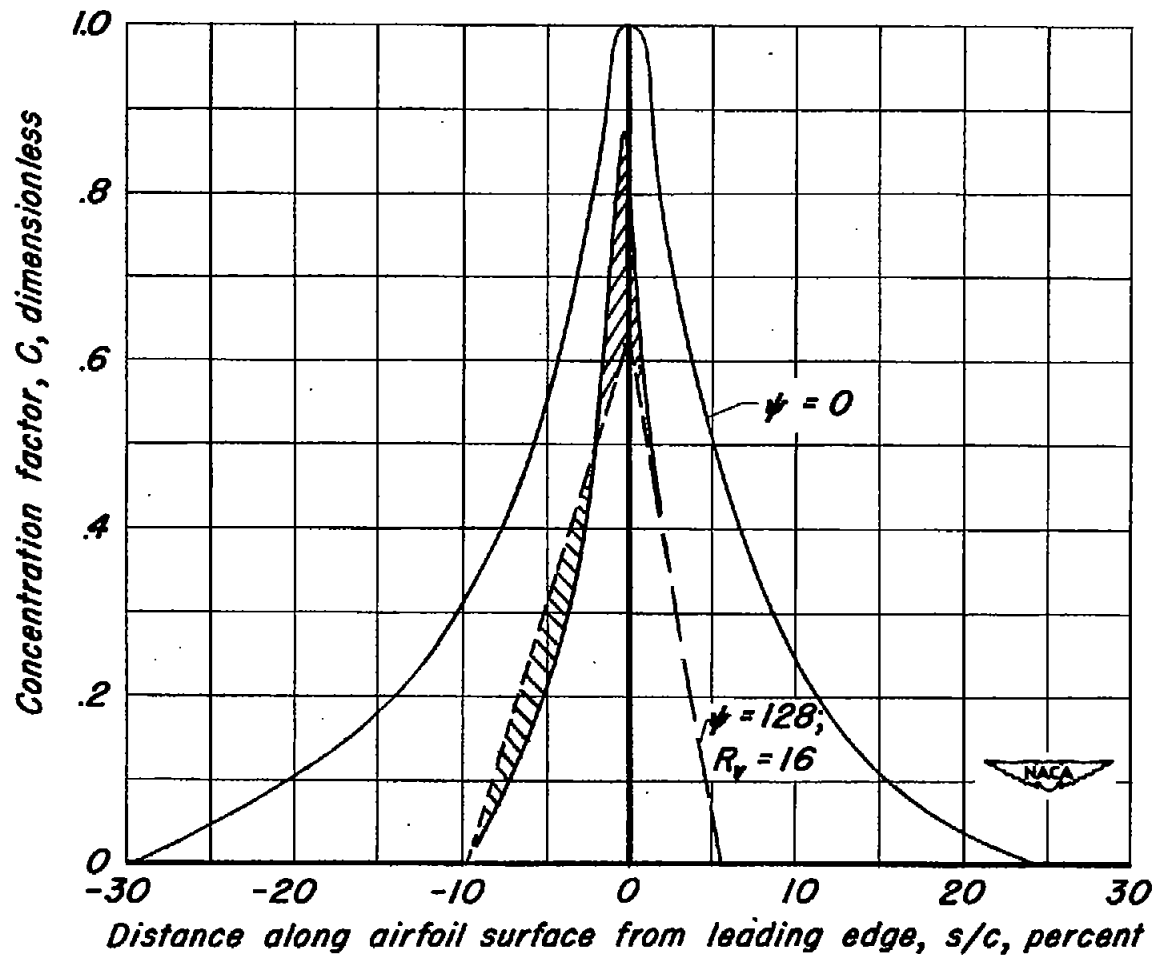
(b) 15-percent-thick symmetrical Joukowski airfoil; a = 2°.

Figure 17.—Continued.
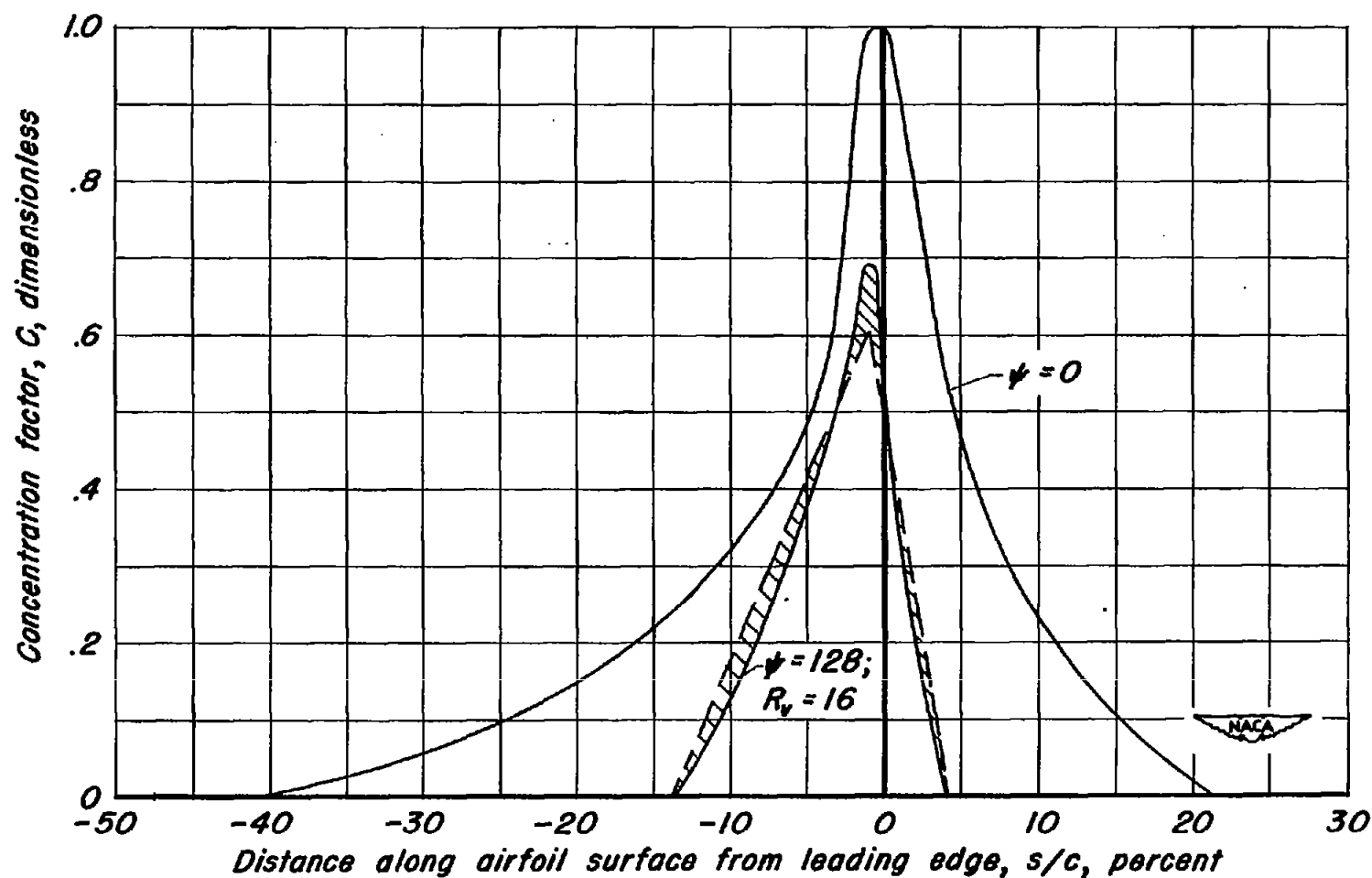
(c) 15-percent-thick symmetrical Joukowski airfoil; a = 4°.

Figure 17.- Continued.
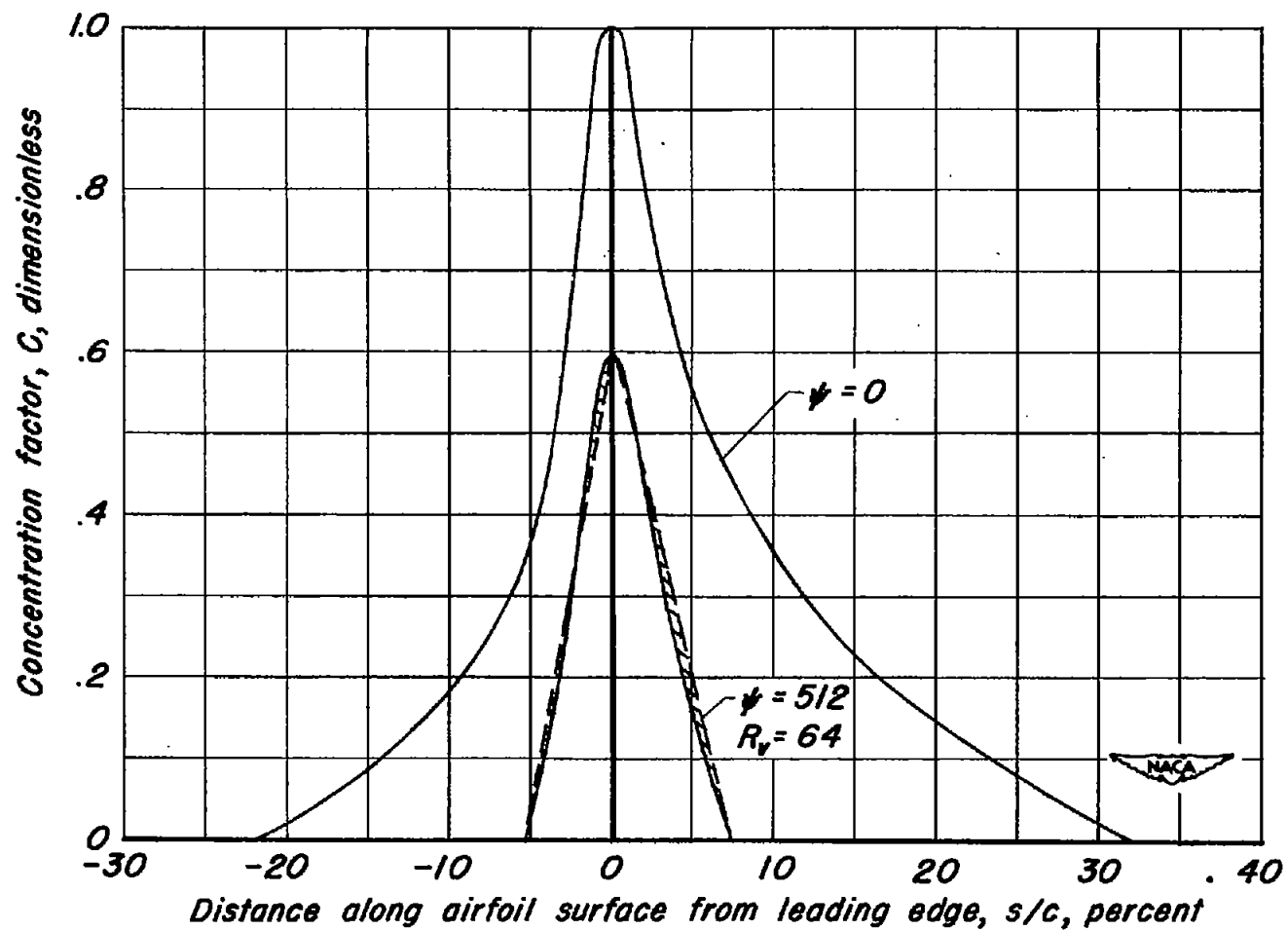
(d) 15-percent-thick cambered Joukowski airfoil; a = 1.0 mean line; α = 0°.

Figure 17.— Continued.

(e) NACA 65_2-015 airfoil; $a = 4°$.
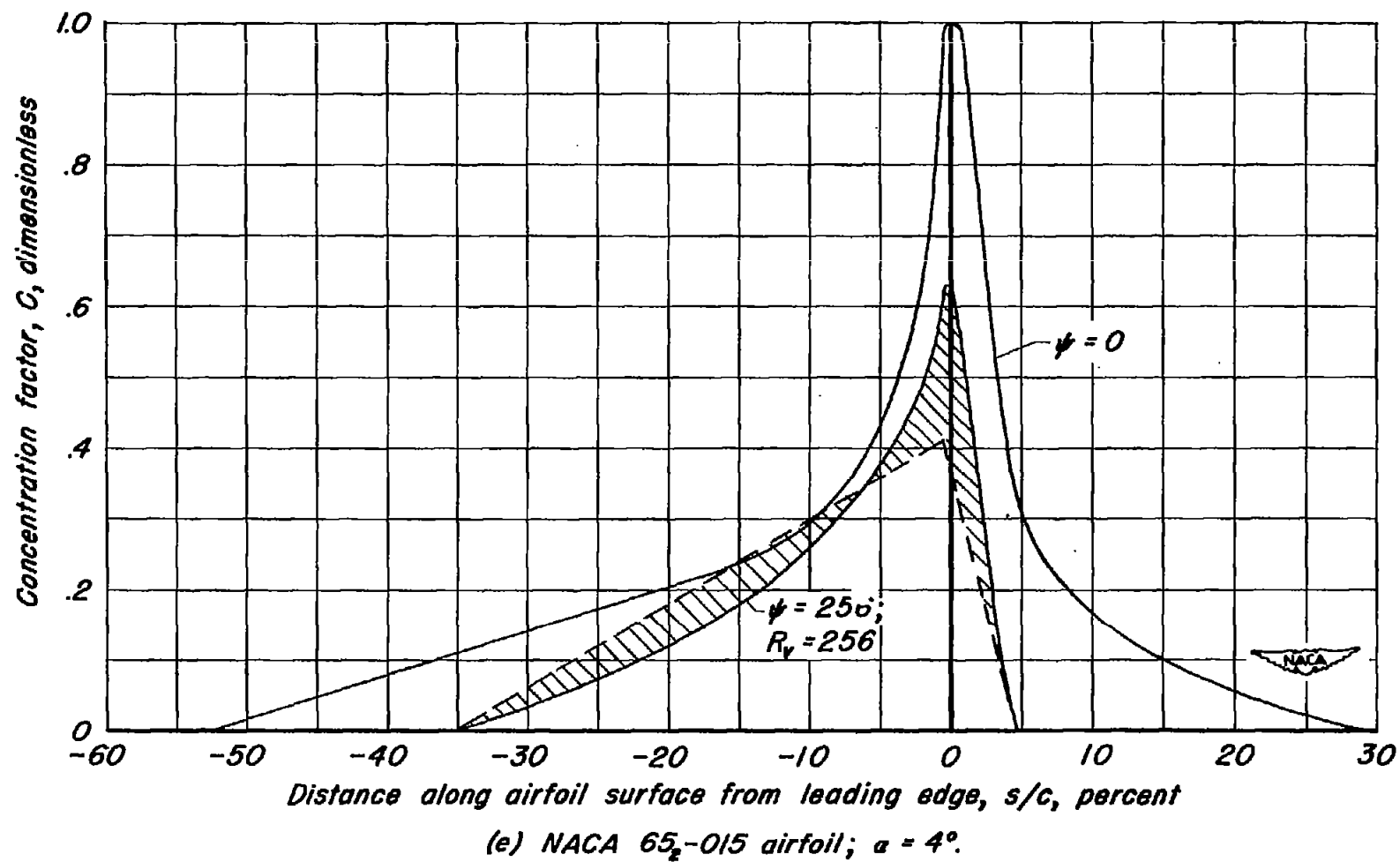
Figure 17. — Concluded.
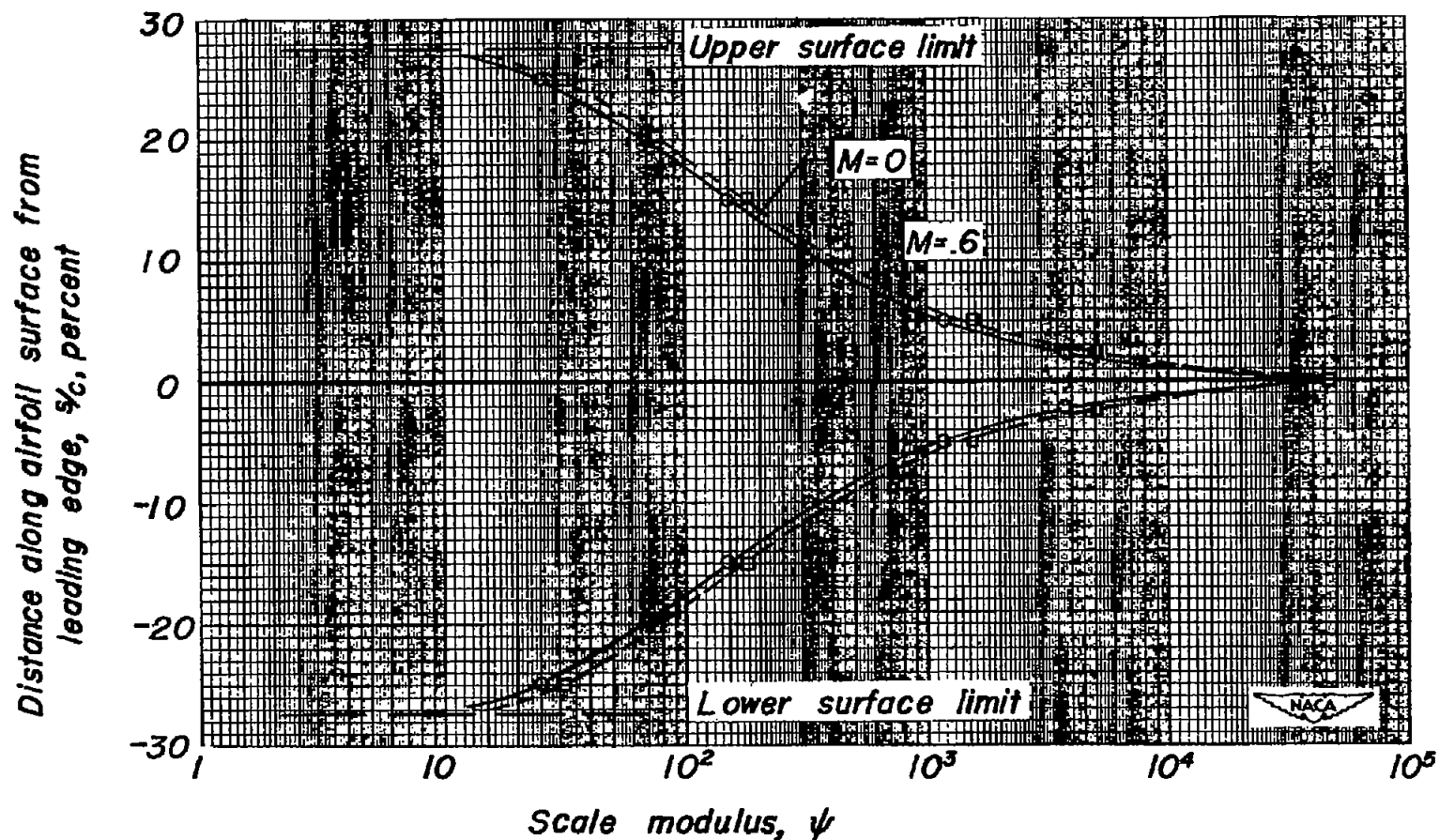
(a) Farthest position of impingement.

Figure 18.— Comparison between empirically calculated values of farthest position and efficiency of impingement for a 15-percent-thick symmetrical Joukowski airfoil, $c_l=0$, at different Mach numbers; $R_V=225$.
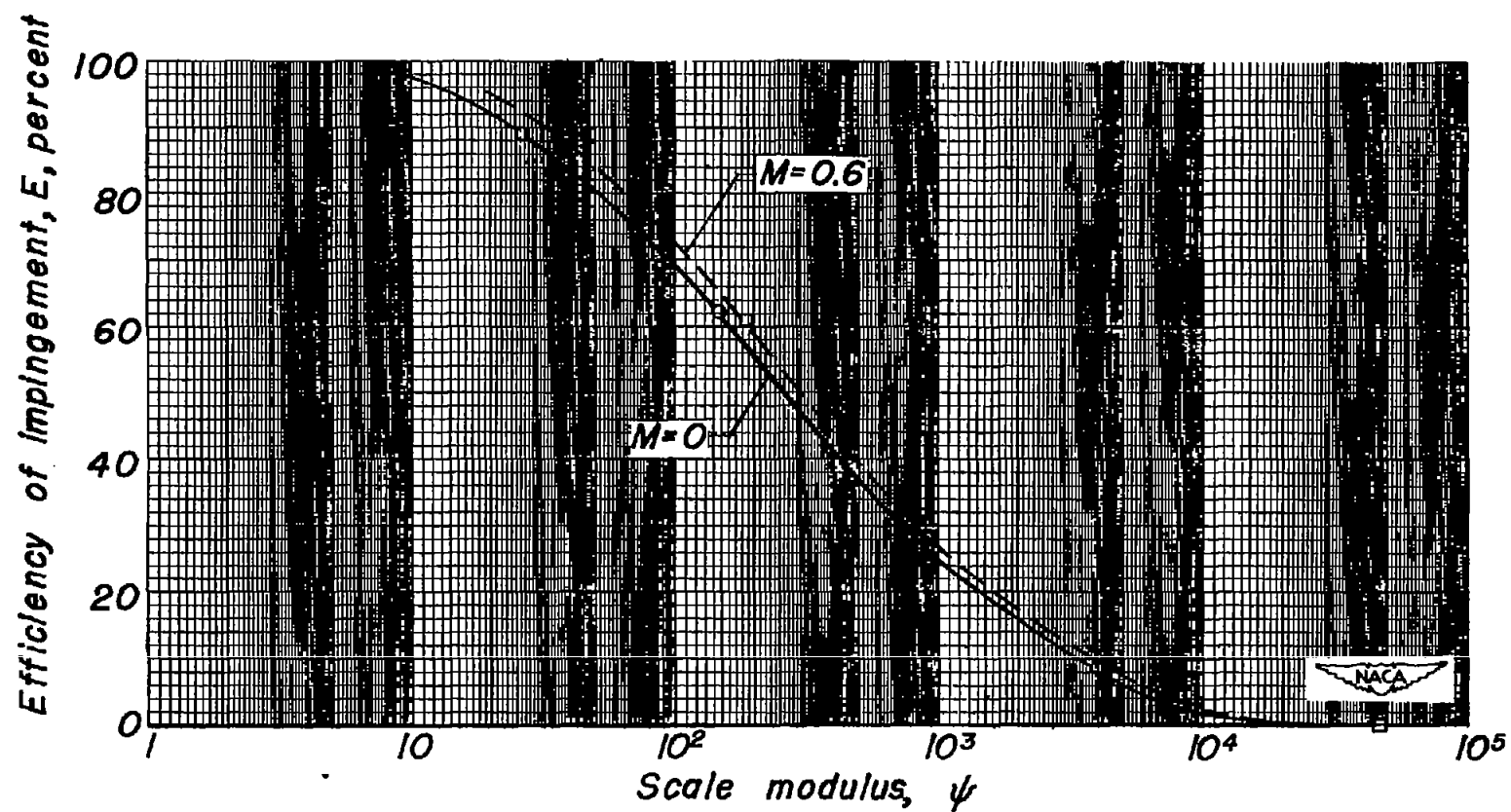
(b) Efficiency of Impingement.

Figure 18.— Concluded.
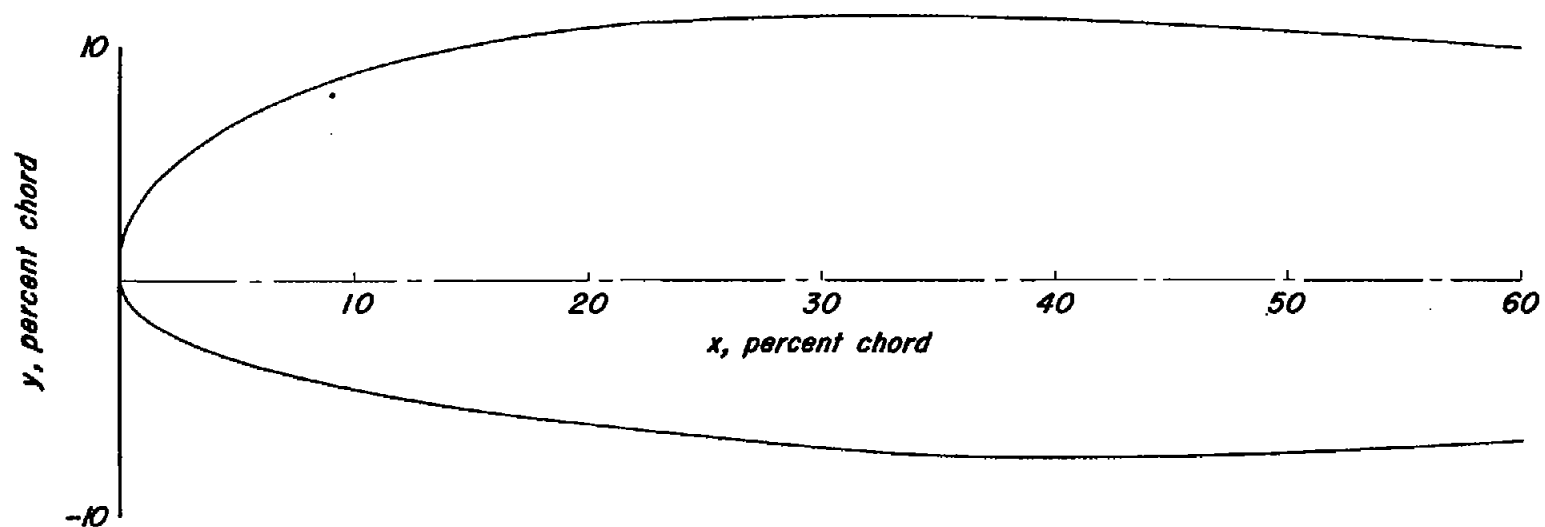
(a) Airfoil contour.

Figure 19. – Graphical relationships used in evaluating farthest position of impingement for an
NACA 23015 airfoil; $\alpha = 3.6°$; $c_l = 0.5$.
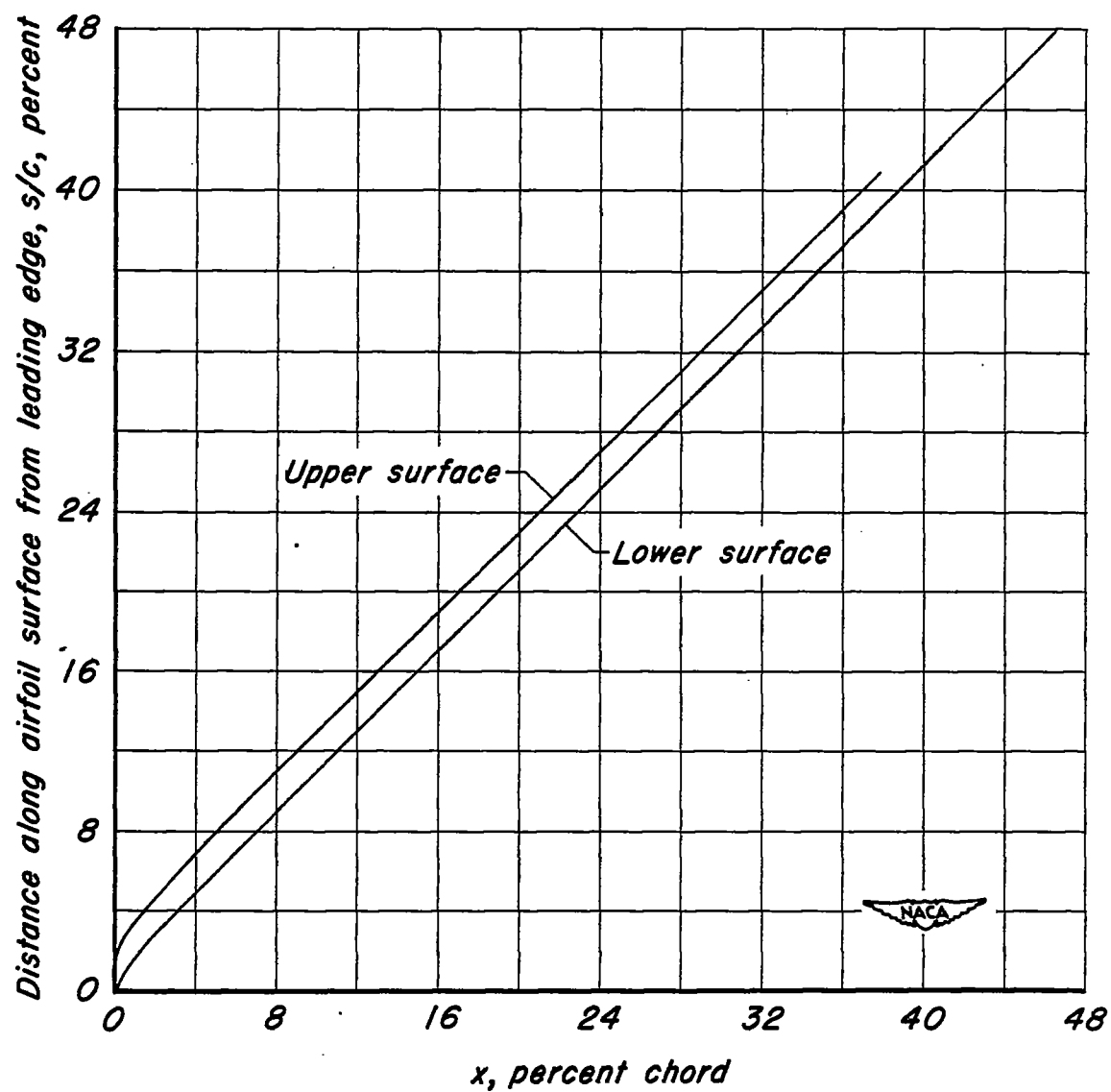
(b) Variation of s/c with chordwise position.

Figure 19. – Continued.
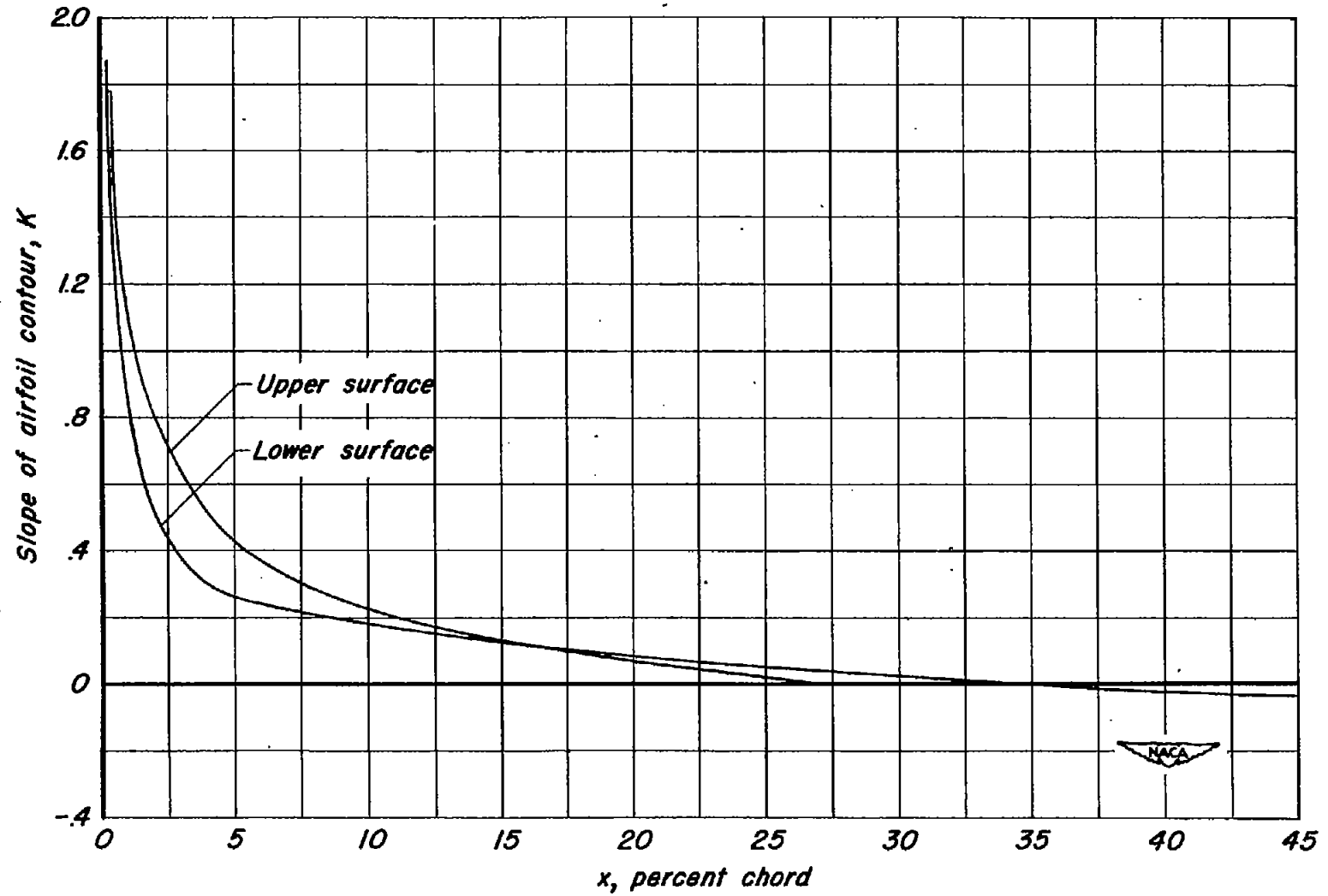
(c) Slope of airfoil contour as a function of chordwise position.

Figure 19. — Continued.
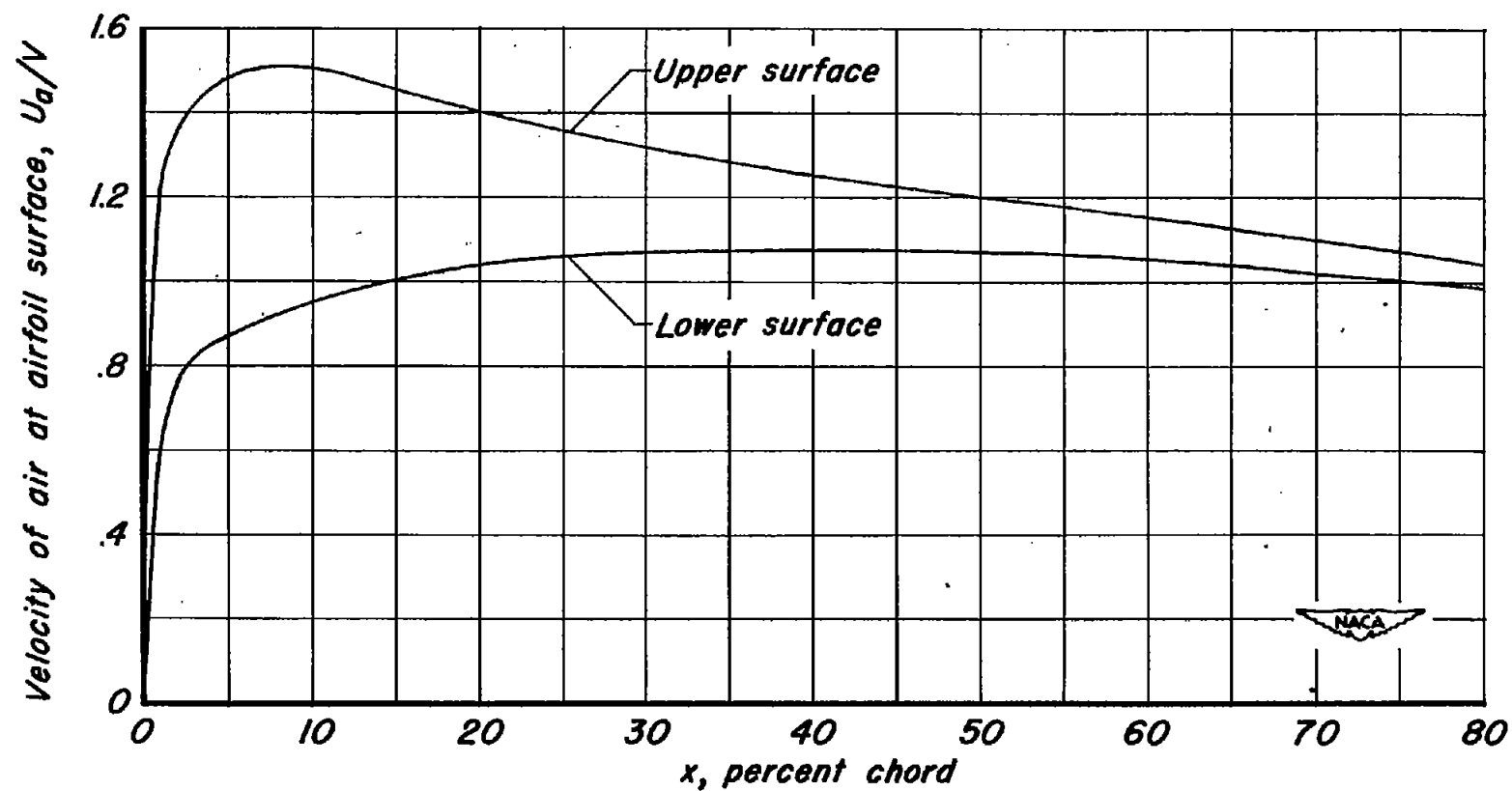
(d) Chordwise velocity distribution.

Figure 19. - Continued.
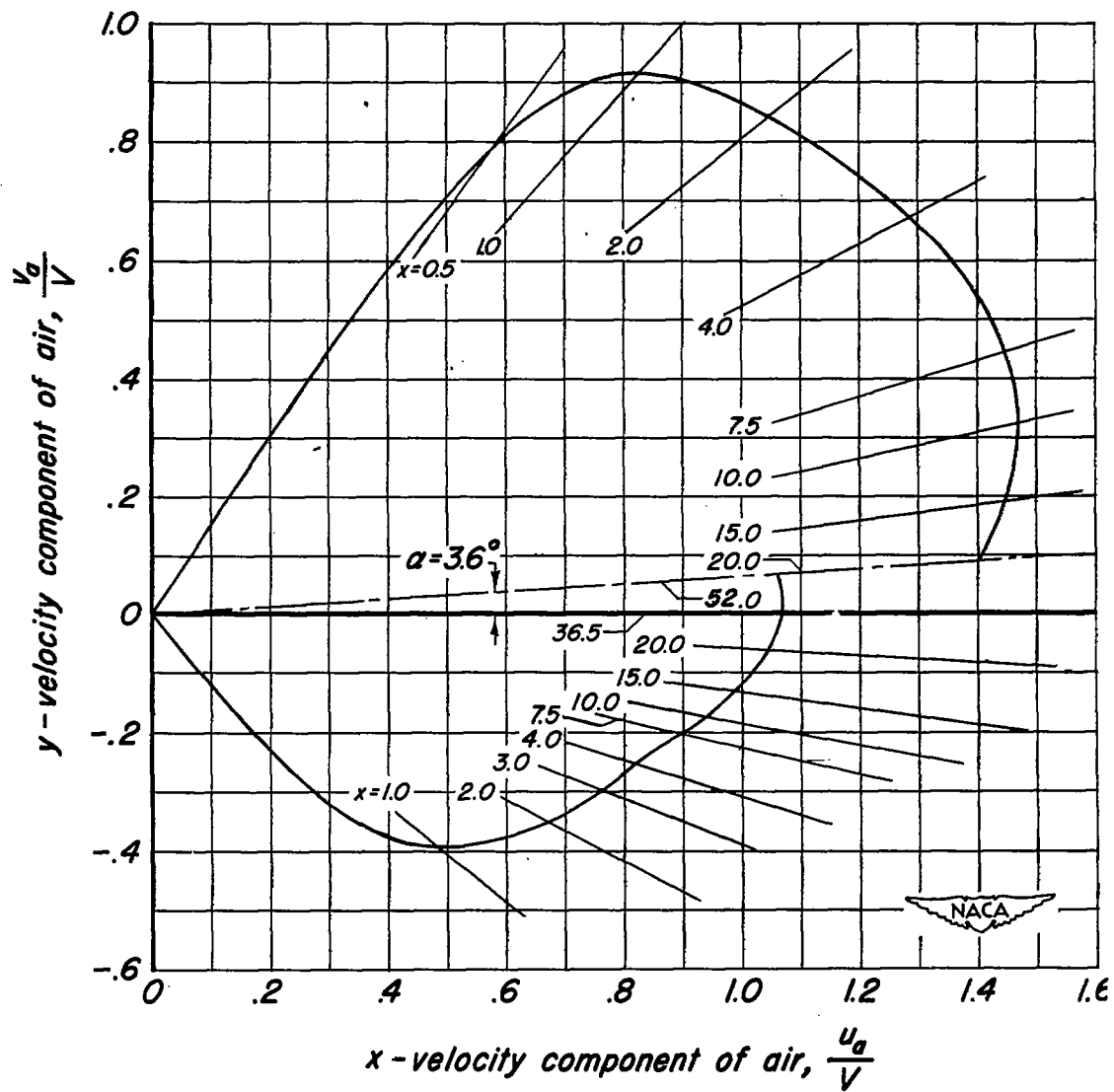
(e) Hodograph for air.

Figure 19. – Continued.
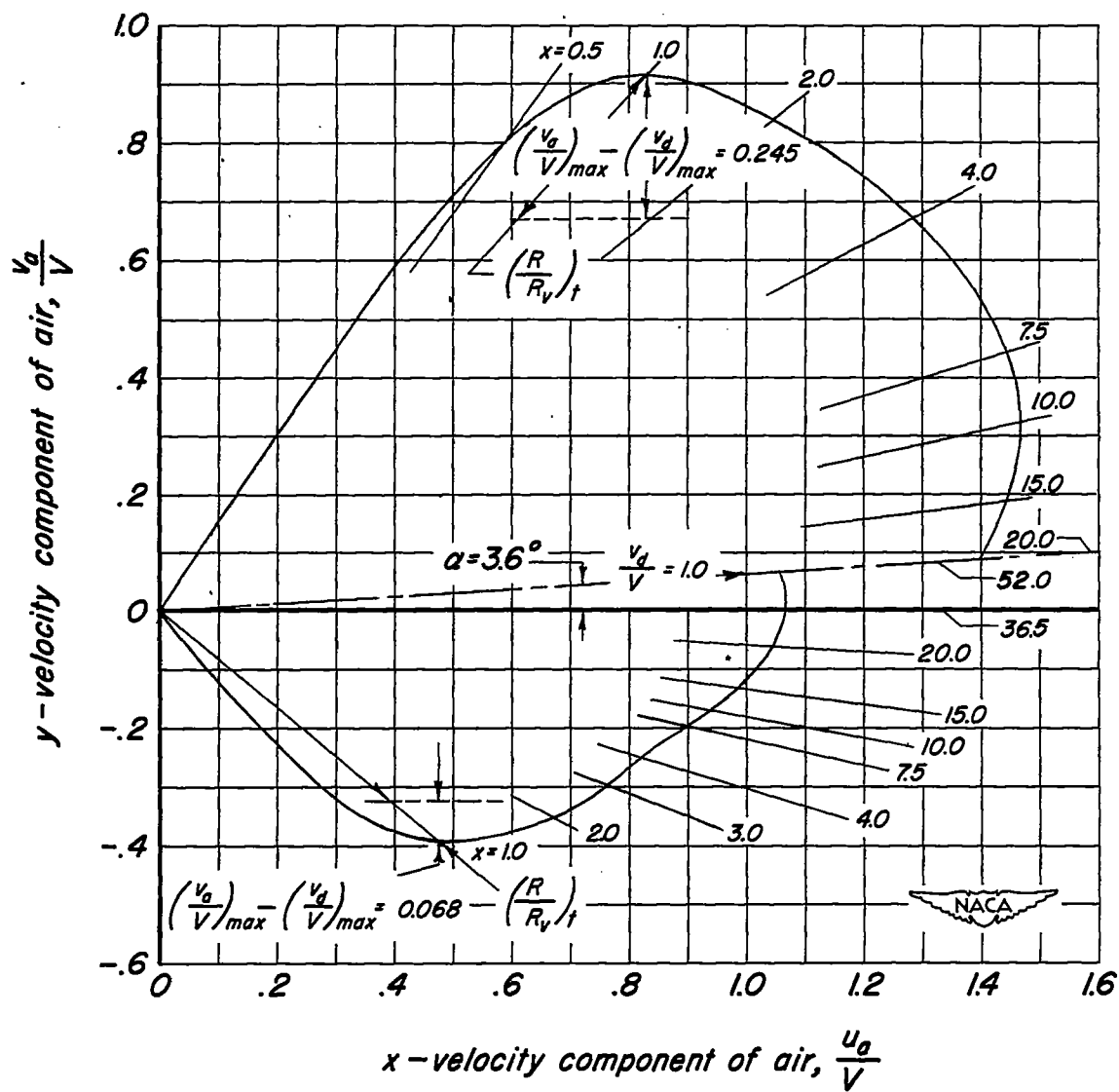
(f) Initial phase of drop hodograph.

Figure 19. – Continued.

(g) Completed drop and air hodographs.

Figure 19. – Continued.

Ratio of Reynolds number of drops impinging tangentially on airfoil to free-stream drop Reynolds number, $(R/R_V)_t$, dimensionless

$\frac{s}{c}$, percent
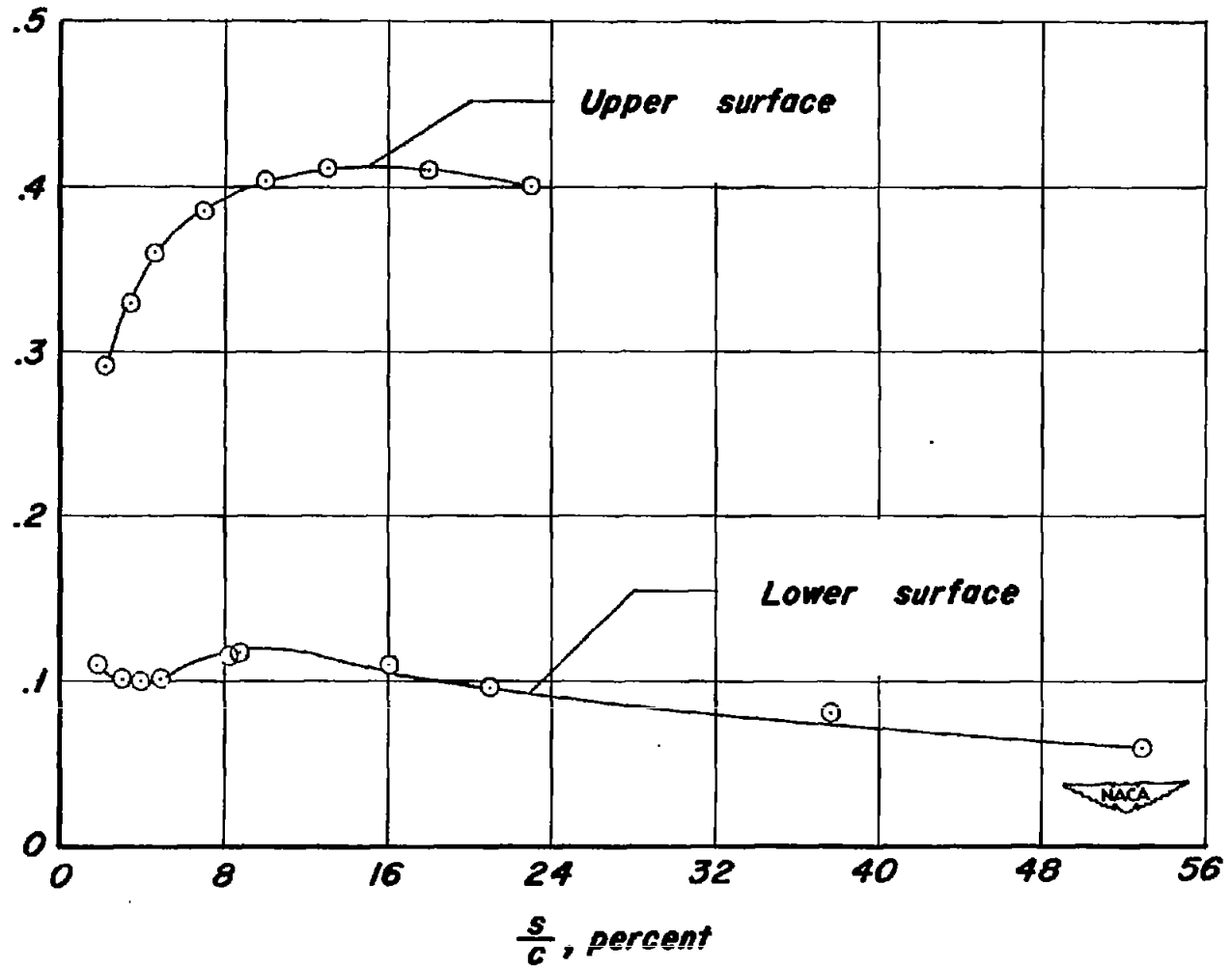
(h) $\left(\frac{R}{R_V}\right)_t$ as a function of $\frac{s}{c}$

Figure 19. — Continued.
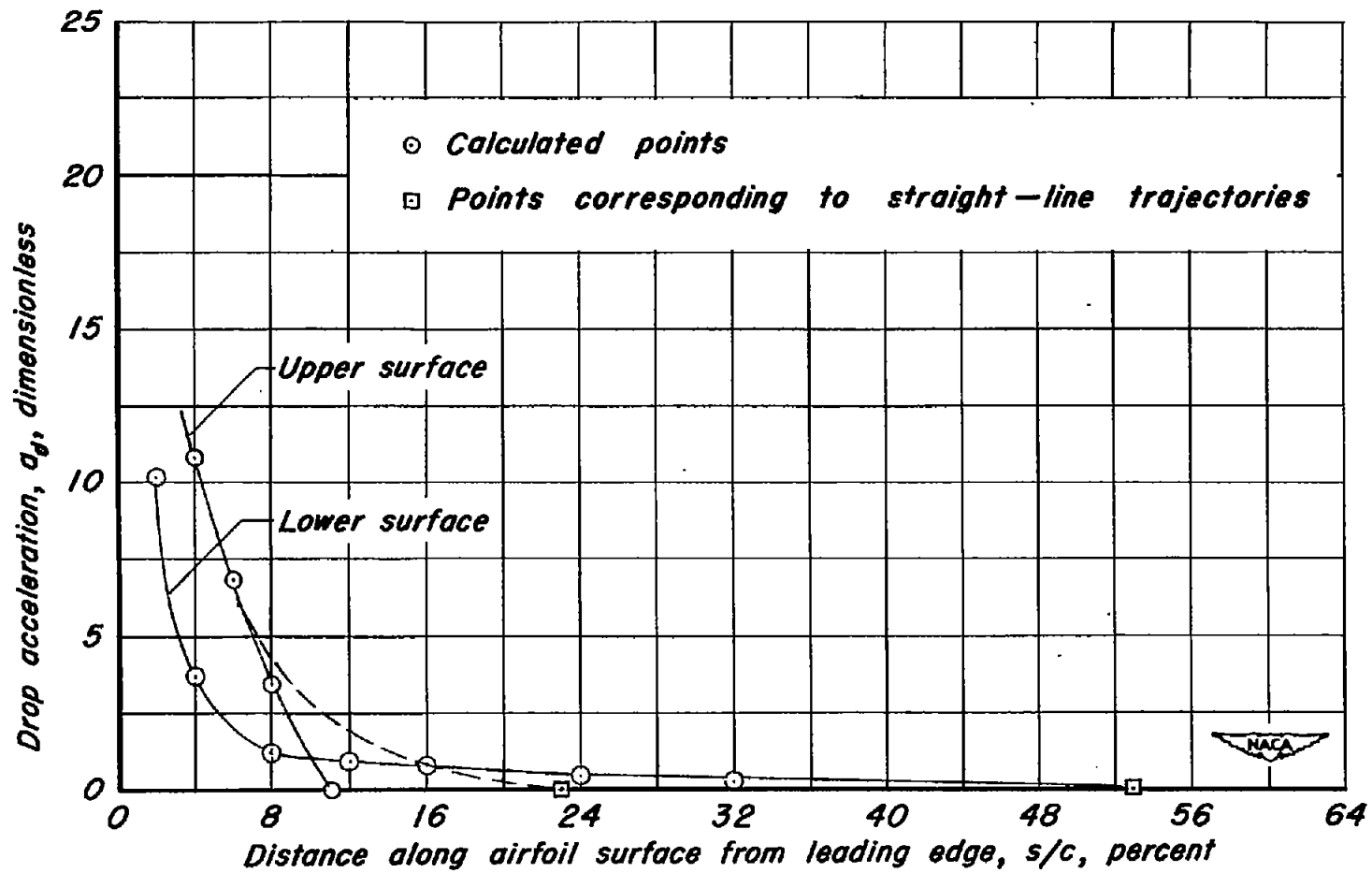
(i) Distribution of drop acceleration values over airfoil surface.

Figure 19.—Continued.

Local drop Reynolds number, R, dimensionless
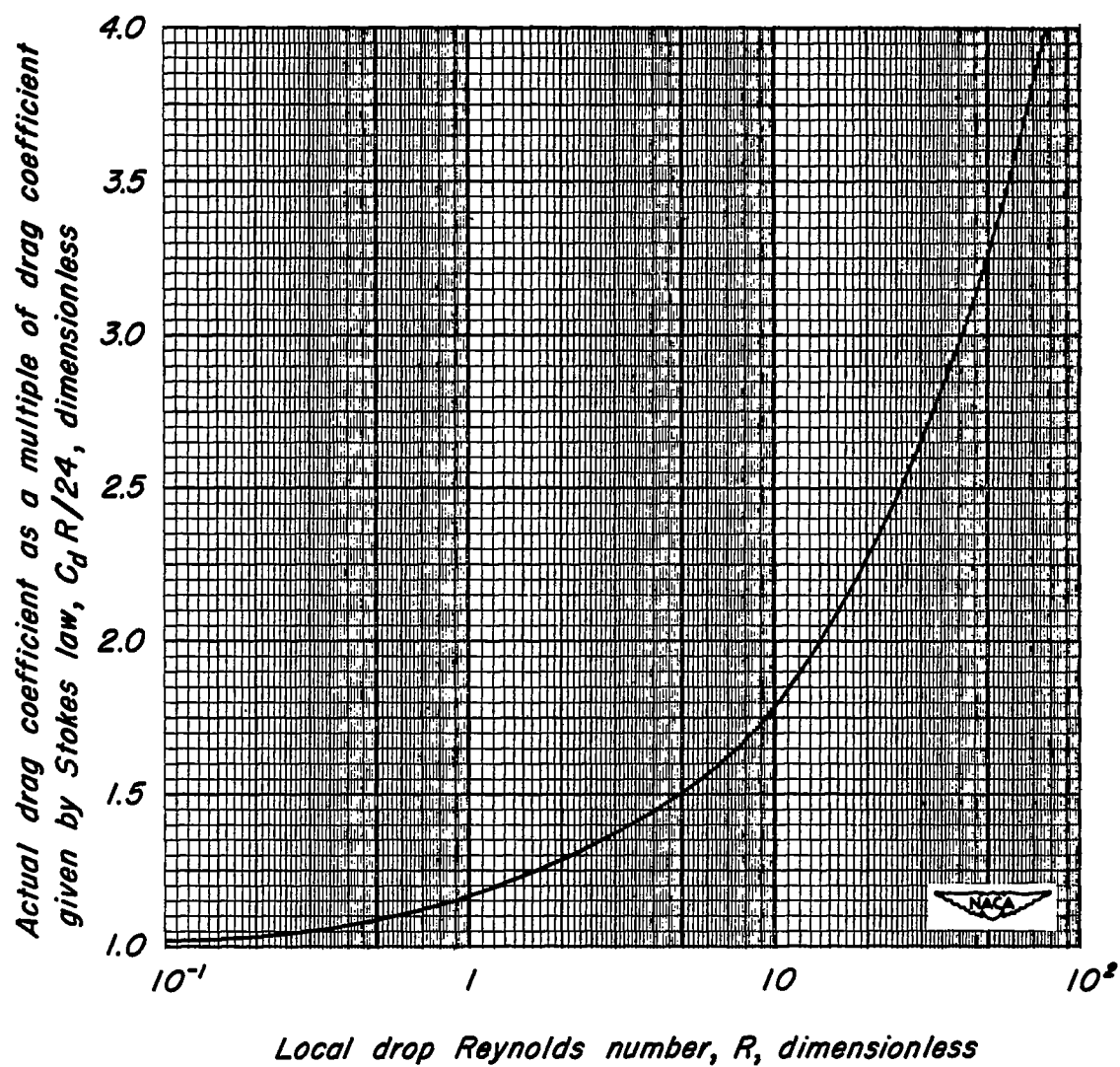
(J) $\dfrac{C_d R}{24}$ as a function of R.

Figure 19.-Continued.
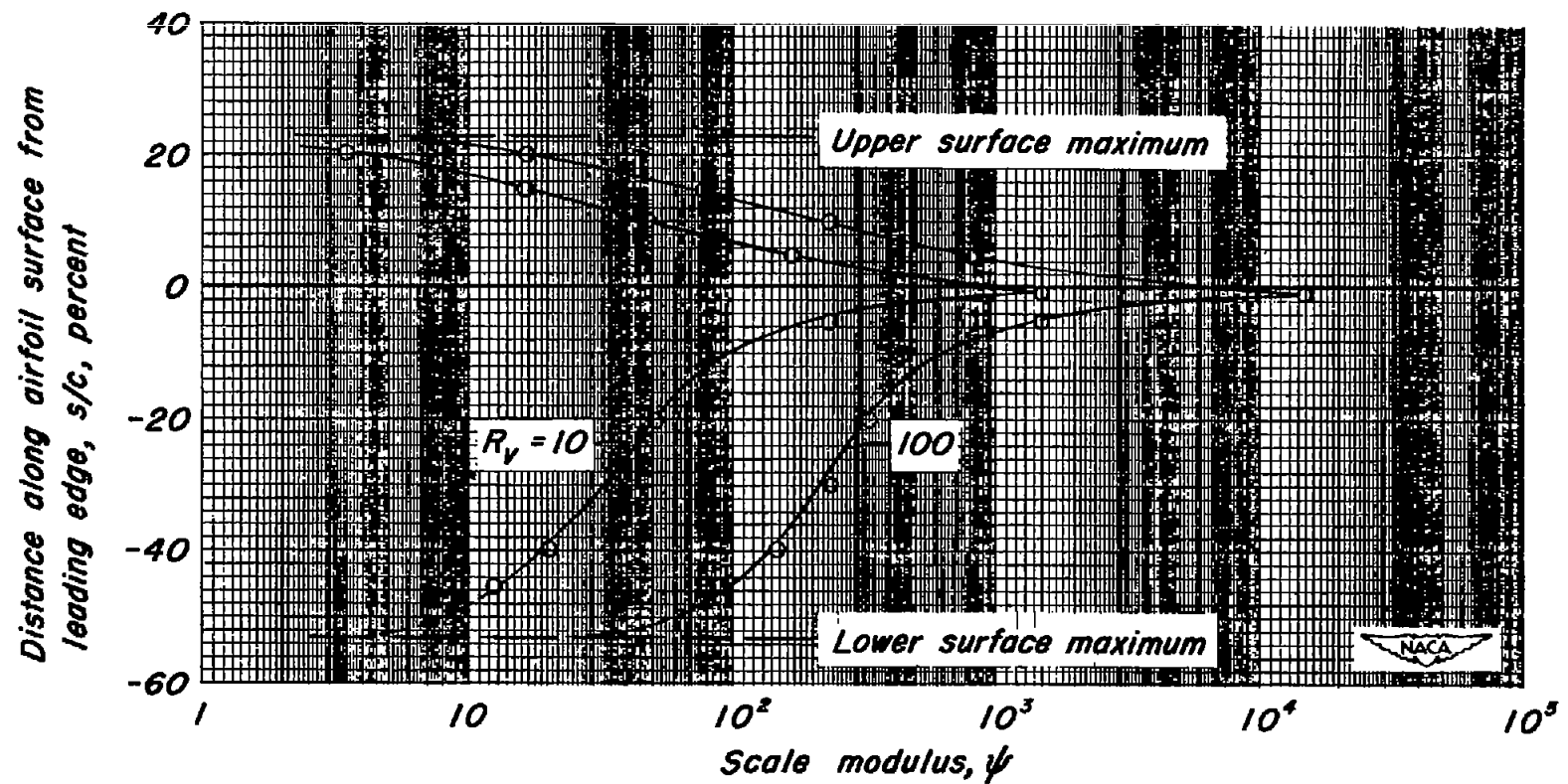
(k) Farthest position of impingement.

Figure 19.—Concluded.
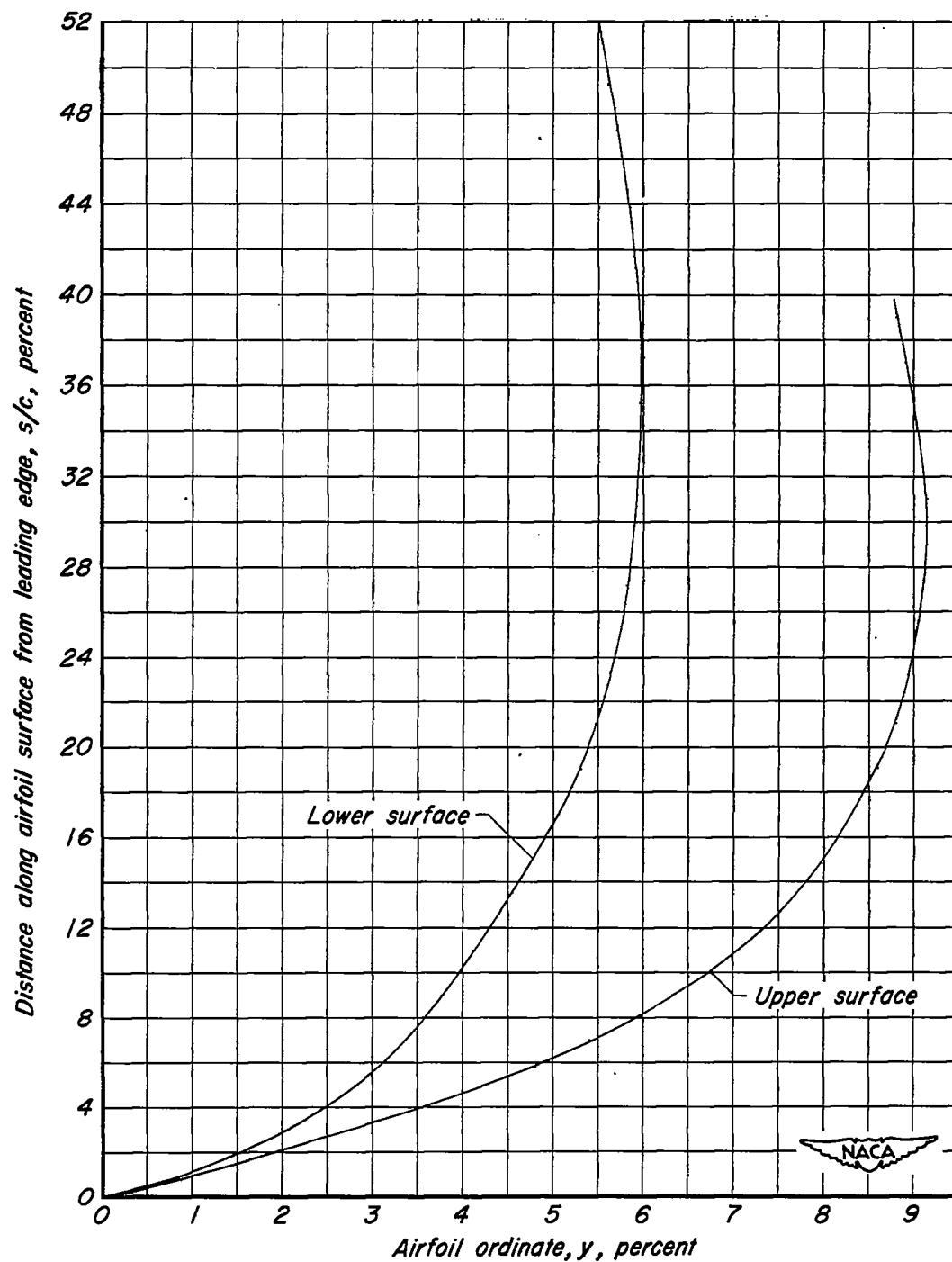
(a) Variation of s/c with airfoil ordinates.

Figure 20. – Graphical relationships used in evaluating impingement efficiency for an NACA 23015 airfoil; $a = 3.6°$; $c_l = 0.5$.
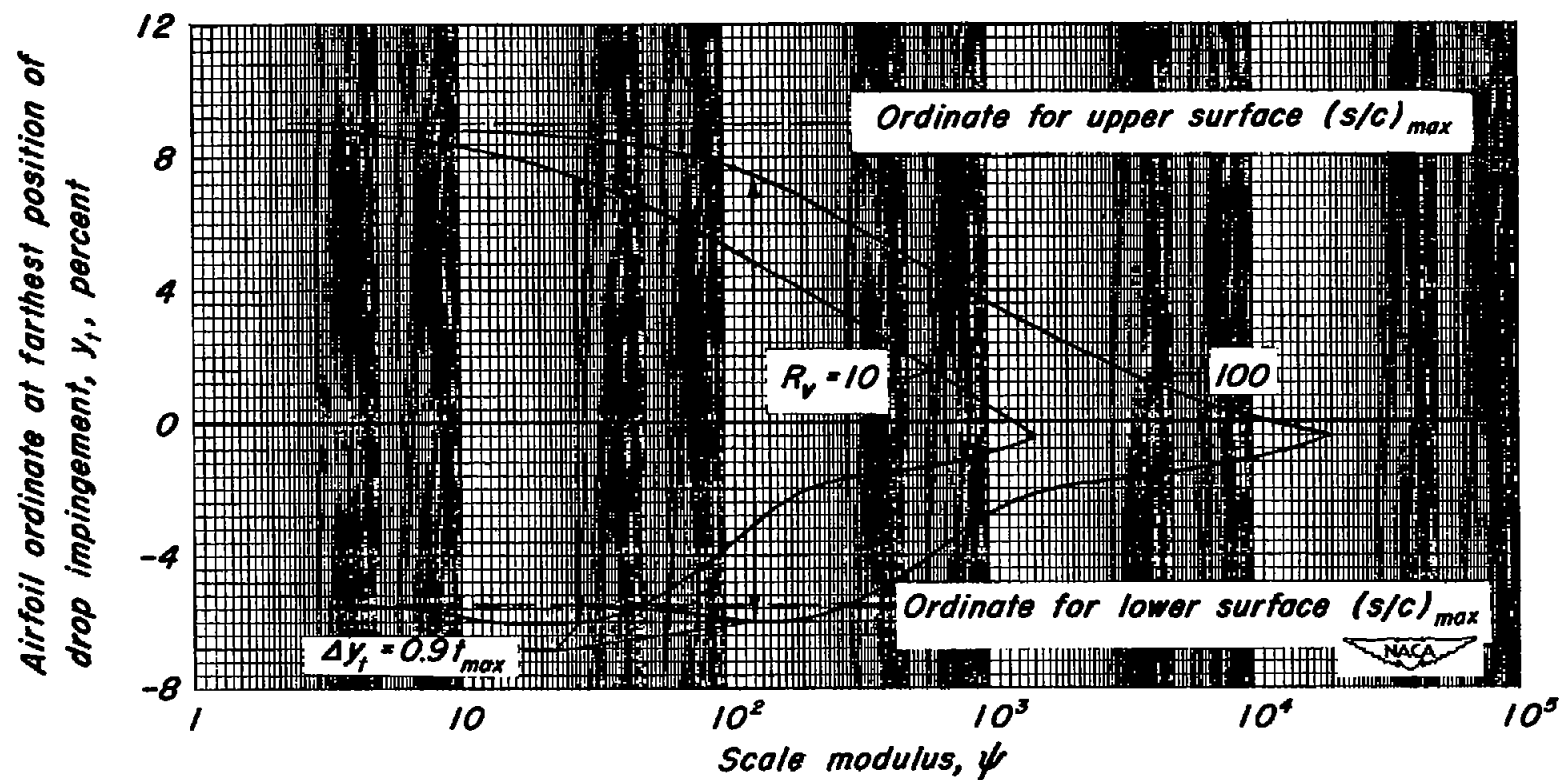
(b) Airfoil ordinate at farthest position of impingement.

Figure 20.-Continued.
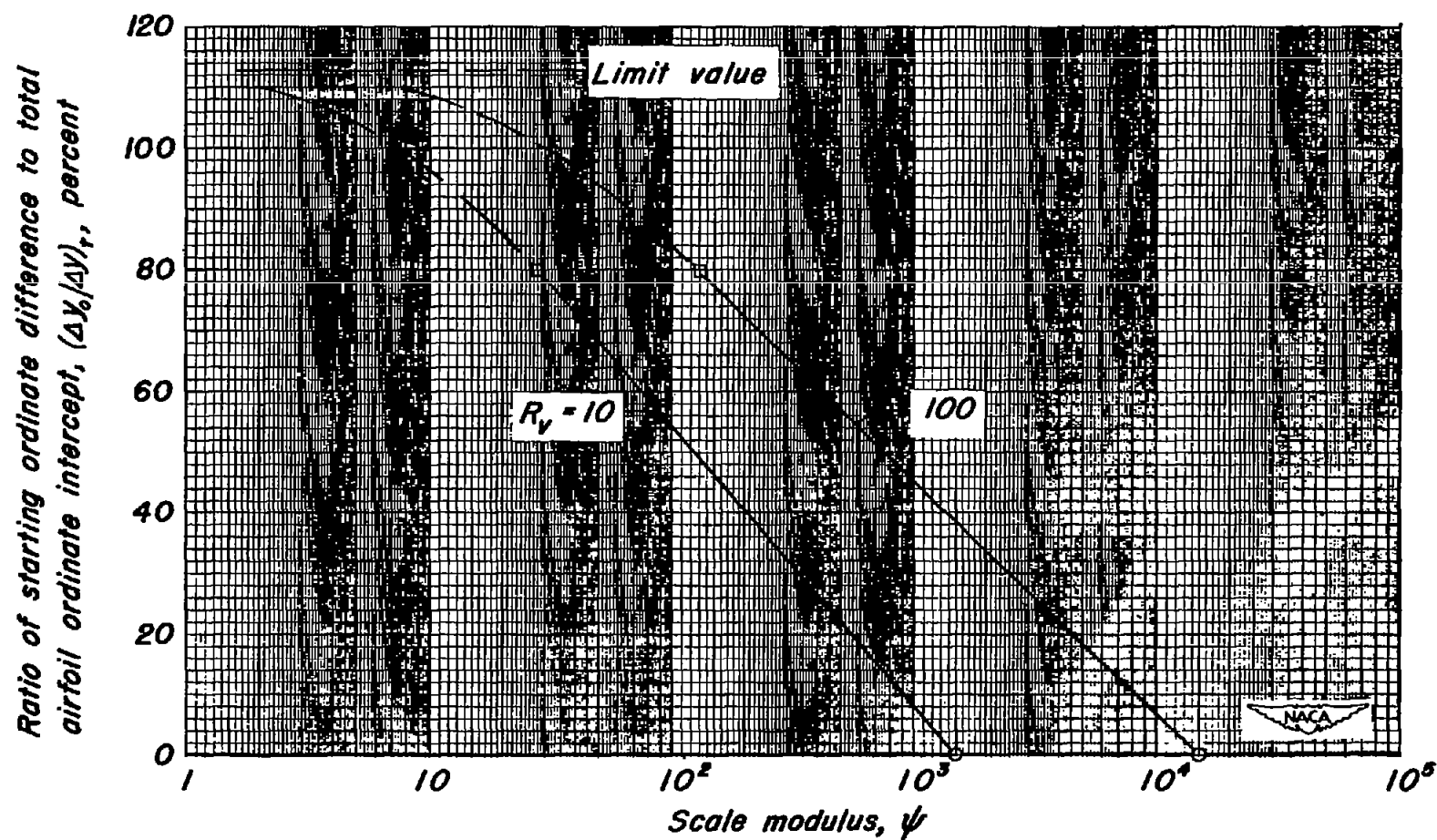
(c) Ordinate-ratio isopleths.

Figure 20.-Continued.
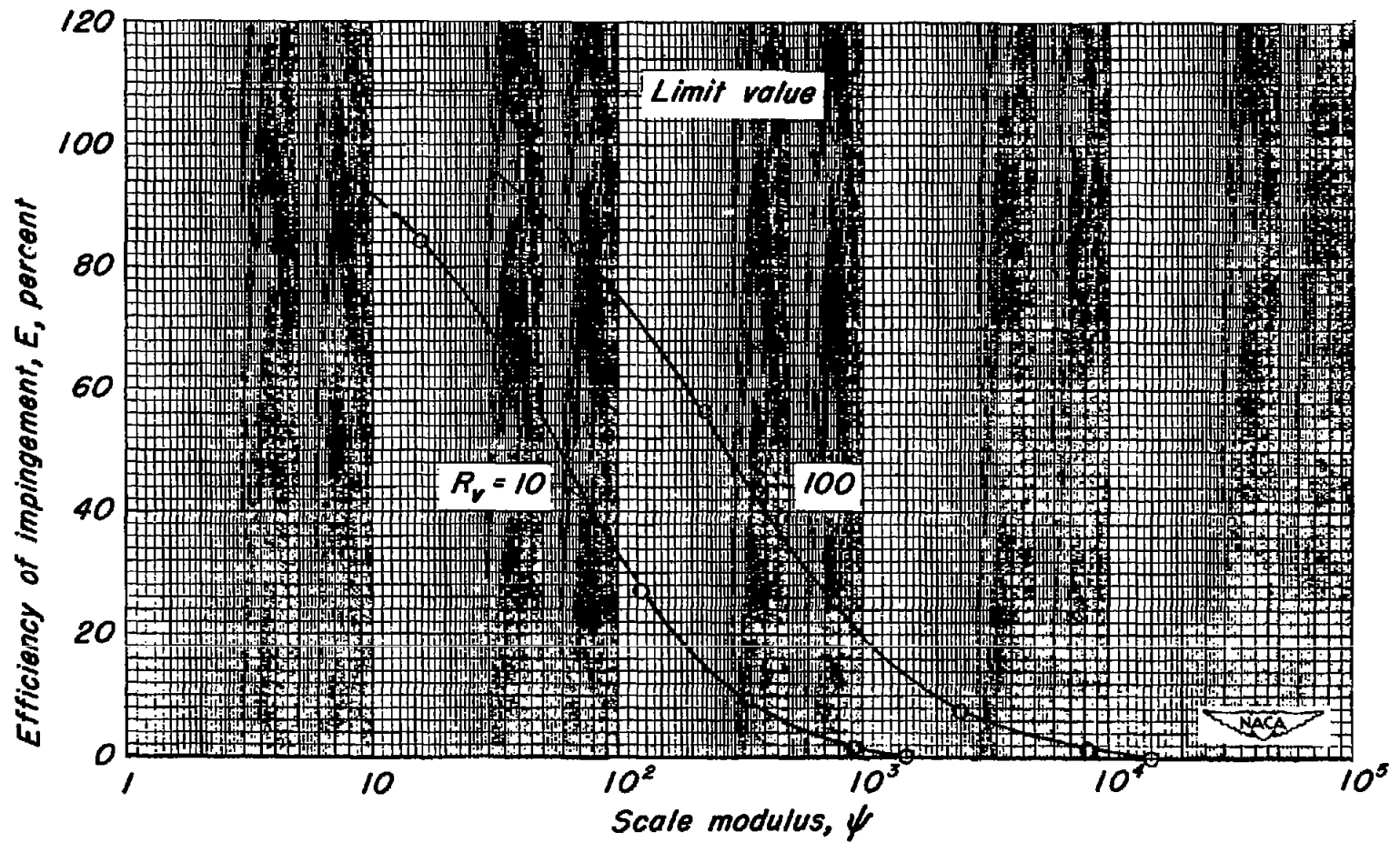
(d) Efficiency of impingement.

Figure 20.- Concluded.
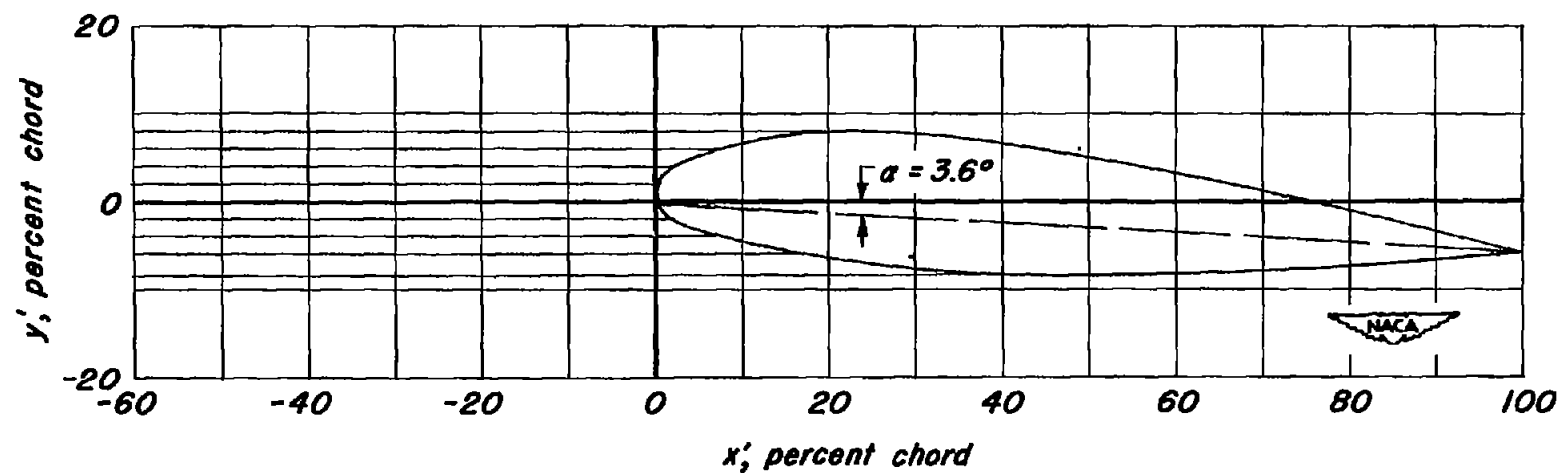
(a) Straight-line trajectories impinging on airfoil.

Figure 21. — Graphical relationships used in evaluating distribution of impingement for an NACA 23015 airfoil; $\alpha = 3.6°$; $c_l = 0.5$.
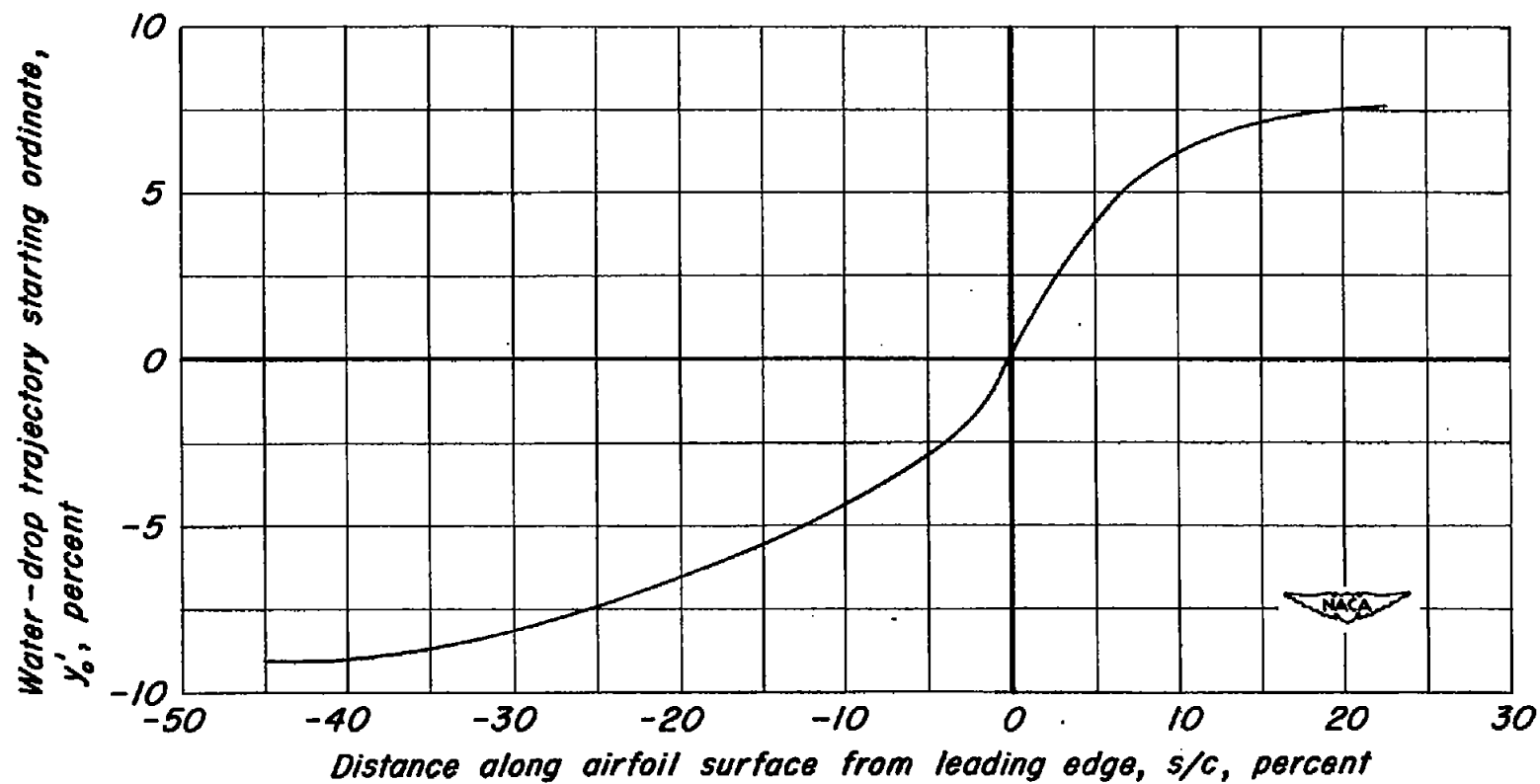
(b) Straight-line trajectory starting ordinates as a function of s/c.

Figure 21.- Continued.
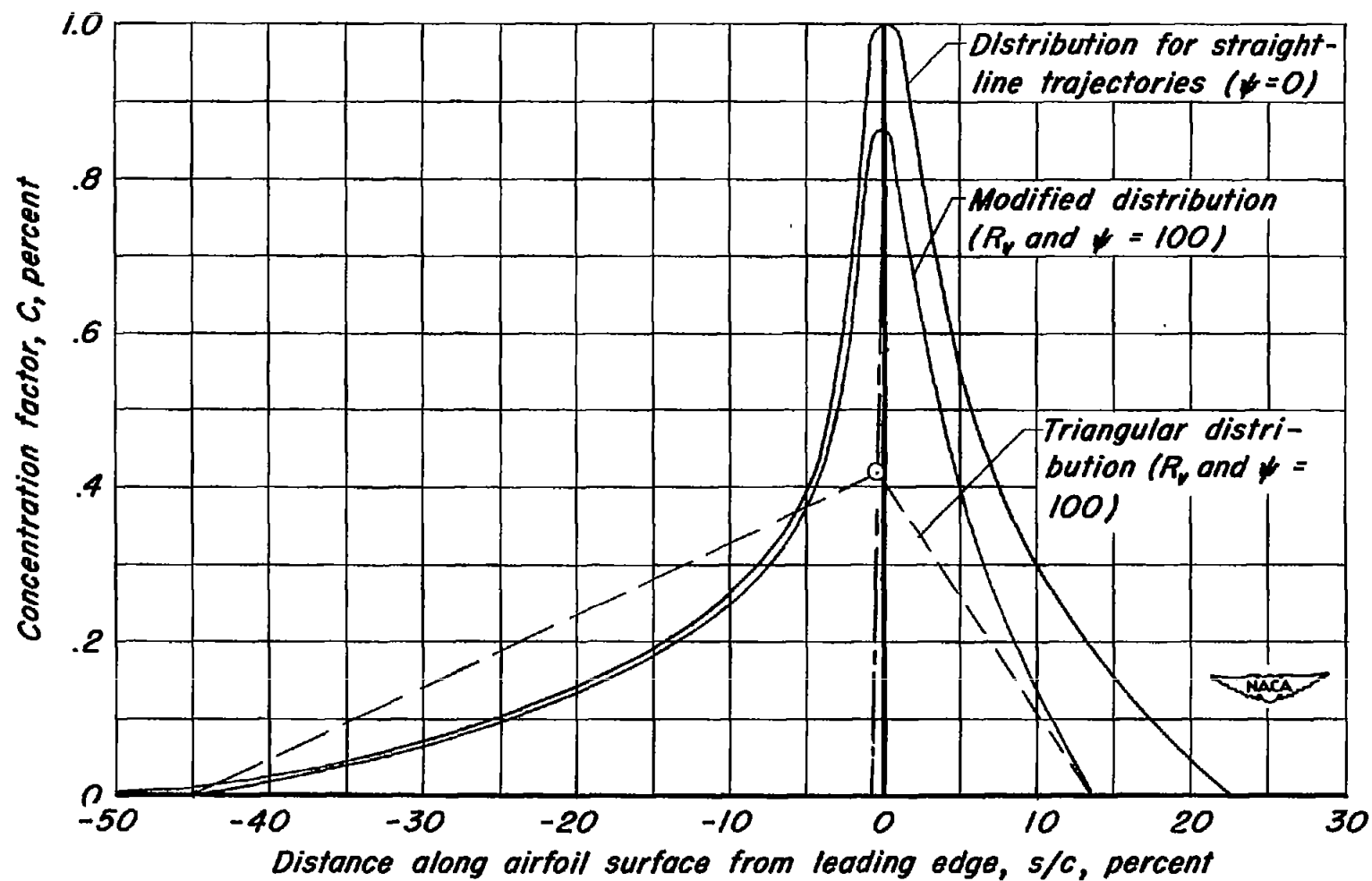
(c) Distribution of impingement.
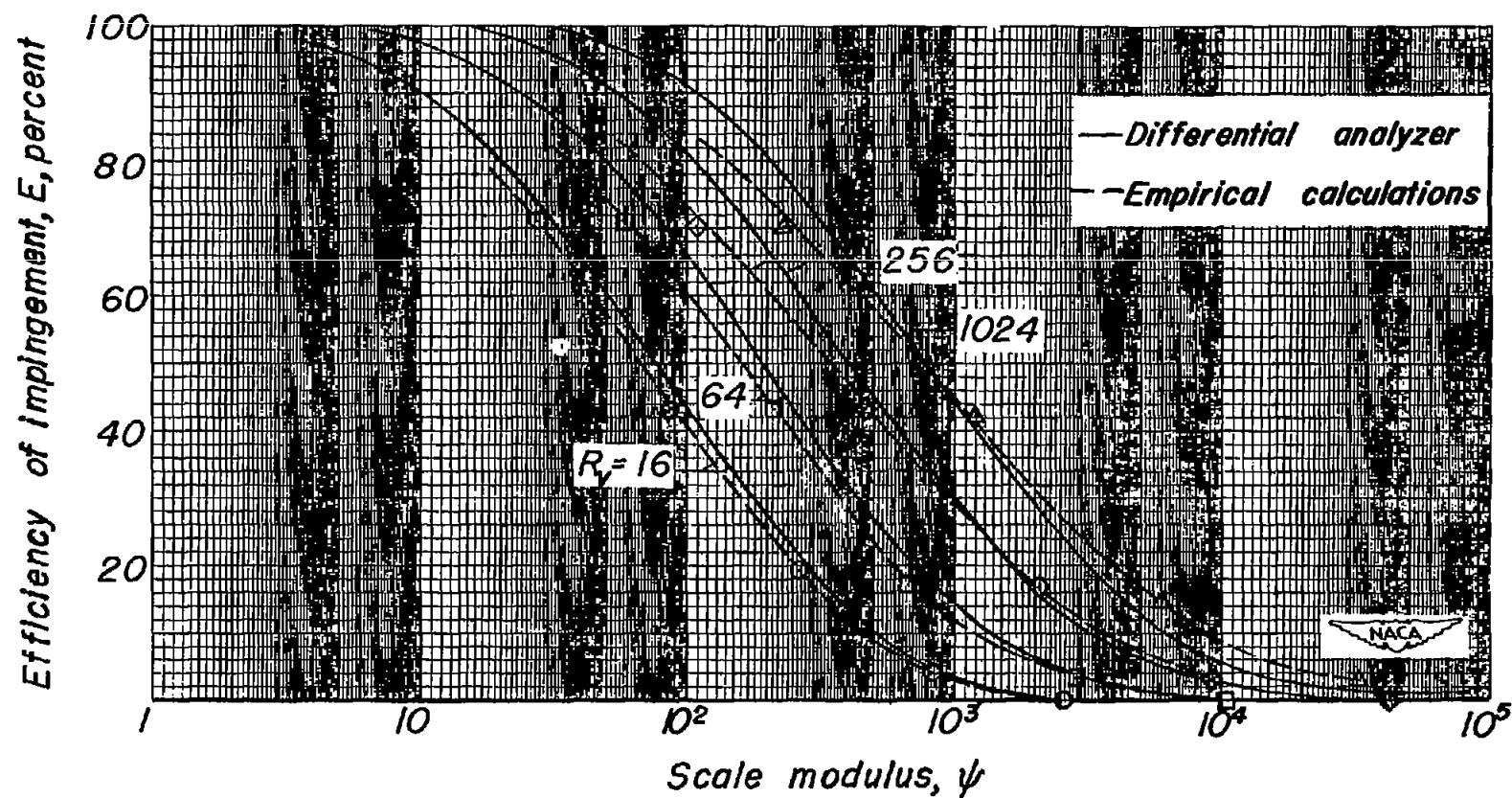
Figure 21. - Concluded.
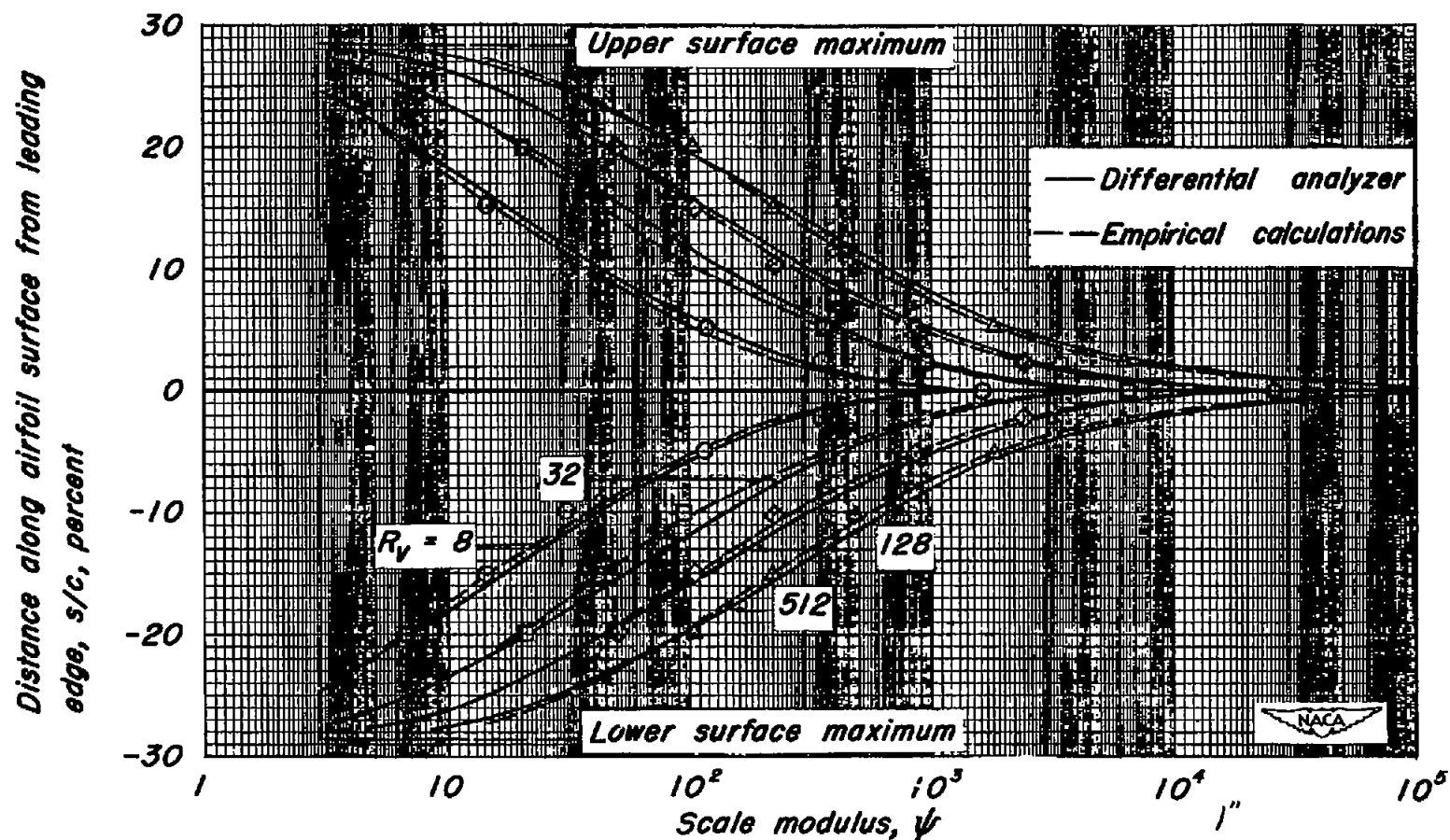
(a) 15-percent-thick symmetrical Joukowski airfoil; $\alpha = 0°$.

Figure 22.—Empirically calculated point values of farthest position of impingement for five airfoils in comparison with curves obtained from a differential analyzer.
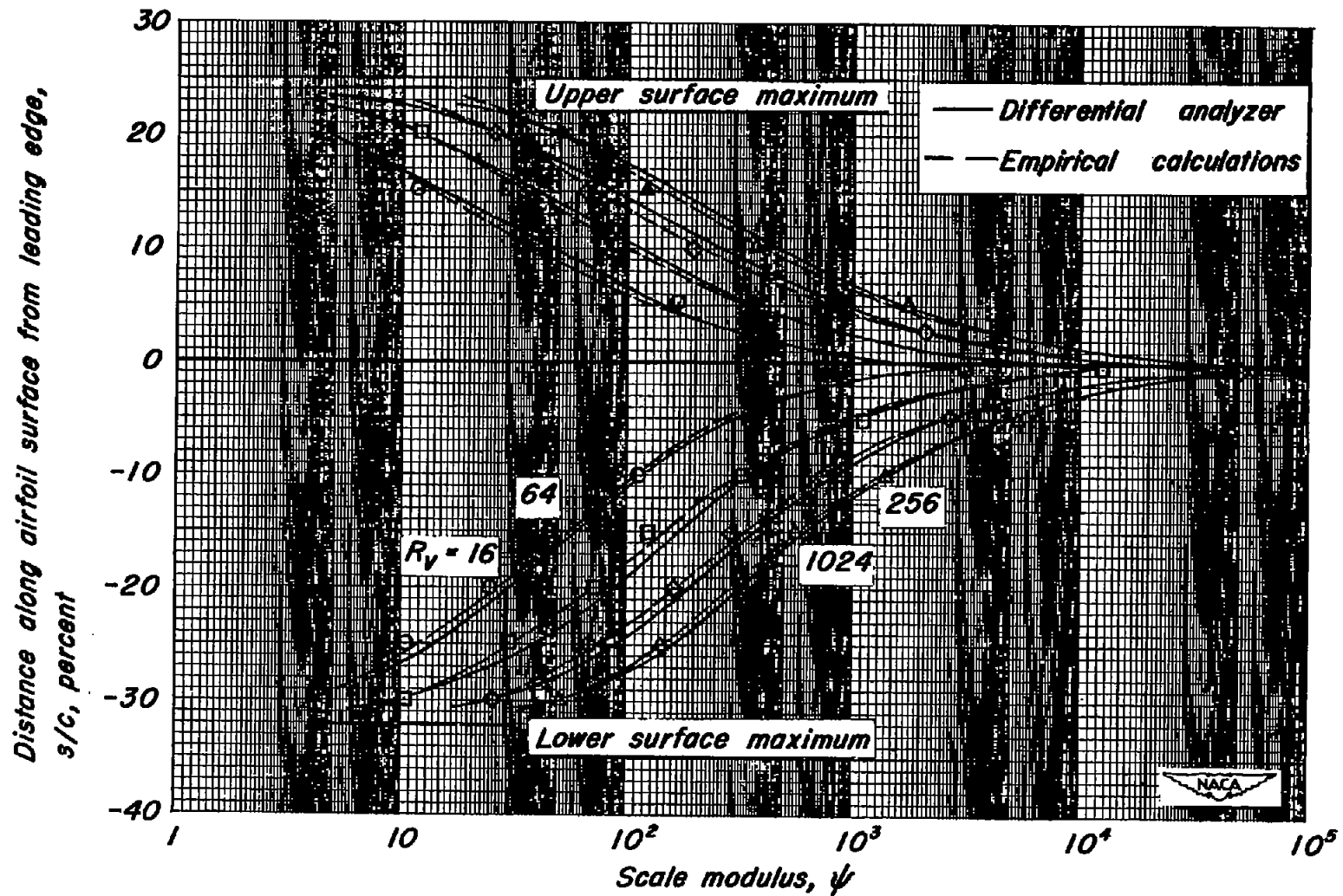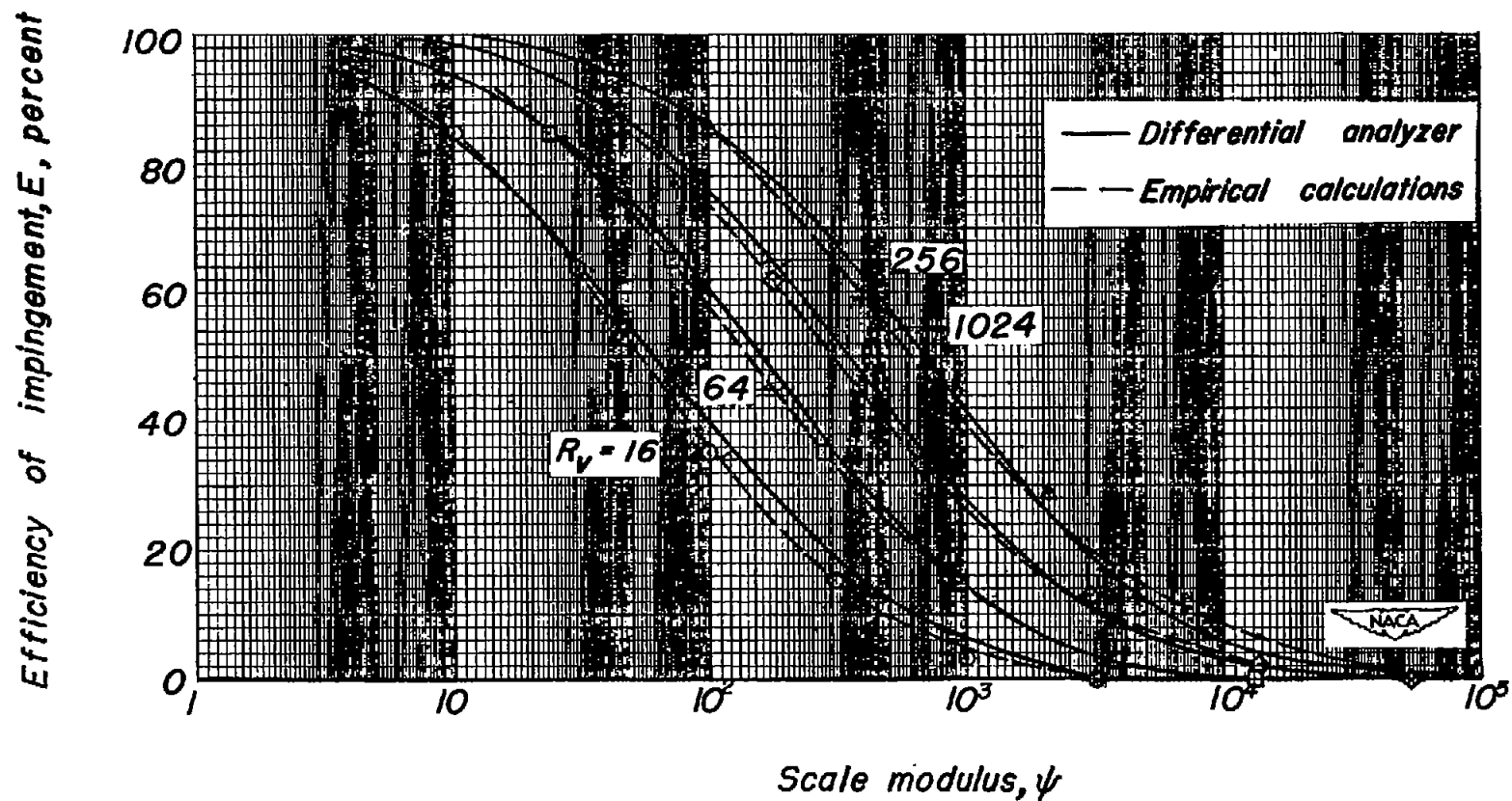
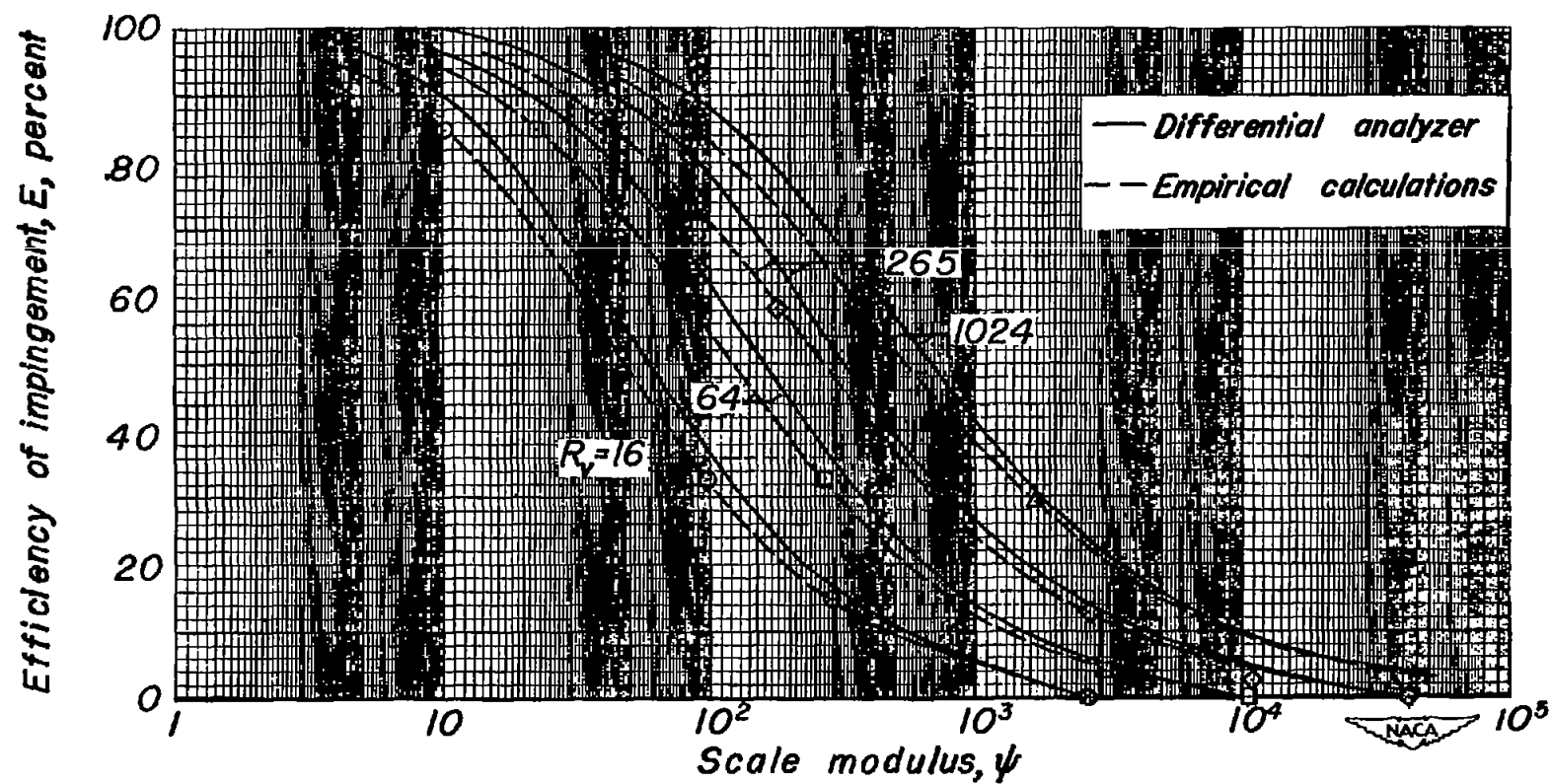(b) 15-percent-thick symmetrical Joukowski airfoil; $a = 2°$.

Figure 22.- Continued.
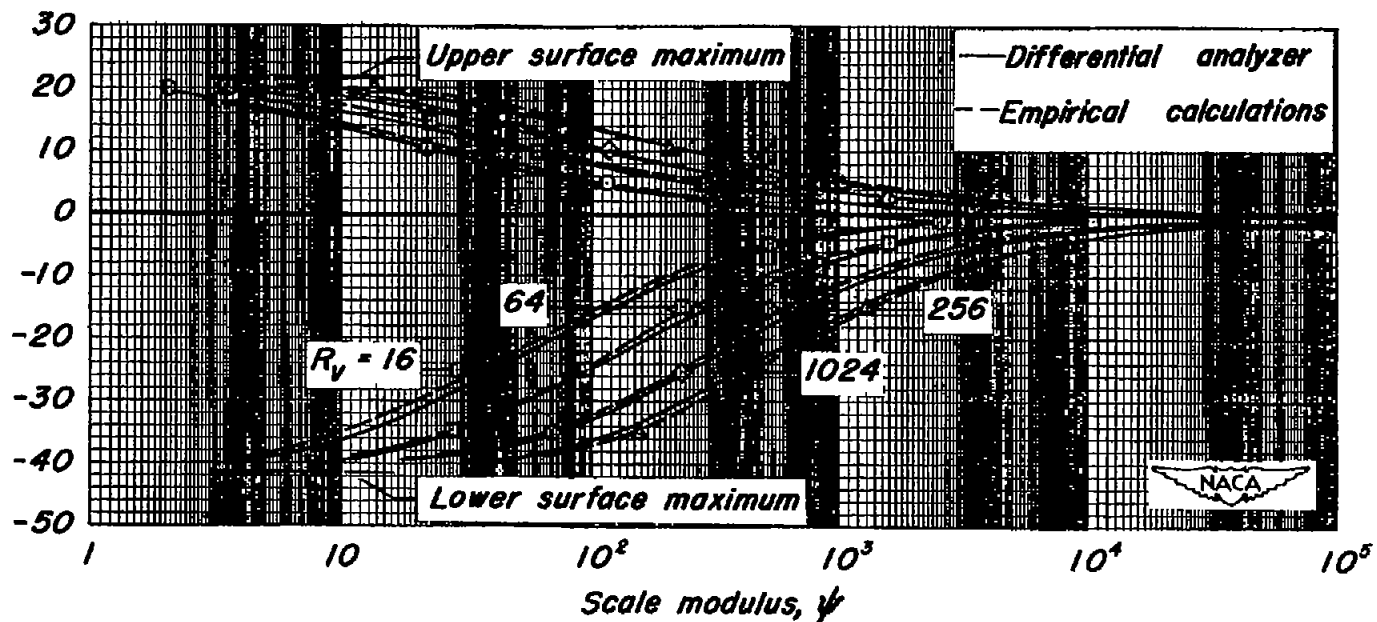
(c) 15-percent-thick symmetrical Joukowski airfoil; $\alpha = 4°$.

Figure 22.- Continued.
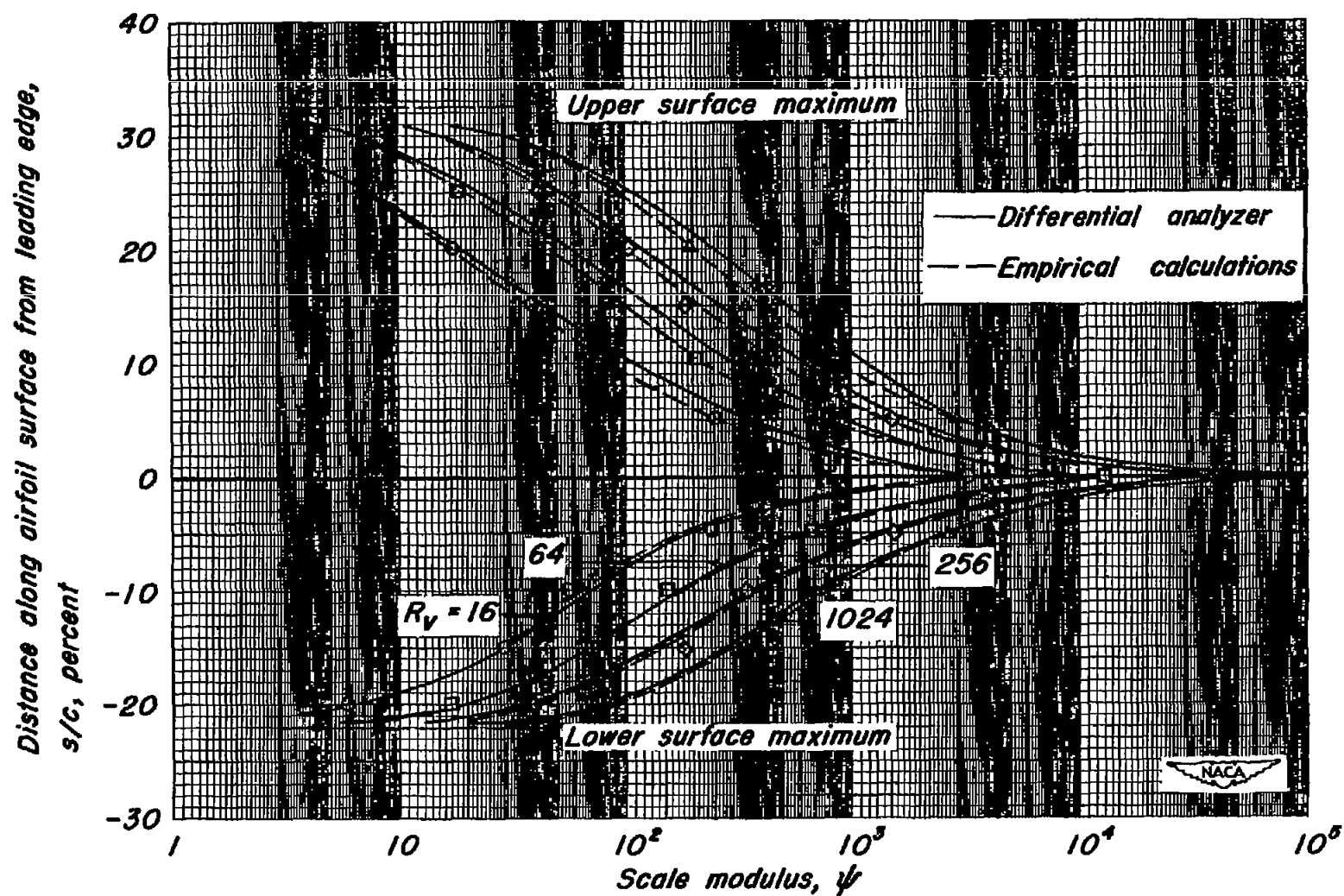
(d) 15-percent-thick cambered Joukowski airfoil ; a = 1.0 mean line ; α = 0°.

Figure 22.- Continued.
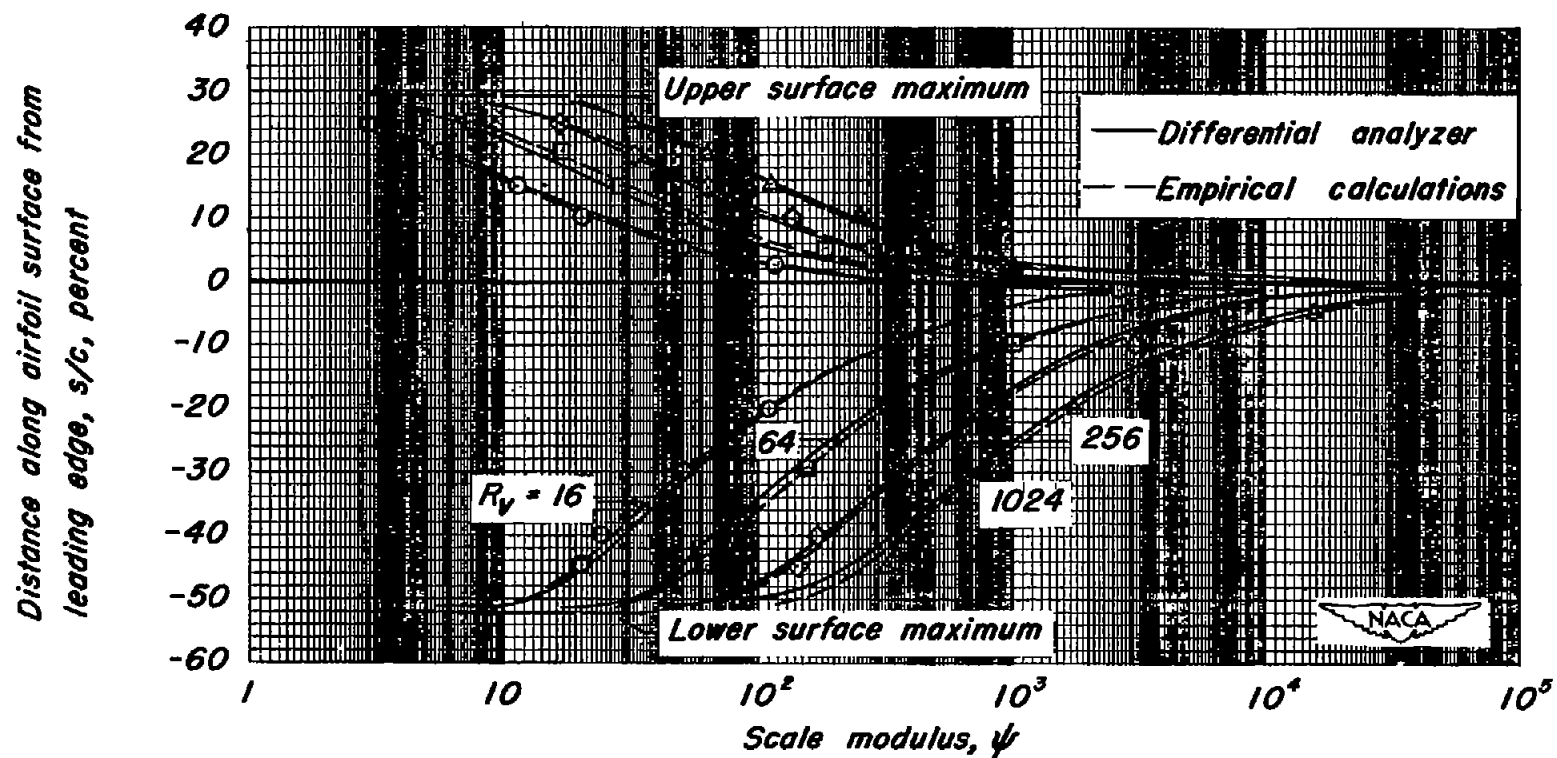
(e) NACA 65_2-015 airfoil; $\alpha = 4°$.

Figure 22.- Concluded.
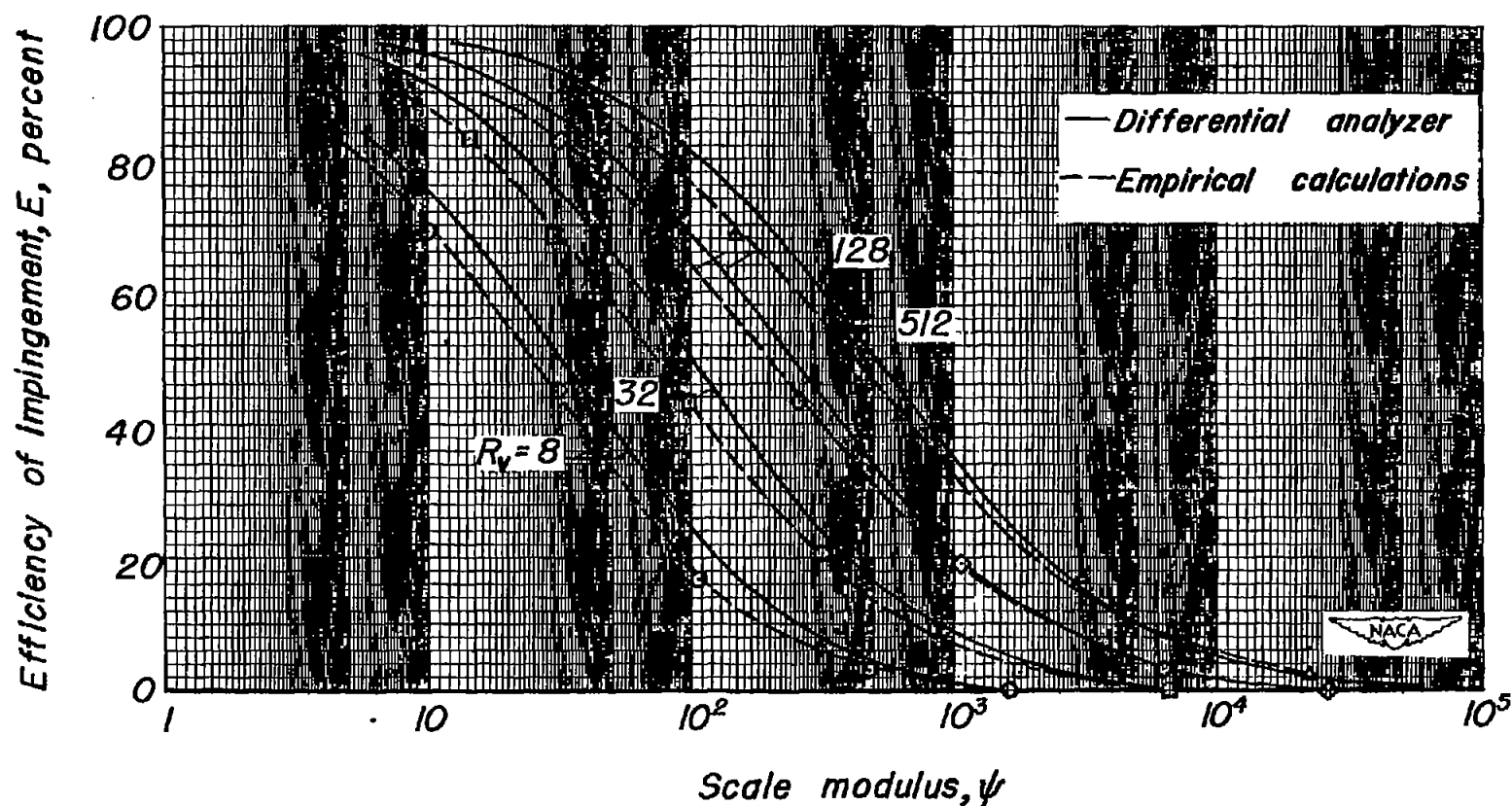
(a) 15-percent-thick symmetrical Joukowski airfoil; a= 0°

Figure 23.— Empirically calculated point values of efficiency of impingement in comparison with curves obtained from a differential analyzer.
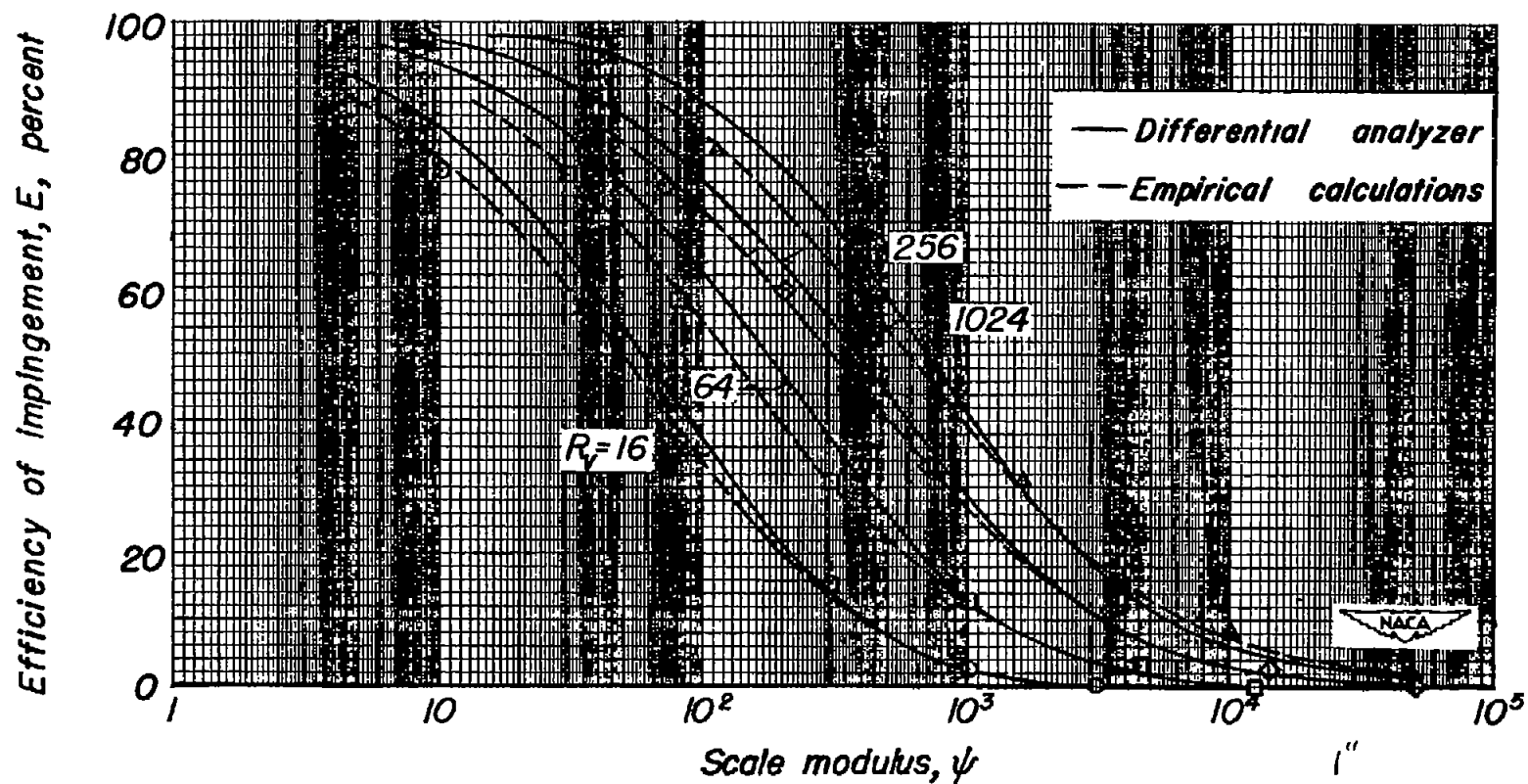
(b) 15-percent-thick symmetrical Joukowski airfoil; $\alpha = 2°$.

Figure 23.— Continued.

(c) 15-percent-thick symmetrical Joukowski airfoil; a=4°.

Figure 23.— Continued.

(d) 15-percent-thick cambered Joukowski airfoil; a = 1.0 mean line; α = 0°.

Figure 23.— Continued.
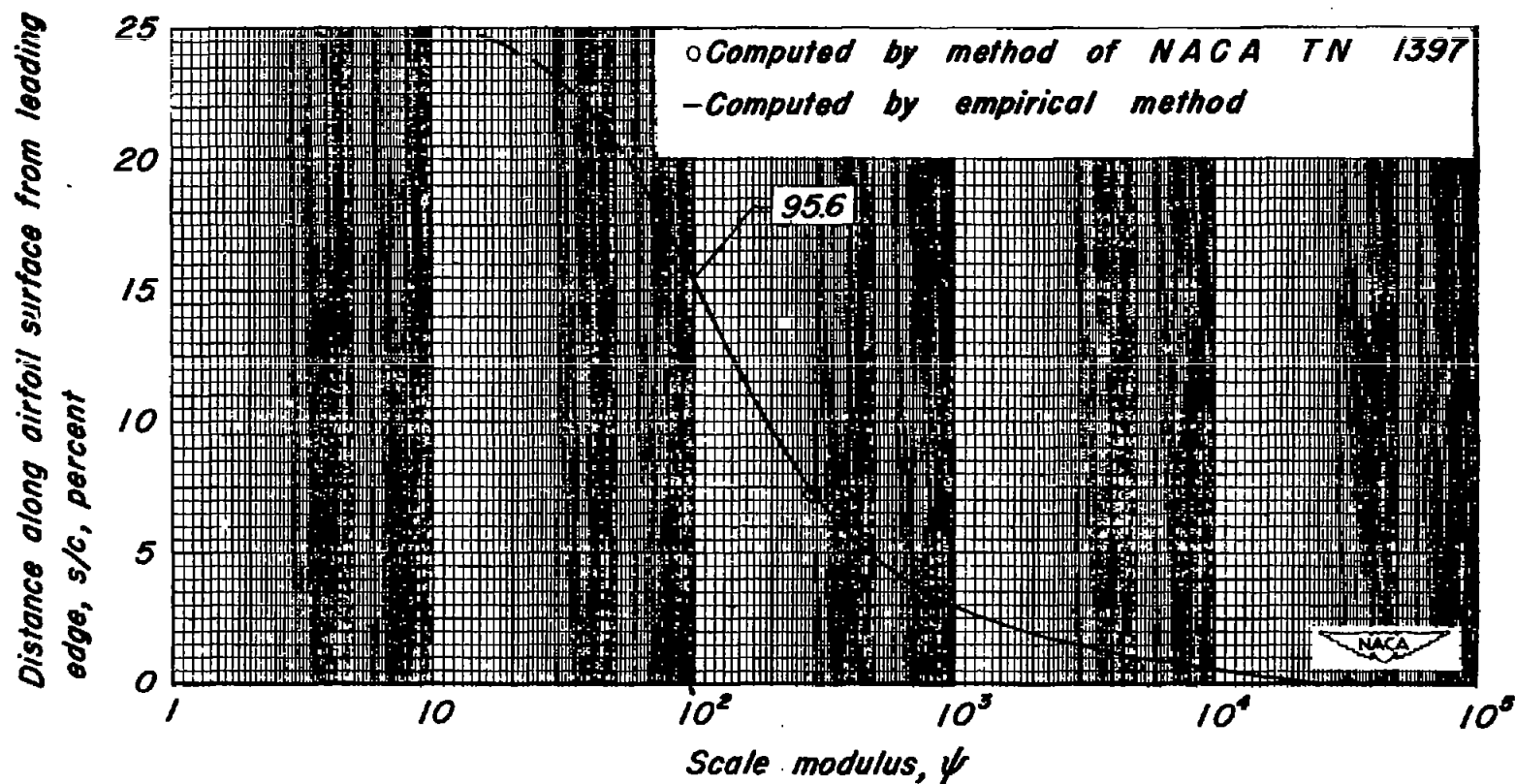
(e) NACA 65₂-015 airfoil; a = 4°.

Figure 23.— Concluded.

Figure 24.- Empirically calculated curve of farthest position of impingement in comparison with point values obtained by stepwise computations for a 12-percent-thick symmetrical Joukowski airfoil, a = 0°.
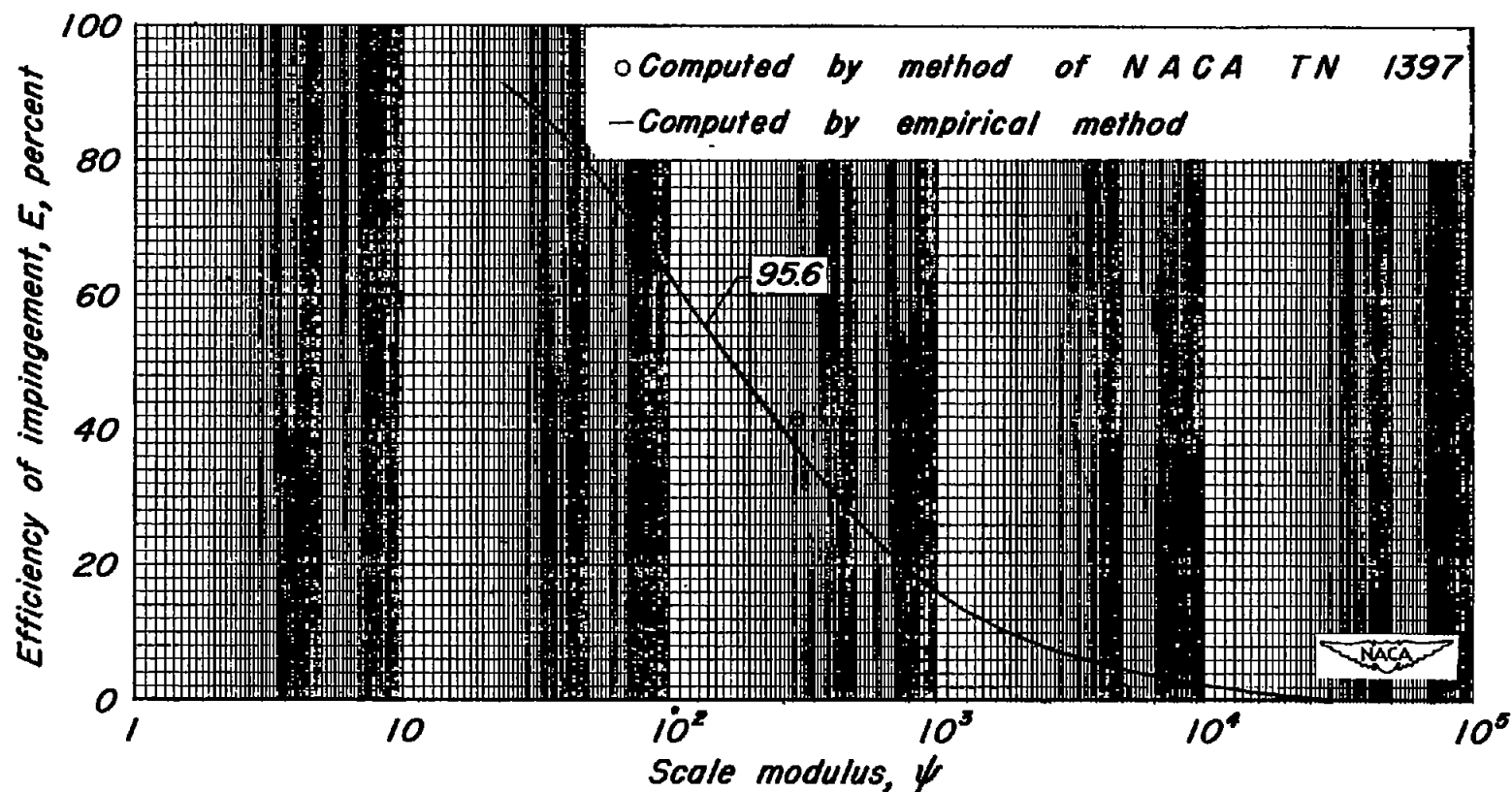
Figure 25.- Empirically calculated curve of percent impingement in comparison with point values obtained by stepwise computations for a 12-percent-thick symmetrical Joukowski airfoil, $\alpha = 0°$.